Designing greener catalysts for vegetable oil oxidation and arene hydrogenation

A thesis submitted to McGill University

In partial fulfillment of the requirements of the degree of Doctor of Philosophy

by Luis Carlos de la Garza Becerra

October 2020

Centre for Green Chemistry and Catalysis, Department of Chemistry

McGill University, Montreal, Quebec, Canada

Abstract

The works presented in this thesis are encompassed under the subject of catalyst design. Although the different chapters cover very different subjects, the common feature is the development of improved catalysts which are superior within the context of green chemistry. The main features I attempted to achieve are higher reaction rates, milder reaction conditions, recyclable heterogeneous catalysts, and reducing the quantity of noble metals needed.

The first subject presented is vegetable oil oxidation, which is a form of biomass valorization. Oxidizing vegetable oils is very important because it increases the range of products made from a recyclable source of hydrocarbons. Many products made from oxidized vegetable oils already exist and their industry is rapidly growing. My research intended to make better catalysts that make these oxidations cheaper and greener. Chapter 2 introduces a new phase transfer agent developed to create a heterogeneous peroxophosphotungstate catalyst. Although the use of peroxophosphotungstate for this reaction is not novel, literature reports of supported heterogeneous phosphotungstates show significantly lower reaction rates than their homogeneous counterparts. Our catalyst was designed to achieve a heterogeneous and recyclable catalyst without compromising activity. Our research also showed that the activity of heterogeneous phosphotungstates depended on the proper formation of the active species before being immobilized and avoiding the formation of less active tungstate side products. We devised methods to achieve the adequate formation of the active species, which we further support via solid-state magic-angle spinning (MAS) nuclear magnetic resonance (NMR) characterization, so this discovery can be applied to other types of heterogeneous phosphotungstates as well.

The second subject presented is photocatalytic enhancement via localized surface plasmon resonance (LSPR), which involves plasmonic metal nanoparticles. This research on Chapter 3 is directed towards hydrogenation of alkenes and arenes using the antenna effect of LSPR, thereby enhancing the reaction rate of ruthenium-based hydrogenations. Although ruthenium is already known to perform this reaction, the enhancement provided by LSPR allows for the reaction to be performed under milder conditions or with a lower loading of ruthenium, therefore making it more efficient. Our research showed how this can be accomplished using gold nanoparticles as the source of LSPR. We designed a catalyst by depositing Ru on the surface of Au NPs, which

were then immobilized onto Al_2O_3 and used for hydrogenations of alkenes and arenes under light. The activity of this catalyst was significantly enhanced when exposed to irradiation at a wavelength that overlapped with the LSPR of Au NPs, which demonstrated that the methodology was viable. Reaction rates observed under light irradiation were 11 times higher than those in the dark. It was also observed that LSPR-enhanced hydrogenation of arenes did not affect the rate order of the reaction. This result suggests that the enhancement was not due to a photothermal effect or an increased desorption of the substrates.

Following that, Chapter 4 presents our efforts researching a similar system where Au is replaced with Al in an attempt to make the system greener, since Al is much more abundant than Au. Catalysts were synthesized by depositing Ru on Al NPs. Characterization by transmission electron microscopy (TEM) showed that the Al NPs conformed to literature reports and that the Ru was successfully grown on the surface of the Al NPs. However, we were unable to observe rate-enhancement towards the hydrogenation of styrene when irradiating the catalyst with visible light. Further characterization using electron-energy loss spectroscopy (EELS) demonstrated a large variation between the LSPR energy profile of our sample and the ones of Al NPs with similar size, shape and capping agents reported in the literature.

Résumé

Les travaux présentés dans cette thèse visent tous à la conception de catalyseurs. Bien que les différents chapitres couvrent des sujets très différents, ils ont pour point commun le développement de catalyseurs améliorés et supérieurs dans le contexte de la chimie verte. Les principales caractéristiques que j'ai tenté d'obtenir sont des vitesses de réaction plus élevées, des conditions de réaction plus douces, des catalyseurs hétérogènes recyclables et une réduction de l'utilisation de métaux nobles.

Le premier sujet présenté est l'oxydation des huiles végétales, qui est une forme de valorisation de la biomasse. Les huiles végétales oxydantes sont très importantes car elles élargissent la gamme de produits fabriqués à partir d'une source recyclable d'hydrocarbures. De nombreux produits à base d'huiles végétales oxydées existent déjà et leur industrie est en pleine croissance. Mes recherches visent à fabriquer de meilleurs catalyseurs qui rendent ces réactions d’oxydation moins chères et plus vertes. Le chapitre 2 présente un nouvel agent de transfert de phase développé pour créer un catalyseur peroxophosphotungstate hétérogène. Bien que l'utilisation du peroxophosphotungstate pour cette réaction ne soit pas nouvelle, la littérature sur les phosphotungstates hétérogènes supportés montrent des taux de réaction significativement plus faibles que leurs homologues homogènes. Notre catalyseur a été conçu pour obtenir un catalyseur hétérogène et recyclable sans perte d'activité. Nos recherches montrent également que l'activité des phosphotungstates hétérogènes dépend de la formation de l'espèce active désirée avant d'être immobilisée et d'éviter la formation de produits secondaires de tungstate moins actifs. Nous avons conçu des méthodes pour atteindre la formation adéquate des espèces actives, ainsi que le démontre la caractérisation par résonance magnétique nucléaire (RMN) à l’état solide par rotation à l’angle magique (RAM), de sorte que cette découverte peut être appliquée à d'autres types de phosphotungstates hétérogènes.

Le deuxième sujet présenté est l'amélioration photocatalytique par résonance des plasmons de surface localisée (RPSL), qui implique des nanoparticules métalliques plasmoniques. Cette recherche, au chapitre 3, est orientée vers l'hydrogénation d'alcènes et d'arènes en utilisant l'effet d'antenne du RPSL, augmentant ainsi la vitesse de réaction des hydrogénations à base de ruthénium. Bien que le ruthénium soit déjà connu pour effectuer cette réaction, l'amélioration

fournie par RPSL permet d’effectuer la réaction dans des conditions plus douces ou avec une charge plus faible de ruthénium, la rendant ainsi plus efficace. Notre recherche a montré comment cela peut être accompli en utilisant des nanoparticules d'or comme source de RPSL. Nous avons conçu un catalyseur en déposant du Ru à la surface des NP Au, qui ont ensuite été immobilisés sur Al_2O_3 et utilisés pour les hydrogénations d'alcènes et d'arènes sous lumière. L'activité de ce catalyseur était significativement améliorée lorsqu'il était exposé à une irradiation à une longueur d'onde qui chevauchait le RPSL des NP Au, ce qui a démontré que la méthodologie était viable. Les vitesses de réaction observées sous irradiation ont été 11 fois plus élevées que celles dans l'obscurité. On a également vu que l'hydrogénation des arènes assistée par LSPR n'affectait pas l'ordre de réaction. Ce résultat suggère que l'amélioration n'était pas due à un effet photothermique ou à une désorption accrue des substrats.

Ensuite, le chapitre 4 présente nos efforts pour rechercher un système similaire dans lequel l'or est remplacé par de l'aluminium afin de rendre le système plus vert, car l'aluminium est beaucoup plus abondant que l'or. Les catalyseurs ont été synthétisés en déposant Ru sur Al NPs. La caractérisation par microscopie électronique en transmission (TEM) a montré que les NP Al étaient conformes aux précédents de la littérature et que le Ru a pu être déposé avec succès à la surface des NP Al. Cependant, nous n'avons pas pu observer une augmentation de la vitesse de l'hydrogénation du styrène lors de l'irradiation du catalyseur. Une caractérisation plus poussée à l'aide de la spectroscopie de perte d'énergie des électrons (SPEE) a démontré une grande variation entre le profil énergétique du RPSL de notre échantillon et ceux des NP de Al rapportés dans la littérature avec des tailles, des formes et des fonctionnalisations similaires.

Acknowlegments

I would like to thank Dr. Audrey Moores above everyone else for her exemplary role as a supervisor. Not only was she very knowledgeable and help direct my research in the right direction, she was also extremely supportive and engaged in making sure I was improving in a personal level.

To my parents, who are always extremely supportive at all times and constantly try to help me even though they are far away while I'm studying abroad.

My colleagues, especially Madhu, Alain, Blaine and Alexandra, who were always willing to discuss the science and give advice, even though our research subjects often didn't overlap. Along with them, all the members of the Moores Group always provided a great environment and I'm happy to have met and worked together with Huizhi, Mary, Julio, Tony, Aude and Thomas.

Research staff from McGill University, in particular Robin Stein and David Liu, both of which taught me a lot about NMR and TEM respectively. I appreciate all the time and effort they spent helping me and I hope they get more recognition for the fantastic job they perform.

A great thanks to Chantal Marotte, who was by far the most helpful person in the university. She was essential from before I even arrived in Canada, until the very end of my degree. Professors at the chemistry department, especially Dr Nicolas Moitessier, Dr. C.J. Li and Dr. Bruce Arndtsen which were in my review committees and taught me a lot of how a researcher needs to think and present itself. Also thanks to Dr. Samuel Sewall and Mr. Jean-Marc Gauthier, who I worked for as a TA multiple times and were very friendly.

I would like to thank all the people that co-authored my publications: Mr. Nicolas Brodusch, Dr. Raynald Gauvin, Dr. Karine De Oliveira Vigier and Dr. Gregory Chatel. Nicolas was especially involved in the characterization of my nanoparticles, which was an enormous help. Thanks to Dr. Chatel for hosting me at Poitiers University, allowing me to use their facilities and teaching me about sonochemistry. Thanks to Oleotek for hosting me and introducing me to

oleochemistry at their facility in Thetford-Mines, as well as training me in GC maintenance. Thanks to Jacqueline Farrell as well, who helped make those collaborations possible.

I also thank the funding sources that allowed the research to happen. The France–Canada Research Fund, the Natural Science and Engineering Research Council of Canada (NSERC) Discovery Grant program, the Canada Foundation for Innovation (CFI), the Canada Research Chairs (CRC), the Fonds de Recherche du Québec – Nature et Technologies (FRQNT) Equipe program, the Centre for Green Chemistry and Catalysis (CGCC), NSERC-Collaborative Research and Training Experience (CREATE) in Green Chemistry and McGill University for their financial support.

Thesis Overview and Contribution of Authors

Chapter 1

The author wrote the content. Audrey Moores edited the manuscript.

Chapter 2

Luis Carlos de la Garza, Karine De Oliveira Vigier, Gregory Chatel and Audrey Moores, "Amphiphilic dipyridinium-phosphotungstate as an efficient and recyclable catalyst for triphasic fatty ester epoxidation and oxidative cleavage with hydrogen peroxide", Green Chemistry, 2017, 19, 2855-2862.

The author designed the experiments, collected all data and wrote the manuscript. Audrey Moores, Gregory Chatel and Karine de Oliveira Vigier edited the manuscript.

Chapter 3

Luis Carlos de la Garza, Nicolas Brodusch, Raynald Gauvin and Audrey Moores, "Plasmon-Enhanced Hydrogenation of 1-Dodecene and Toluene Using Ruthenium-Coated Gold Nanoparticles", ACS Applied Nano Materials, 2021, DOI:10.1021/acsanm.0c03077

The author designed the experiments, collected all experimental data, performed characterization of the catalyst (UV-vis and TEM) and wrote the manuscript. Nicolas Brodusch performed characterization of the catalyst (EDS, SEM and EELS) and edited the manuscript. Raynald Gauvin and Audrey Moores edited the manuscript.

Chapter 4

Luis Carlos de la Garza, Nicolas Brodusch, Raynald Gauvin and Audrey Moores· "Plasmon-enhanced hydrogenation of alkenes and arenes using ruthenium-decorated aluminium nanoparticles". (manuscript in preparation).

The author designed the experiments, collected all experimental data, performed characterization of the catalyst (TEM) and wrote the manuscript. Nicolas Brodusch performed characterization of the catalyst (SEM and EELS) and edited the manuscript. Raynald Gauvin and Audrey Moores edited the manuscript.

Table of contents

List of figures

List of schemes

List of tables

List of abbreviations

CTAB	Hexadecyltrimethyl ammonium bromide
DMF	Dimethylformamide
DMSO	Dimethylsulfoxide
DP^{2+}	4,4′-(trimethylene)bis(1-tetradecylpyridinium)
EELS	Electron energy loss spectroscopy
EtOAc	Ethyl acetate
EDS	Energy-dispersive X-ray spectroscopy
EF	Energy-filtered
ESI	Electronic supplementary information
FE	Field emission
GC	Gas chromatography
HAADF	High-angle annular dark-field
ICP	Inductively coupled plasma
LSPR	Localized surface plasmon resonance
MAS	Magic-angle spinning
MeCN	Acetonitrile
MeOD	Deuterated methanol
MeOH	Methanol

MOF	Metal-organic framework
MS	Mass spectrometry
NMR	Nuclear magnetic resonance
NP	Nanoparticle
PEG	Polyethylene glycol
POM	Polyoxometalate
PVP	Polyvinylpyrrolidone
PPW^{3-}	Peroxophosphotungstate: $[PO_4[W(O)(O_2)_2]_4]^{3-}$
PVC	Polyvinyl chloride
SE	Secondary electron
SEM	Scanning electron microscopy
STEM	Scanning transmission electron microscopy
TEM	Transmission electron microscopy
THF	Tetrahydrofuran
TGA	Thermogravimetric analysis
TOF	Turnover frequency
TON	Turnover number
UV	Ultraviolet

1. Introduction

With the goal of greener catalyst design, the projects presented in this thesis cover several different topics which will be presented sequentially in this introduction. The first topic concerning biomass valorization through vegetable oil oxidation is relevant for the research presented in Chapter 2. The second and third topics are plasmon-enhanced catalysis and hydrogenation, which are relevant for the research presented in Chapters 3 and 4.

1.1. Vegetable oil oxidation

The chemical industry relies on petroleum as its main source of hydrocarbons. But due to the non-renewable nature of petroleum, there is a pressing need to develop renewable feedstocks of carbon-based materials that can replace petroleum for a wide range of applications.[1] It is well established that renewable organic materials can be obtained from biomass, which is defined as animal or plant material, which can come from a large variety of sources such as food crops, forestry, waste from food processing, animal farming, algae or even sewage sludge.[1-5]

Vegetable oils are the most prominent source of biomass currently used in the chemical industry.[6] As such, there is a lot of ongoing research devoted to valorization of vegetable oils by transforming the raw triglycerides into different products for multiple applications.[7-10] Vegetable oils are composed of triglycerides, which are molecules that contain a glycerol unit bound to three long-chained hydrocarbons via ester groups. These long-chained hydrocarbons can be separated from the glycerol via acid hydrolysis, a process that also occurs naturally during digestion of edible oils, which makes what is commonly known as a fatty acid.[11] Although triglycerides are always formed of esters, the term “fatty acid” is generally used to refer to all hydrocarbon chains in vegetable oils.

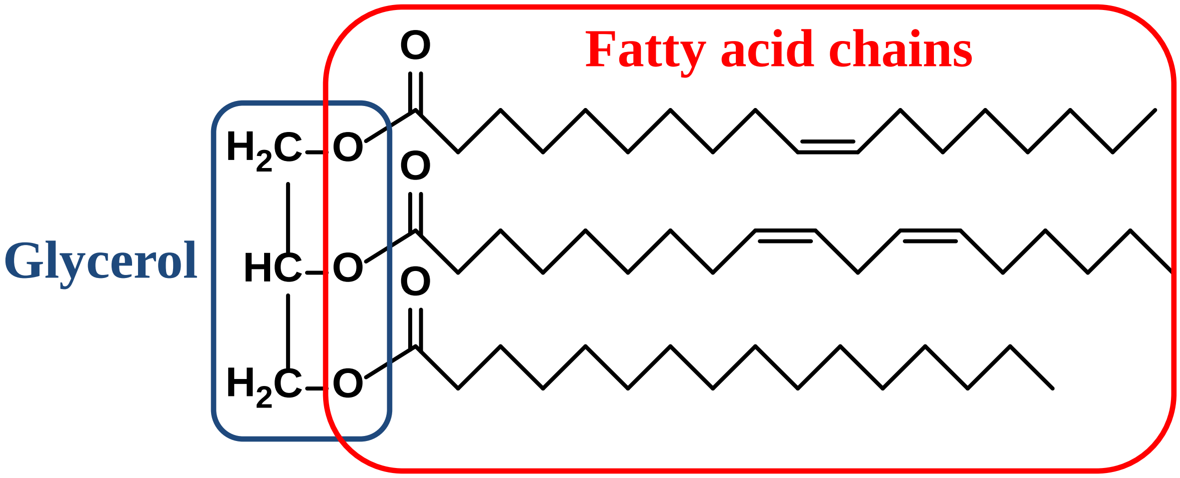

Figure 1: General composition of triglycerides.

The fatty acid chains are the main component in vegetable oil, and its main defining features are the carboxylic group, the length of the hydrocarbon chain, and the amount of double bonds present, as seen in Figure 1. Fatty acids are typically classified by the number of double bonds, which is also called the degree of unsaturation. Fatty acids without double bonds are called saturated fatty acids, and are generally much less prevalent than unsaturated fatty acids, with oleic and linoleic acid being the most common fatty acids found in vegetable oils.[12-13] Some common fatty acids are depicted in Figure 2. An important characteristic about these unsaturations is that fatty acids from vegetable oils have exclusively cis double bonds. Trans double bonds only appear in fatty acids sourced from animals or after isomerizing the cis bonds via partial hydrogenation.[14]

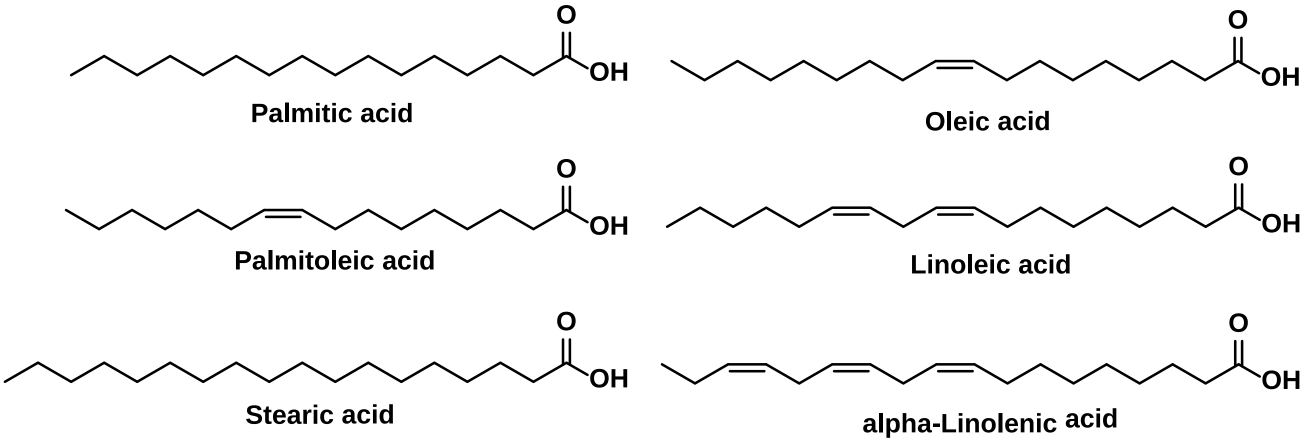

Figure 2: Common fatty acids found in vegetable oils.

Reactions involving vegetable oils and fatty acids focus either on the carboxylic moiety or the double bonds in the hydrocarbon chains. Reactions involving the carboxylic moiety in triglycerides lead to individual fatty acids, amines, glycerol or biodiesel (fatty acid methyl esters), while reactions involving the hydrocarbon chain focus on transforming the double bonds via epoxidation, cleavage, metathesis, dimerization or hydroformylation.[7] An overview of these reactions is shown in Scheme 1

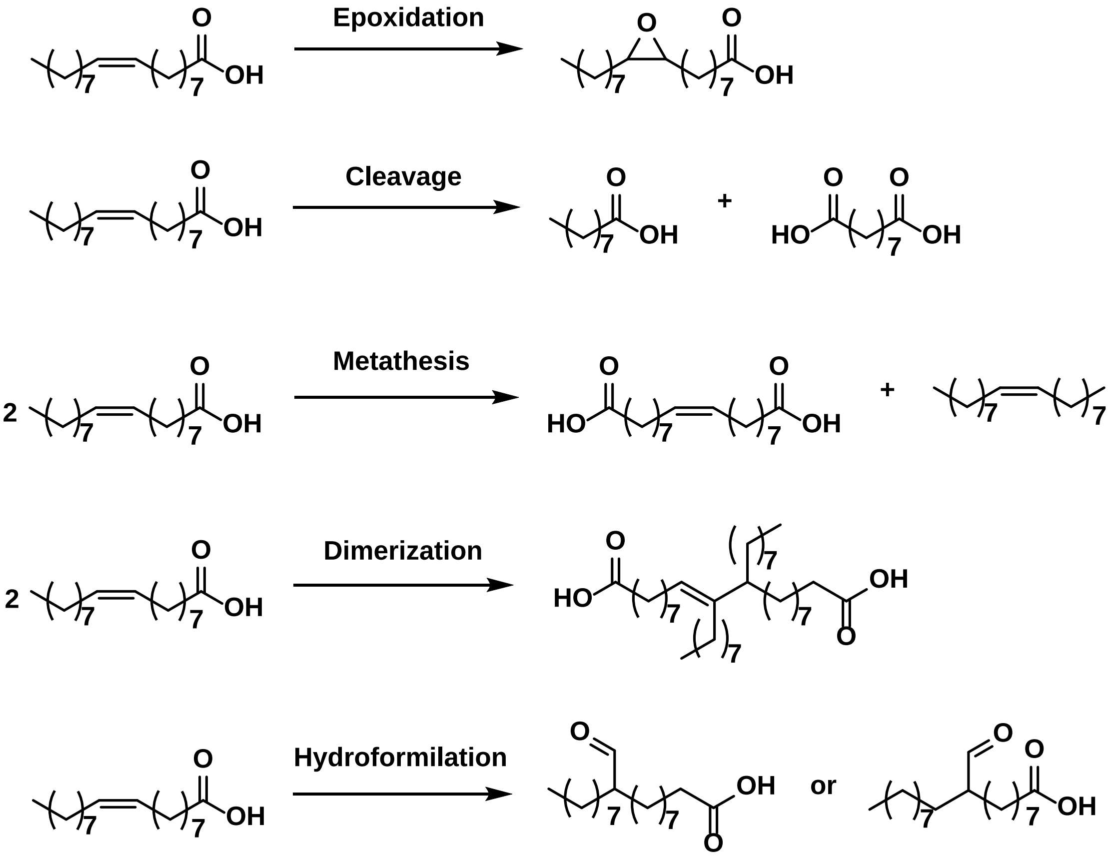

Scheme 1: Valorization reactions of fatty acids involving double bonds.

Epoxidized fatty acids are useful both as intermediates for further transformations and as products themselves. The most common use of these epoxides is as polymer additives, specifically as plasticizers and stabilizers.[7] For example, epoxidized soybean oil is commonly used as an additive in PVC resins, which increases its softness and flexibility, while also acting as a stabilizer by reacting with hydrochloric acid that is slowly released when PVC is exposed to light and heat.[7, 15] Uses of epoxides as intermediates rely mostly on ring-opening reactions. Epoxides readily react with many nucleophiles like amines, alcohols and carboxylic acids, or they can also be transformed into polyols by hydrolysis or polymerized via acid catalysis.[16]

Cleavage reactions as defined as the complete rupture of the double bond, which forms two shorter unsaturated products: a carboxylic acid and a dicarboxylic acid, as seen in Scheme 1. Cleavage of polyunsaturated fatty acids will lead to additional products by cleaving multiple double bonds. This reaction is usually performed via ozonolysis or oxidative cleavage using strong oxidants like chromic acid or peroxyacids.[7] The oxidative cleavage can be performed by successive oxidation of the epoxide. Scheme 2 shows a summary of the reaction pathway and applications of the multiple products that can be obtained using this methodology. The main desired products from cleavage are the diacids, which have applications as plasticizers, lubricants, pharmaceutics, monomers for polymers, greases and cosmetics.[7] For example, azelaic acid, the diacid formed from cleavage of oleic acid, has bactericidal, anti-inflammatory and antioxidative properties, which makes it a useful active ingredient against acne.[17] The shorter monocarboxylic acids produced from the cleavage of the double bonds are less interesting in this case, since they can be readily obtained through other feedstocks, but they are still byproducts that increase the value of the functionalization of vegetable oils and have applications as diet supplements, dyes, perfumes and surfactants.

Metathesis is a reaction where two alkenes replace one of their substituent chains with each other at the same time. This reaction can be used to create two new products or even to cyclize large molecules, while retaining the double bonds, and is typically catalyzed using molybdenum or ruthenium carbene complexes, developed respectively by Schrock and Grubbs.[18-19] Homometathesis between two identical fatty acids forms a long-chained alkene and a long-chained diacid, but the reaction can also be performed with other alkenes, which is known as Cross Metathesis.[20] This leads to a large variety of possible products, most of which are considered intermediates. Since the double bond is maintained after the metathesis reaction, these products can be further functionalized which leads to numerous applications, including lubricants, polyolefins, pharmaceuticals, surfactants, fragrances, polyamides and polyesters, among others.[7]

Dimerization of fatty acids is another route other than cleavage which leads mainly to dicarboxylic acids. However, this reaction makes molecules larger instead of shorter. These diacids feature long branching chains which result in less oily materials, with applications such as hot melt adhesives, epoxy coatings, and printing inks. They are also known to be useful for the production of polyesters and polyamides, or they can also hydrogenated into diols in order to make polyethers and polyurethanes.[7]

Hydroformylation is the most common method to introduce a carbonyl group to a double bond. The reaction involves a metal-catalyzed insertion of carbon monoxide and H_2 which reduces the double bond and forms a branched aldehyde, with cobalt carbonyl and rhodium nanoparticles being the most commonly used catalysts for this reaction.[21] The addition of an aldehyde to a fatty acid allows for the formation of polyols, polyacids, polyesters, and polyamides, which have similar applications to those formed via epoxidation, namely as plasticizers, lubricants, coatings and monomers for polymer synthesis.[7]

Among these valorization reactions, our research focused on the design of catalysts for the oxidation reactions including both epoxidation and oxidative cleavage of unsaturated fatty acids, the results of which are reported in chapter 2.

Oxidations can lead to several different products, so specific reaction conditions are required to reach the desired product. Oxidations proceed via multiple sequential reactions, where reaction selectivity depends on the ability to neatly stop reaction at a given intermediate, or making it proceed all the way to the end. The oxidation sequence first epoxidizes the double bonds, then hydrolizes the epoxide to form two diols, then oxidizes the alcohols to form ketones, and finally breaks the carbon chain to form two carboxylic acids when fully oxidized. This leads to the formation of five possible products for every double bond: the epoxide, the diol, the hydroxyketone, the diacid and a shorter carboxylic acid. The intermediates between the hydroxyketone and the carboxylic acid are not stable under oxidizing conditions so they are generally not isolable.

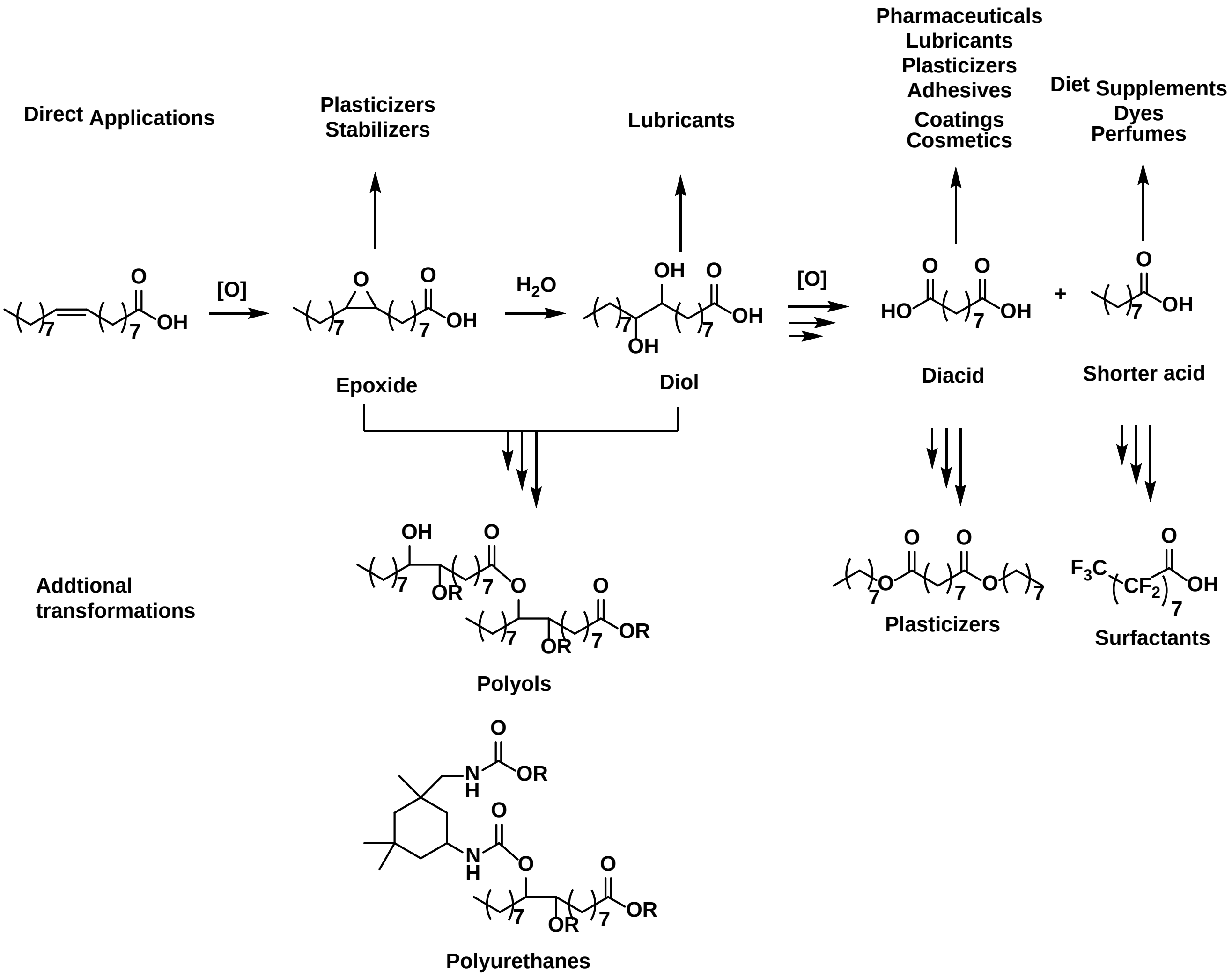

Scheme 2: Oxidation pathway of fatty acids and applications.

The most common oxidizer used to epoxidize vegetable oils is hydrogen peroxide (H_2O_2), due to its relatively low cost compared to organic peroxides, and the fact that the only byproduct from reducing H_2O_2 is water, which is generally easy to separate from most of the desired products since oils are not miscible with water. H_2O_2 is a chemical that is commercially available as a solution in water since pure H_2O_2 is a strong oxidant that can cause fires and explosions when in contact with organic materials, and decomposition of H_2O_2 releases oxygen and heat, which makes pure H_2O_2 hazardous to handle and unsuitable for long-term storage.[22] H_2O_2 is therefore commercially available as an aqueous solution and also contain small amount of stabilizers, with solutions between 30 and 35 wt% being the most commonly used in chemical research.[23-32] However, aqueous solutions of H_2O_2 do not mix with vegetable oils. The reaction rate between the two immiscible phases is consequentially very slow, which makes the aqueous H_2O_2 solution very ineffective towards vegetable oil oxidation by itself. A simple method to solve the issue of two phases is to mix all the reagents with a solvent, such as ethanol, which is capable of mixing with both aqueous and organic compounds. However mixing oil and water into a single phase has some important disadvantages. Mixing oil and water into a single phase with a solvent is inconvenient if the desired product is the epoxide, since doing so will enhance the reaction rate of the epoxide hydrolysis, and cause the formation of the diol. The solvent also increases the production costs, both by the addition of large amounts of solvent to the reaction mixture, and by having to remove the solvent afterwards to purify the product. Indeed, the presence of a co-solvent prevents the possibility to easily separate the aqueous phase from the product.

Instead of using solvents to mix both phases, the reaction can be carried out in biphasic mixture using catalysts or additives that increase the activity of the oxidizing species and transport the oxidizing species between the two immiscible phases. Additives whose purpose is to transport the oxidizer between the two phases are called phase-transfer agents in this context, and will be discussed in more detail in section 1.1.2.

1.1.1. Catalysts for oxidation of vegetable oils with H_2O_2

Catalysts designed to perform the oxidation of vegetable oil are compounds that form organic or metallic peroxides when mixed with aqueous H_2O_2 solutions. The most common epoxidation process is the Prilezhaev reaction, which uses formic acid or acetic acid as catalysts.[7, 33] These organic acids form organic peroxyacids when mixed with aqueous H_2O_2 solutions under acidic conditions and are capable of oxidizing the oils quite effectively.[34-35] Formic acid and acetic acid have been extensively used because they are fairly cheap, but they have some important drawbacks that prevent them from being ideal catalysts. The peroxyacids degrade after a few catalytic cycles. To solve this issue, the reaction requires high loading of the peroxyacids, as well as sulfuric acid as co-catalyst, which in turn makes the reaction mixture very corrosive. The high acidity of the mixture also promotes the hydrolysis of epoxides, which limits the selectivity towards epoxidation. For example, as shown in Scheme 3, the epoxidation of soybean oil reported by Santacesaria *et al*. reaches only 67% selectivity towards the epoxide at 98% conversion.[36] The formation of the peroxyacids is also very exothermic, which is both a safety hazard and a productivity issue, since the reaction needs to be purposely slowed down to prevent a runaway reaction.[36]

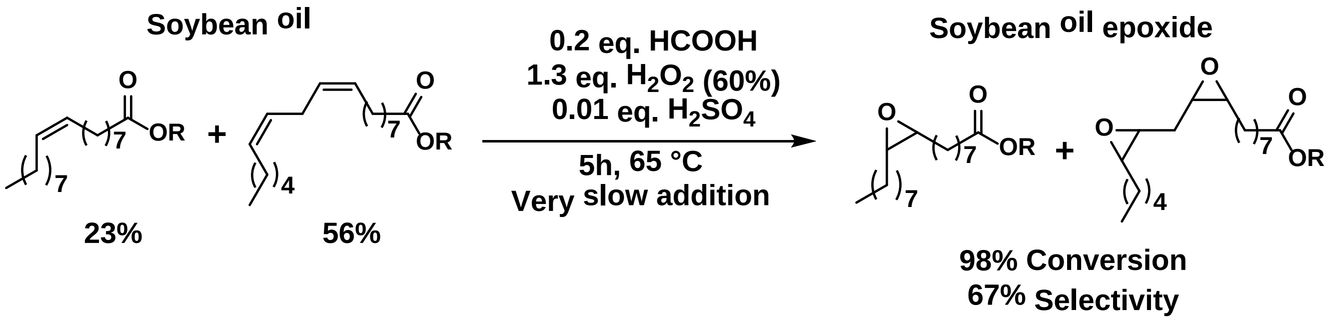

Scheme 3: Example of a Prilezhaev epoxidation of soybean oil.[36]

In order to improve on the drawbacks of organic peroxyacids, there has been a lot of research to develop new catalysts for alkene epoxidation with aqueous H_2O_2. There is now a large variety of promising catalysts, such as manganese carbonates,[37] metal-organic frameworks like MIL-101,[38-39] ruthenium complexes,[40] ionic liquids,[41] molybdenum complexes,[42] among many others.[33, 43-44]

Most of these catalysts achieve higher selectivities than peroxyacids and are less dangerous to handle. However, the main disadvantage of most of these new catalysts is price. In order for any new catalyst to be viable, they need to be able to perform many more cycles than the cheap peroxyacids. Either by increasing its activity so much that the loading required is extremely small, or by being stable enough to be recycled and reused, effectively reducing its price per mole of oxidized oil produced. Another critical parameter is the compatibility with biphasic solutions. Although all of these catalysts can epoxidize non-polar alkenes using aqueous H_2O_2, the reaction rates are heavily influenced by the catalyst's ability to interact with both of the immiscible aqueous and organic phases. Long-chained fatty acids are typically less reactive than small alkenes like cyclohexene, so this effect becomes more prominent when optimizing catalysts towards vegetable oil oxidation.

A type of catalyst that works very well for vegetable oil oxidations are polyoxometalates (POM). POMs are a large class of molecular inorganic compounds consisting of three or more oxyanions linked by shared oxygen atoms to form 3-dimensional frameworks.[45] Several POMs have been found to form peroxides when mixed with aqueous H_2O_2 solutions, and are uniquely effective towards vegetable oil oxidation due to their stability and ionic structure. Although an inorganic oxyanion would not normally mix with organic oils, the anionic POMs can be paired with cationic surfactants to form an amphiphilic catalyst that can interact with both the water and oil phases. Among POMs, research has shown that tungsten-based POMs are more active towards oxidation of double bonds than its molybdenum and silicon counterparts.[23, 27, 46] This has led to research on oxidation being focused towards tungsten POMs, specifically the peroxophosphotungstate known as Venturello's catalyst ($PW_4O_{24}^{3-}$).[47] $PW_4O_{24}^{3-}$is easily obtained by mixing the Keggin-structured phosphotungstic acid ($H_3PW_{12}O_{40}$) with aqueous solutions of H_2O_2 as shown in Scheme 4. This catalyst is the main focus of the research presented in chapter 2.

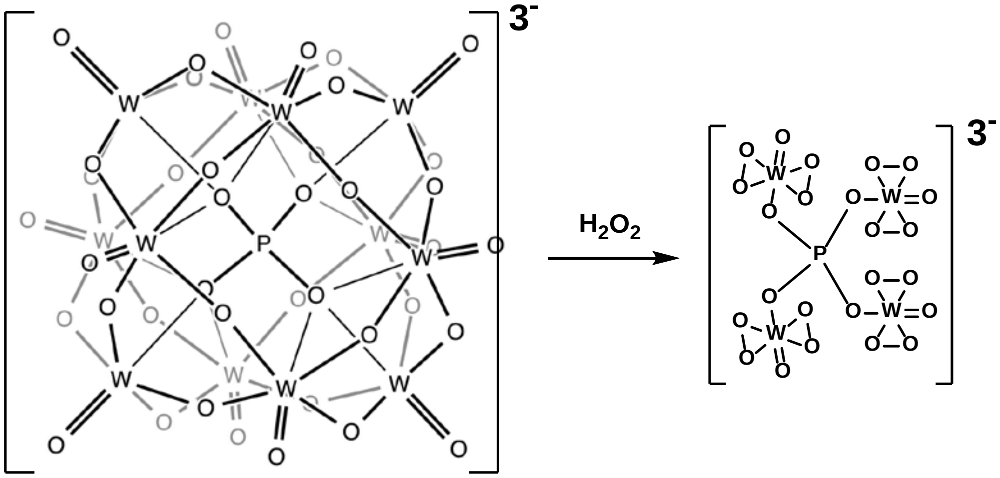

Scheme 4: Structures of phosphotungstic acid ($H_3PW_{12}O_{40}$) and Venturello's catalyst.

The oxidation of $PW_{12}O_{40}$ by aqueous H_2O_2 to form Venturello's catalyst requires multiple oxidation reactions to reach $PW_4O_{24}^{3-}$ as well as removing 8 units of WO_6^{2-}. At a minimum, 24 oxidation steps are required to form Venturello's catalyst and remove all the peroxotungstates, but the reaction is typically carried out with an excess as large as 200 equivalents. However, the exact stoichiometry of this oxidation is not known with precision.[48] Furthermore, spectroscopic studies have shown that PW_3 and PW_2 species are also formed during the reaction,[27, 48] which means that there are a large amount of intermediate species between the precursor and Venturello's catalyst. Each oxidation step involves the oxygen transfer from H_2O_2 to a WO_x unit to form a $WO_{x-2}(O_2)$ unit, subsequently breaking two W-O-W bonds, as shown in Scheme 5.

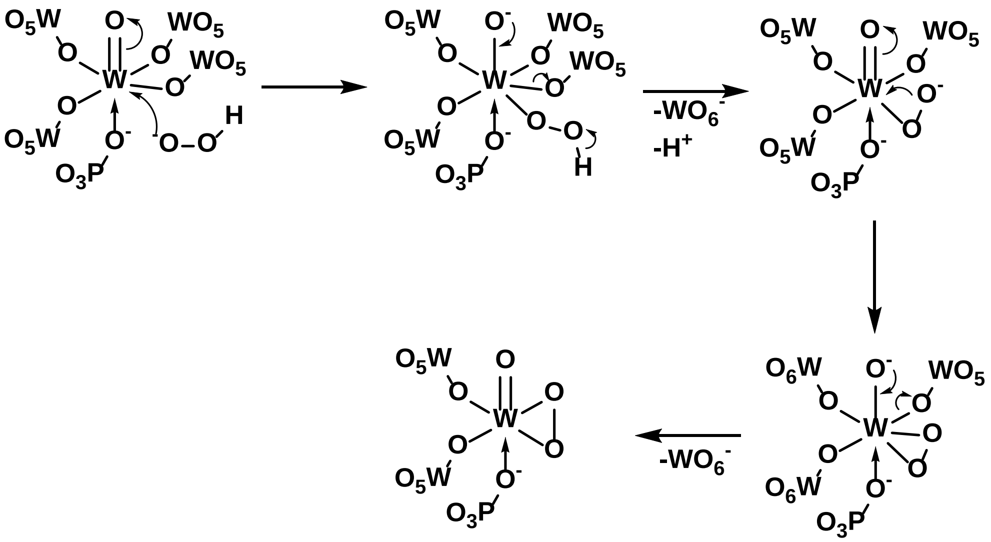

Scheme 5: Peroxidation mechanism of phosphotungstate with H_2O_2.

Characterization of homogeneous Venturello catalysts using ammonium salts as phase transfer agents have shown that $PW_4O_{24}^{3-}$ is preferentially formed with excess H_2O_2 and can be extracted with $CHCl_3$ with high yields.[27] However, heterogeneous Venturello catalysts have not been properly characterized due to their inherent insolubility, so the formation of the fully peroxidized phosphotungstate is usually inferred by following a similar procedure. My own characterization presented in Chapter 2 and Appendix 1 shows that insoluble phosphotungstate species do not produce the fully peroxidized Venturello catalyst under the same reaction conditions as the homogeneous systems, which requires modifying the peroxidation method to achieve fully peroxidized heterogeneous phosphotungstates.

1.1.2. Phase-transfer agents

As mentioned previously, oils are immiscible with aqueous H_2O_2 solutions. This generates a biphasic mixture and hinders direct contact between reagents. Catalysts are required for the oxidation reaction to proceed smoothly, but most catalysts will exhibit a higher affinity for only one of the two phases, thus not contributing to improve the contact between reagents. For this reason, anionic POMs paired with cationic surfactants are very attractive for vegetable oil oxidation. In this context, the cationic surfactants are called phase-transfer agents because their purpose is solely to transport the catalyst between the two phases, instead of affecting the surface tension of the two immiscible liquids.

The features of phase-transfer agents are to have one cationic end that will pair with the anionic POM, and a long hydrocarbon chain that can interact with the organic phase, typically between 12 and 16 carbons in length. The complex formed by the POM and the phase-transfer agent acts as a catalyst that can interact with both organic and aqueous phases independently. Ammonium, pyridinium and imidazolium compounds with long hydrocarbon chain are the most commonly used phase-transfer agents paired with POMs in the literature.[24, 26, 49-50]

The catalytic cycle is split into two phases, with the catalyst precursor reacting with H_2O_2 in the aqueous phase to generate the active catalytic species, and then the catalyst can move into the organic phase to react with the vegetable oil. The catalyst needs to return to the aqueous phase to regenerate. As shown in Scheme 6, the complex formed by the POM and the phase-transfer agent (denoted at Q^+) is capable of interacting with both phases as necessary.

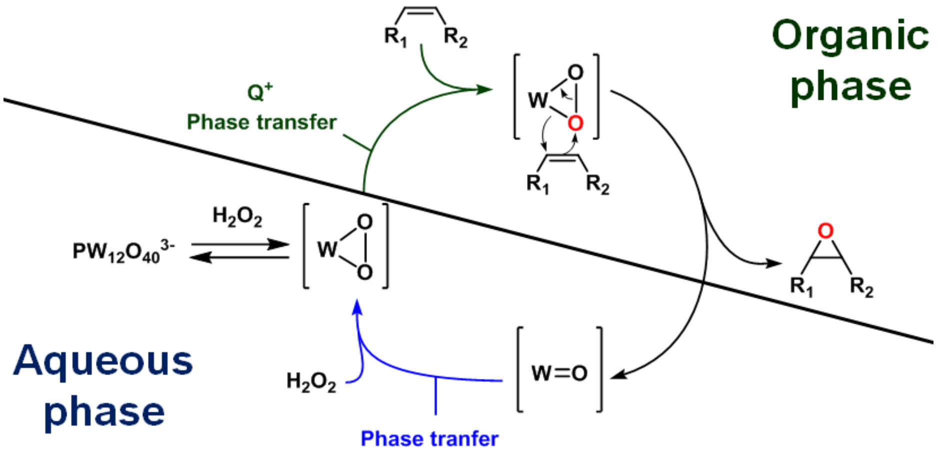

Scheme 6: General catalytic cycle of peroxophosphotungstate catalyst with phase transfer agent to epoxidize a double bond from vegetable oil.

Phase-transfer agents can also be designed to generate solid catalysts that do not dissolve, therefore forming a third phase which can be easily separated from the oil and water, and facilitate the recycling of the catalyst. This is done by attaching the cationic moiety to an insoluble matrix like a polymer[29] or a support like mesoporous silica[51] or functionalized nanoparticles.[30] The amphiphilic properties of the insoluble catalyst will still require careful consideration to be an effective phase-transfer agent, so these structures will still need long hydrocarbon chains attached to the solid matrixes in some form to increase the lipophilicity of the catalyst.

Table 1: Reported activities of selected, best performing tungstate catalysts for the epoxidation of methyl oleate or olefins

Catalyst	**Substrate**	**Eq. H_2O_2**	**Solvent**	**Temp (°C)**	**Time (h)**	**Conv.[a]**	**Sel.**	**TON**	**TOF (h^{-1})**	**TON**	**REF**
$[Me(n\text{-}C_8H_{17})_3N]_3$ $[PO_4[WO(O_2)_2]_4]$	Methyl oleate	2	Neat	60	5	94%	95%	940	188	940 Not recyclable	32
Fe@PILPW-AM	Methyl oleate	0.4	MeCN	70	6	37%	95%	124	21	375[b] 3 cycles	30
DIM-CIM-PW	Cyclooctene	1.2	EtOAc	60	6	100%	100%	167	28	830 5 cycles	29
$(Bu_4N)_4$ $(SiW_{10}O_{34}(H_2O)_2)$	Cyclooctene	0.2	MeCN	32	2	20%	99%	124	62	620 5 cycles	24
W-Zn/SnO_2	Cyclooctene	2[c]	DMC	60	4	99%	99%	30	8	149 5 cycles	25
Poly(dipyridinium) $PW_{12}O_{40}$	4-decen-1-ol	2.5	Neat	50	24	92%	100%	460	19	2885 6 cycles	31

However, designing effective heterogeneous phase transfer agents is an area of research that is still in progress. Recyclable heterogeneous phosphotungstate catalysts reported using these immobilization techniques exhibit reaction rates approximately one order of magnitude lower than their homogeneous counterparts. A brief comparison between literature reports and is shown Table 1. Designing a heterogeneous peroxophosphotungstate catalyst that can bridge this gap in activity is the main objective of the research shown in chapter 2. This active heterogeneous phosphotungstate achieves high selectivities and is easily separable, which makes it superior to the classic Prilezhaev reaction.

1.2. Plasmonic Catalysis

1.2.1. Metal nanoparticles

Nanoparticles are generally defined as particles which have a diameter between 1 and 100 nanometers. Nanoparticles feature high specific surface area, due to the increased proportion of atoms present at the surface the smaller the particle becomes, which can lead to improved reactivity compared to larger particles. But beyond this obvious fact, nanoparticles possess properties which are inherently different from the ones of bulk materials with identical composition, and are not thoroughly accounted by the simple size considerations.[52]

One of the most noticeable properties of nanoparticles is the change in the surface chemistry. In particular, small nanoparticles below 30 nm in size are characterized by having an excess of energy at the surface, which makes them thermodynamically unstable. This instability can lead to crystallographic changes such as lattice contraction or deformation, the formation of defects, rearrangements of surface atoms or more drastic changes in morphology, which affect the interfacial reactivity and some of the intrinsic properties of the nanoparticles.[52] These nanoscale features can affect electronic properties like bandgap energy,[53] thermal properties like melting point,[54] magnetic properties like the Néel temperature,[55] quantum-size effects,[56] and optical properties like LSPR,[57] among others. The LSPR is the main interest for the research in this thesis are the will be presented in more detail in section 1.2.2.

Metal nanoparticles can be synthesized by two general methods: top-down and bottom-up. The top-down approach refers to breaking down bulk material into smaller particles through mechanical means. The bottom-up approach starts from dissolved metal salts and generates the NPs by controlled reduction of the ionic metal species in the presence of capping agents.[58] The bottom-up approach is usually favored because it allows for a better control of nanoparticle size.[59] By purposely performing the reduction at low concentration of metal ions, the formation of solid species will favor nucleation of new particles over growth of existing particles. Aggregation of the nanoparticles is prevented by the addition of capping agents, small molecules which bind strongly to the surface of the metal nanoparticles, therefore preventing fully formed NPs from fusing together into larger particles.[60] Capping agents are usually carboxylic acids, amines or thiols, since these nucleophilic moieties coordinate strongly with the electrophilic metal surface of the nanoparticles, and form stable bonds that do not provoke secondary reactions.[61] Some polymers like PEG and PVP are also quite commonly used as capping agents.[62] Covering the surface of NPs with organic molecules help stabilize the NPs via electrostatic repulsion, steric stabilization, or a combination of these two.[63] Capping agents also strongly affect the dispersion properties of the resulting nanoparticles. For example, a lipophilic capping agent like oleylamine will cover the surface with long hydrocarbon chains that will make the nanoparticle suspend in nonpolar solvents, while a hydrophilic capping agent like citric acid will cover the surface with carboxylic acids that will make the nanoparticles suspend in polar solvents. As depicted in Figure 3, this is the result of how the capping agents orient themselves when binding with the NP surface, leaving the opposite end to interact with the surrounding solvent in suspension.

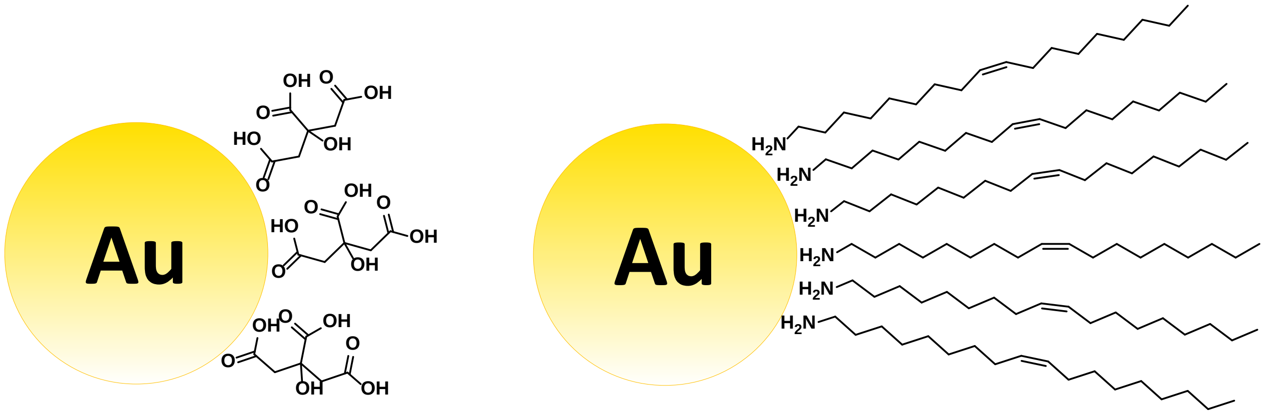

Citric acid capping

Oleylamine capping

Figure 3: Representation of how capping agents orient when bound to NPs (partial coverage depicted for clarity).

Nanoparticles are not exclusively made out of a single metal. Bimetallic nanoparticles can be produced by alloying, or by growing a second metal onto premade nanoparticles.[64] Depending on the growth mechanism and molar proportion, these second metal may be present in the form of decoration or a full coverage, also called a core/shell NP, as shown in Figure 4.

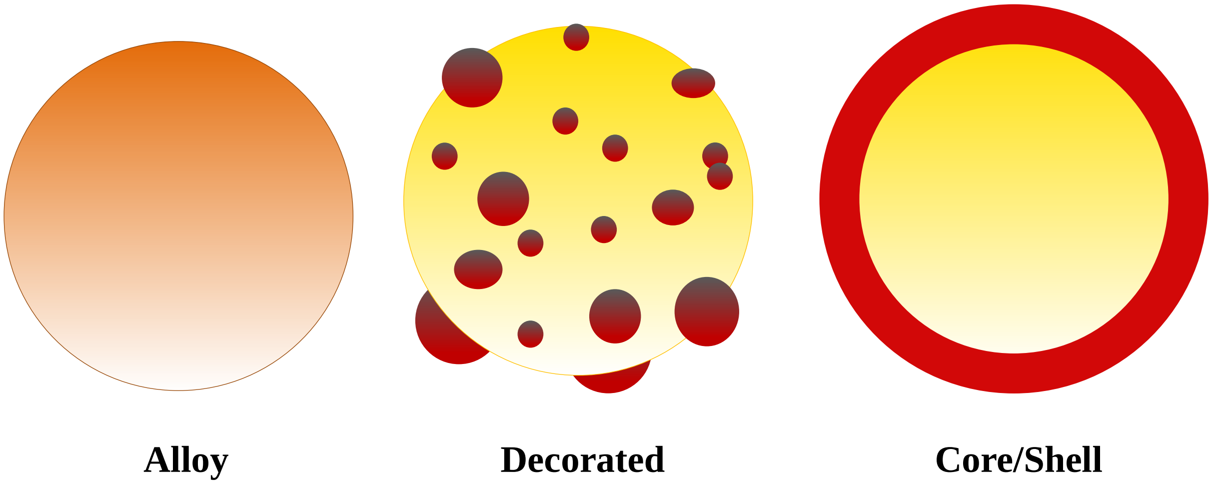

Figure 4: Depiction of the different types of bimetallic nanoparticles.

Bimetallic alloy NPs can be synthesized by co-reduction of the two metals in solution, which has shown to work well for AuAg and AuCu alloy NPs.[65-66] A similar method called the co-impregnation reduction technique has been reported to produce alloy AuPd NPs, in which the metal precursors are reduced in situ in the presence of a metal oxide support.[67] Other methods like deposition precipitation, digestive ripening, and photodeposition have also been reported.[64]

Decorated bimetallic NPs are generated by partial coverage of the NPs with a second metal, and can be readily obtained by reduction of metal salts using premade NPs as a support.[68] This means that the synthesis needs to be done in two separate steps. First the synthesis of pure metal NPs and then the deposition of the second metal. Core/shell NPs follow the same principle. The two steps can be done independently or by successive reactions *in situ*. The main difference between decorated and core/shell NPs is that the methodologies to produce core/shell NPs need to maintain a uniform coating and control the shell’s thickness. This control can be obtained by methods such as sol-gel condensation, the layer-by-layer adsorption, redox-transmetalation, and using microemulsions, among others.[69]

Core/shell NPs can also be the result of oxidation of the surface of metal nanoparticles instead of introducing a second material to form the shell. Depending on the characteristics of the metal oxides and the oxidation method, the oxide shell may act as a passivizing layer that protects the core of the nanoparticle.[70-72]

1.2.2. Localized Surface Plasmon Resonance

The main feature of nanoparticles discussed in this thesis is the localized surface plasmon resonance (LSPR). Unlike crystallographic-dependent features, surface plasmon resonance is an optical phenomenon caused by a resonant oscillation of conduction electrons with incoming light.[73] LSPR is the result of confinement of the surface plasmon due to the nanoparticle having a smaller size than the incident wavelength, which means that the plasmon cannot propagate across the surface since the entire volume of the nanoparticle is activated at once. The resonant frequency depends on the composition, size, geometry, dielectric environment and separation distance of the nanoparticles.[74] Since the size of the nanoparticles necessary to exhibit LSPR is relative to the wavelength of incident light, the size required is not dependent on the general definition of nanoparticles, and structures larger than 100 nm that exhibit LSPR have been reported.[75]

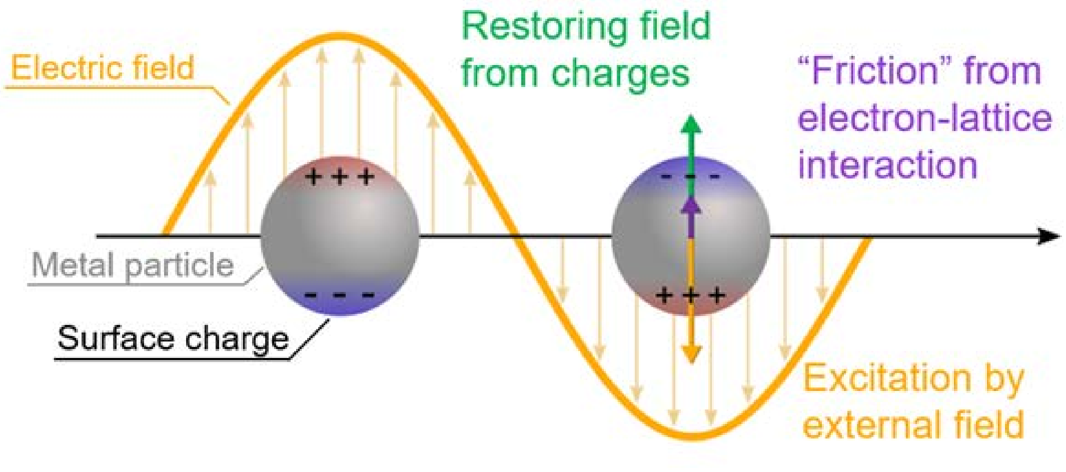

Figure 5: Depiction of electron dynamics of plasmonic NPs during irradiation. Reproduced with permission from the American Chemical Society.[64]

Figure 5 shows a representation of a plasmonic NP irradiated with light. The conductive electrons in metal NPs are mobile, so they can travel across the NP guided by the incident electric field, which results in an excited state that polarizes the nanoparticle. These localized charges create a depolarization field that creates a restoring force on the electron cloud. If the external field oscillates at the same frequency of the resonant mode of the NP, both external and restoring fields will synchronize, greatly enhancing the total field in and around the particle, which is what is called the LSPR.[64]

All conductive metals can exhibit surface plasmon resonance. However, in practice, research of LSPR is dominated by a few metals: Au, Ag, Cu, Mg and Al.[76-80] This is mostly because NPs of these metals exhibit LSPR absorbance within the visible range of light.[64] Most other metals show resonance in the infrared region or have a weaker LSPR response so they have not sparked as much interest from researchers.[73]

LSPR is a useful tool for catalysis. When a nanoparticle exhibits LSPR, the cloud of conductive electrons of the nanoparticle oscillates in resonance with the electromagnetic field, which causes a near-field electromagnetic enhancement at the vicinity of the nanoparticles. As a result, there are three main effects that occur which are relevant to catalysis:

1. Localized heating: The excitation of nanoparticles by LSPR can produce a local photothermal effect.[81-82] Although the total amount of energy from the absorption of light does not heat a suspension of nanoparticles significantly at a macromolecular level, the heat from the LSPR excitation is generated exclusively at the surface of the nanoparticles so a large temperature differential can be generated and molecules in the vicinity of the surface will experience an increased temperature. This photothermal effect has been shown to be a major contributor to enhancing some catalytic reactions. For example, Zhang *et al*. reported using a UV-absorbent plasmonic Rh/TiO_2 catalyst for CO_2 methanation and measured the contributions of thermal and nonthermal effects, showing that the light illumination could increase the local temperature on the catalyst by up to 100°C.[83] Stamplecoskie *et al*. reported using the localized heating generated by the LSPR of Ag NPs to selectively polymerize nylon-6 at the surface of the

NPs.[84] Localized heating has also proven to be broadly useful in non-catalytic applications such as cancer therapy, drug delivery, nanofluidics, gasification and phononics.[64, 81, 85-86]

2. Field Enhancement: The excitation of nanoparticles by LSPR causes a strong enhancement to the surrounding electromagnetic field. In particular, the intensity of the incident field is increased within the range of the LSPR, which reaches up to a few nanometers from the surface of the nanoparticle. In this way, the plasmonic nanoparticle can work as an antenna which harnesses light and amplifies its effects, coupling with nearby molecules.[87] This is useful to improve the reactivity of independent catalytic molecules if they are placed at the appropriate distance from the plasmonic nanoparticles.[88] In terms of catalysis, the field enhancement effect of LSPR has been mostly used to increase reaction rates of photocatalysts, since the direct effect of increasing the amplitude of the electromagnetic field results in a stronger absorption by an independent photocatalyst placed within the range of the LSPR.[89-90] but other applications such a polymer crosslinking,[91] hydrogenations[92] and oxidations[93] have also been reported, among others.[64] This shows that the field enhancement has wider repercussions than simply concentrating light. The increased electromagnetic field from LSPR also has applications related to detection by increasing the magnitude of measuring signals, such as surface-enhanced Raman spectroscopy and fluorescence.[94-96]

3. Charge transfer: The absorption of light of excited nanoparticles can lead to the formation of hot carriers. The LSPR broadens the energy distribution of carriers populating the conduction band which leads to electrons with higher energy than what would correspond to the temperature of the nanoparticle, therefore called hot electrons.[97-98] These hot electrons can be transferred to other molecules and occupy excited electronic states. Hot electron transfer is particularly useful for redox and coupling reactions.[99-104]

These characteristics make LSPR a very versatile tool that can be used to enhance catalytic activity. So by designing catalysts that are compatible with LSPR we expect to be able to improve existing catalysts and carry out reactions under milder conditions. The research presented in chapters 3 and 4 are devoted to the application of LSPR towards Ru-based hydrogenations by decorating LSPR-active NPs with Ru. Literature reports have shown that

LSPR can enhance Pt and Pd-based hydrogenations of olefins,[92, 105-107] so our research is intended to expand the scope of LSPR applications to Ru-based hydrogenations.

1.3. Metal-catalyzed Hydrogenation

1.3.1. Scope and mechanism

Hydrogenation is a reaction where an H_2 molecule is introduced to reduce or saturate another compound. Several functional groups are prone to be hydrogenated such as alkynes, alkenes, aromatics, aldehydes, ketones, esters, carboxylic acids, amides, nitriles, nitros and sulfones, among others. Scheme 7 shows some examples with the resulting products from hydrogenating these substrates.

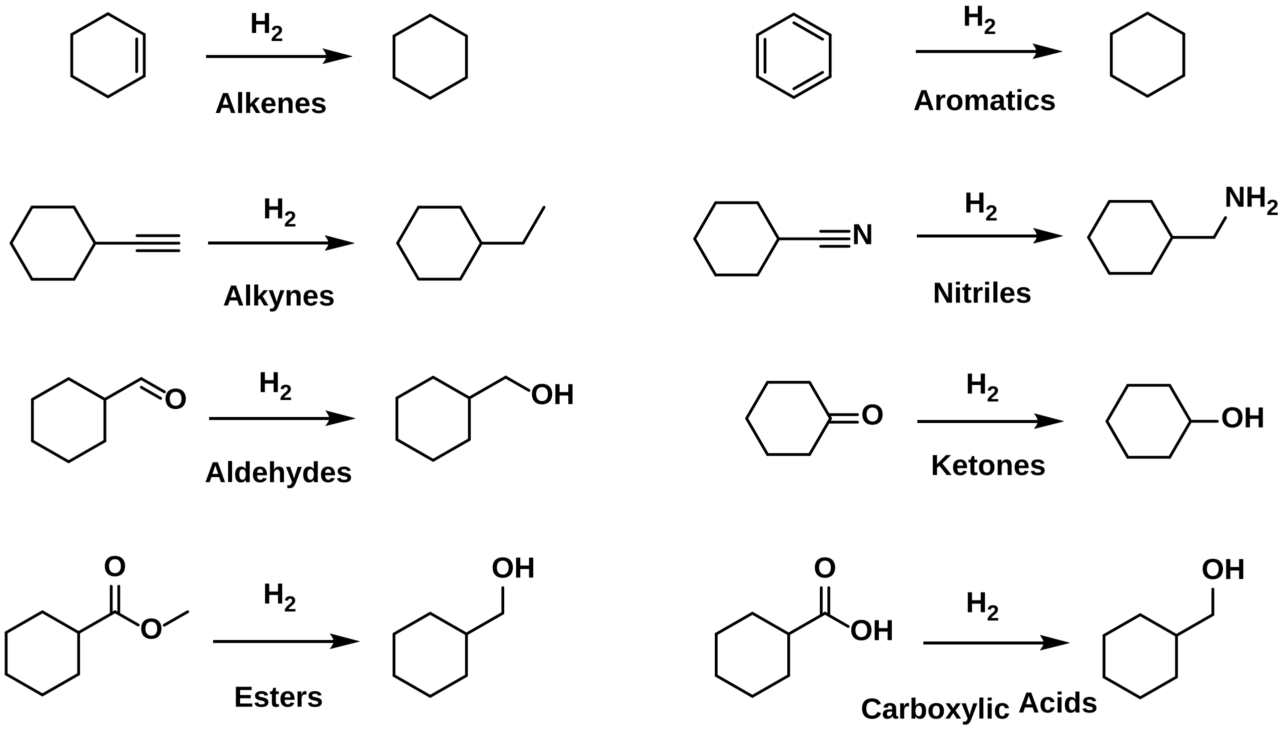

Scheme 7: Examples of some hydrogenation reactions.

Hydrogenation reactions can be performed using H_2 gas, hydrides such as $LiAlH_4$, or molecules that serve as hydrogen donors like hydrazine, isopropanol or formic acid. When using a hydrogen donor the reaction is called a transfer hydrogenation.

Using H_2 gas directly is advantageous since it is cheap and does not generate byproducts, so it is considered the cleanest reducing agent.[108] However, H_2 gas is typically unreactive toward most organic compounds, so in order for the reactions to proceed a metal catalyst is commonly used. The metal catalysts are able to react with gaseous H_2 to form metal hydrides in situ. The catalyst can simultaneously chemisorb the organic substrates and form hydrides, which places the reagents in close proximity, allowing for the transfer of the hydrogen atoms from the metal hydrides to the substrates.[109]

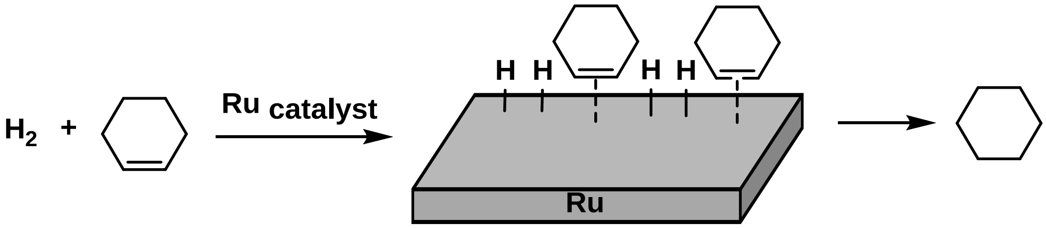

Scheme 8: Reaction pathway of heterogeneous metal-catalyzed hydrogenations.

One of the most important industrial applications of metal-catalyzed hydrogenations is the hydrogenation of aromatic compounds. This is because aromatic compounds have been traditionally used extensively in fuels, but recent studies have shown that high aromatic content, and especially polycyclic aromatics, generates toxic emissions.[110] Therefore, many countries now regulate the amount of aromatic content allowed, and hydrogenation is a useful method to harness the hydrocarbon streams while lowering the aromatic content.[111-112]

Hydrogenating aromatics is similar to hydrogenating alkenes, and follows the same general pathway as shown in Scheme 8. However, there are a few key differences. First, when hydrogenating an aromatic compound, selectivity can be an issue. The reaction of hydrogenating benzene, for example, proceeds as a sequence of hydrogenations which first forms 1,3-cyclohexadiene or 1,4-cyclohexadiene, but this can continue to react to form and cyclohexene which can then continue to react to form cyclohexane, as shown in Scheme 9. Kinetic tests have shown that cyclohexadienes react much faster than benzene, so they can never be isolated, but partial hydrogenation towards cyclohexene is possible in some circumstances.[113] Second, the reaction kinetics of aromatic hydrogenations is controlled by adsorption and desorption rates of the chemisorbed species. Unlike alkenes, aromatic compounds bind very strongly to transition metal catalysts, so much so that the entire surface of the catalyst gets saturated. This creates a situation where the catalyst is maximally used so the concentration of the aromatic compound in the mixture becomes irrelevant. Therefore the reaction shows a zero order rate in aromatic reagents.[114] However, if the reaction is carried out at high temperatures, the reagents will start to desorb and it will no longer behave as a zero order reaction.[113] The desorption rate can also influence selectivity, since partially hydrogenated species desorb much faster than aromatics.[113] Therefore, if the reaction is carried at room temperature, the first hydrogenation will be the rate-determining step and a fully hydrogenated alkene will be the expected product. In contrast, at high temperatures the weaker chemisorption can cause the third hydrogenation to become the rate-determining step, which will generate a mixture of partial and fully hydrogenated products.

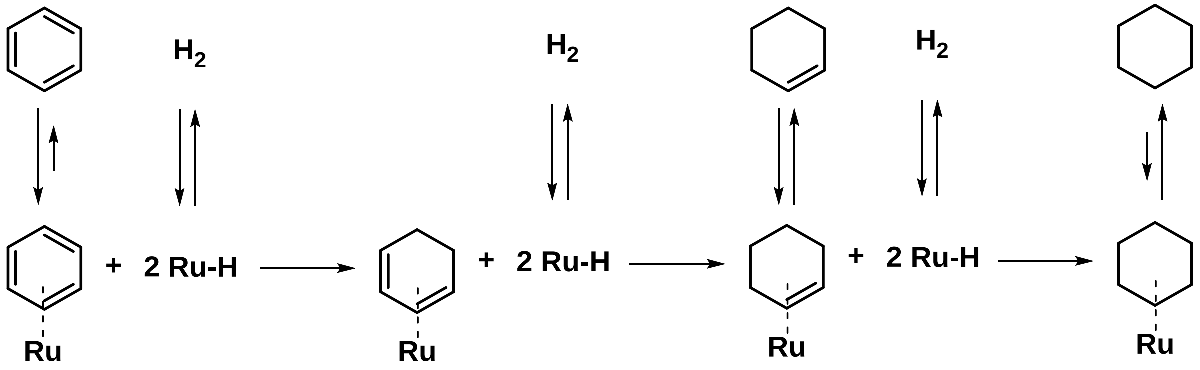

Scheme 9: Reaction pathway for metal-catalyzed arene hydrogenation.

The reaction is also sensitive to the H_2 pressure. Unlike the concentration of aromatic reagents, H_2 pressure does affect the reaction rate, and it is nearly first order at room temperature. But as temperature increases the apparent reaction order also increases. Therefore the reaction is much more favorable when performed at high temperatures and pressures.[115]

Hydrogenation reactions can also be performed with organometallic catalysts. Organometallic catalysts are generally considered to be homogeneous, since the entire complex is dissolved in an appropriate solvent during reaction. It is also possible to graft organometallic complexes onto supports to make them heterogeneous.[116] Alternatively, it is also possible to create metal-organic frameworks (MOFs), where a metal is coordinated to an organic structure that is inherently insoluble, and tailor particular MOFs for aromatic hydrogenation reactions,[117] which would constitute a heterogeneous organometallic catalysts with coordinated reactive sites instead of the metallic surface of traditional heterogeneous catalysts.

In general, heterogeneous catalysts are more robust than homogeneous catalysts, which makes them more practical to use,[118] and the best heterogeneous metallic catalysts reported to date feature higher reaction rates than homogeneous ones.[119] In the specific context of arene hydrogenation, researchers have extensively explored homogeneous catalysts, based in particular on Ir, Rh, and Ru. A significant advantage of organometallic catalysts in aromatic hydrogenation are their ability to perform enantioselective hydrogenations, while their mononuclear active site is more amenable to mechanistic investigations.[118, 120] However, there has been a lot of debate over the nature of the active species, with a number of examples of homogenous catalysts decomposing into nanoparticles *in situ*, causing the observed catalytic activity.[119] Enantioselective homogeneous catalysts can be easily prepared by combining a metal precursor with a chiral ligand. In contrast, enantioselectivity is extremely difficult to control using heterogeneous metallic catalysts due to the complexity of the nanoscale structure and the interplay of surface adsorption and desorption processes. There are very few reports of enantioselective heterogeneous catalysts, which achieve only moderate enantiomeric excess or are limited in scope, being effective exclusively towards activated ketones.[120-122]

1.3.2. Ruthenium-catalyzed hydrogenation

Metals from the platinum group, namely Ru, Rh, Pd, Os, Ir, and Pt are particularly effective at catalyzing hydrogenations using H_2.[115, 123-126] Out of these, the research presented in Chapters 3 and 4 is focused exclusively on Ru. Given that Ru is the cheapest of these metals and also shows excellent activity as a hydrogenation catalyst, it was chosen as being the best candidate to design a greener catalyst.[119, 127-128]

Since the goal of my research is to make greener catalysts, heterogeneous recyclable catalysts are more attractive than homogeneous Ru complexes. In that vein, there have been several reports of either supported metallic Ru or Ru NPs being used as hydrogenation catalysts with H_2.

Simple catalysts such as Ru supported onto silica have been used for decades.[113] The support itself can have a significant effect on the activity of the catalyst. A study by Viniegra *et al*. on the influence of the support have shown that MgO is a better support than SiO_2, Al_2O_3 or C, due to a decrease in the formation of coke, thus leading to a higher stability.[129] A recent report by Zhou et al. also showed that the activity of the Ru catalyst can be improved by engineering the exposed facets of a TiO_2 support. Their results show that nanosheets were more active than nanorods and nanoflower structures, since they contained more open-coordinated sites.[124] Our own research group has also reported supported Ru onto cellulose nanocrystals. This catalyst is particularly easy to synthesize due to a synergistic effect between H_2 and CNCs to reduce Ru(III) and achieved good activity under mild conditions.[124]

Unsupported Ru NPs can also be used as a heterogeneous hydrogenation catalyst. Ru NPs have been shown to be effective at hydrogenating aromatics in both solventless and biphasic conditions.[130] The activity of Ru NPs is also influenced by the ligands used to stabilize the NPs. Rakers *et al*. reported the use of ligands derived from cholesterol. According to their results, the increase in bulkiness of the ligands increased the activity of Ru NPs by reducing the ligand coverage or the Ru NPs which allows for more active sites to be used for hydrogenation.[131]

Combining nanostructured Ru with a support that can boost its activity is the ideal scenario which we intend to create using LSPR. There are already some reports that achieve a good synergy between nanostructured Ru and active supports. Most notably, Ozkar *et al*. reported a very active heterogeneous catalyst formed by stabilizing Ru nanoclusters with a nanozeolite framework, which is able to hydrogenate aromatic substrates at room temperature and only 3 atm of H_2.[119]

1.4. Research Objectives

The objectives throughout this thesis are to develop better catalysts. We define a catalyst to be superior if it provides an improvement based on the principles of green chemistry. In particular, we look to make heterogeneous recyclable catalysts, we seek to perform reactions under mild conditions to make them safer to use, and we intend to reduce the amount of noble metals used through a combination of higher reaction rates and reduced catalyst loadings.

The topic of chapter 2 is oxidation of vegetable oils, with the purpose of biomass valorization. The objective here is to make heterogeneous catalysts more viable, since literature reports show reaction rates roughly an order of magnitude lower for heterogeneous peroxophosphotungstate catalysts, compared to homogeneous peroxophosphotungstate catalysts. A viable recyclable phosphotungstate catalyst could replace the more common method using the Prilezhaev reaction which would make the oxidation of vegetable oils safer, cheaper, and reduce waste.

The topic of chapters 3 and 4 is the hydrogenation of alkenes and arenes, which is an important reaction the chemical industry. The objective of this research is to improve the catalytic activity of Ru using LSPR so that the hydrogenation can be performed under mild conditions and reduce the amount of noble metals required. Chapter 3 focuses on using Au NPs as source of LSPR and provides proof of concept for further research. Chapter 4 focuses on replacing Au NPs with Al NPs which are potentially more sustainable, because Al is much more abundant than Au.

1.5. References

(1) Tuck, C. O.; Perez, E.; Horvath, I. T.; Sheldon, R. A.; Poliakoff, M., Valorization of Biomass: Deriving More Value from Waste. *Science* **2012,** *337*, 695-699.

(2) Simmons, B. A.; Loque, D.; Blanch, H. W., Next-generation biomass feedstocks for biofuel production. *Genome Biol.* **2008,** *9*.

(3) Williams, P. J. L.; Laurens, L. M. L., Microalgae as biodiesel & biomass feedstocks: Review & analysis of the biochemistry, energetics & economics. *Energy Environ. Sci.* **2010,** *3*, 554-590.

(4) Rulkens, W., Sewage sludge as a biomass resource for the production of energy: Overview and assessment of the various options. *Energy Fuels* **2008,** *22,* 9-15.

(5) Mirabella, N.; Castellani, V.; Sala, S., Current options for the valorization of food manufacturing waste: a review. *J. Clean. Prod.* **2014,** *65*, 28-41.

(6) Meier, M. A. R.; Metzger, J. O.; Schubert, U. S., Plant oil renewable resources as green alternatives in polymer science. *Chem. Soc. Rev.* **2007,** *36*, 1788-1802.

(7) Corma, A.; Iborra, S.; Velty, A., Chemical routes for the transformation of biomass into chemicals. *Chem. Rev.* **2007,** *107*, 2411-2502.

(8) Alam, M.; Akra, D.; Sharmin, E.; Zafar, F.; Ahmad, S., Vegetable oil based eco-friendly coating materials: A review article. *Arab. J. Chem.* **2014,** *7*, 469-479.

(9) Rahmat, N.; Abdullah, A. Z.; Mohamed, A. R., Recent progress on innovative and potential technologies for glycerol transformation into fuel additives: A critical review. *Renew. Sust. Energy Rev.* **2010,** *14*, 987-1000.

(10) Clark, J.; Deswarte, F., Introduction to Chemicals from Biomass. *Wiley*, 2014.

(11) Frazer, A. C.; Sammons, H. G., The formation of mono- and di-glycerides during the hydrolysis of triglyceride by pancreatic lipase. *Biochem. J.* **1945,** *39*, 122-128.

(12) Orsavova, J.; Misurcova, L.; Ambrozova, J. V.; Vicha, R.; Mlcek, J., Fatty Acids Composition of Vegetable Oils and Its Contribution to Dietary Energy Intake and Dependence of Cardiovascular Mortality on Dietary Intake of Fatty Acids. *Int. J. Mol. Sci.* **2015,** *16*, 12871-12890.

(13) Andrikopoulos, N. K., Triglyceride species compositions of common edible vegetable oils and methods used for their identification and quantification. *Food Rev. Int.* **2002,** *18*, 71-102.

(14) Albright, L. F.; Wisniak, J., Selectivity and Isomerization During Partial Hydrogenation of Cottonseed Oil and Methyl Oleate: Effect of Operating Variables. *J. Am. Oil Chem. Soc.* **1962,** *39*.

(15) Company, T. C. ChemFlexx Epoxidized Soybean Oil (ESO). https://thechemco.com/chemical/epoxidized-soybean-oil/ (accessed August 2020).

(16) Omonov, T. S.; Curtis, J. M., 7 - Plant Oil-Based Epoxy Intermediates for Polymers. In Bio-Based Plant Oil Polymers and Composites, *Elsevier*, 2016; pp 99-125.

(17) Sieber, M. A.; Hegel, J. K., Azelaic acid: Properties and mode of action. *Skin Pharmacol. Physiol.* **2014,** *27 Suppl 1*, 9-17.

(18) Schuster, M.; Blechert, S., Olefin Metathesis in Organic Chemistry. *Angew. Chem. Int. Ed.* **1997,** *36*, 2037-2056.

(19) Ivin, K. J., Some recent applications of olefin metathesis in organicsynthesis: A review. *J. Mol. Catal. A: Chem.* **1998,** *133*, 1-16.

(20) Patel, J.; Mujcinovic, S.; Jackson, W. R.; Robinson, A. J.; Serelis, A. K.; Such, C., High conversion and productive catalyst turnovers in cross-metathesis reactions of natural oils with 2-butene. *Green Chem.* **2006,** *8*, 450-454.

(21) De, C.; Saha, R.; Ghosh, S. K.; Ghosh, A.; Mukherjee, K.; Bhattacharyya, S. S.; Saha, B., A review of biphasic hydroformylation for long chain substrates. *Res. Chem. Intermed.* **2013,** *39*, 3463–3474.

(22) Hydrogen Peroxide (H_2O_2) Safety and Handling Guidelines. https://www.h2o2.com/technical-library/default.aspx?pid=66&name=Safety-amp-Handling (accessed August 2020).

(23) Mizuno, N.; Yamaguchi, K.; Kamata, K., Epoxidation of olefins with hydrogen peroxide catalyzed by polyoxometalates. *Coord. Chem. Rev.* **2005,** *249*, 1944-1956.

(24) Kamata, K.; Yonehara, K.; Sumida, Y.; Yamaguchi, K.; Hikichi, S.; Mizuno, N., Efficient epoxidation of olefins with >= 99% selectivity and use of hydrogen peroxide. *Science* **2003,** *300*, 964-966.

(25) Kamata, K.; Yonehara, K.; Sumida, Y.; Hirata, K.; Nojima, S.; Mizuno, N., Efficient heterogeneous epoxidation of alkenes by a supported tungsten oxide catalyst. *Angew. Chem. Int. Ed.* **2011,** *50*, 12062-12066.

(26) Ishii, Y.; Yamawaki, K.; Ura, T.; Yamada, H.; Yoshida, T.; Ogawa, M., Hydrogen-Peroxide Oxidation Catalyzed by Heteropoly Acids Combined with Cetylpyridinium Chloride - Epoxidation of Olefins and Allylic Alcohols, Ketonization of Alcohols and Diols, and Oxidative Cleavage of 1,2-Diols and Olefins. *J. Org. Chem.* **1988,** *53*, 3587-3593.

(27) Duncan, D. C.; Chambers, R. C.; Hecht, E.; Hill, C. L., Mechanism and Dynamics in the $H_3[PW_{12}O_{40}]$-Catalyzed Selective Epoxidation of Terminal Olefins by H_2O_2 - Formation, Reactivity, and Stability of $(PO_4[WO(O_2)_2]_4)^{3-}$. *J. Am. Chem. Soc.* **1995,** *117*, 681-691.

(28) Sato, K.; Aoki, M.; Noyori, R., A "green" route to adipic acid: Direct oxidation of cyclohexenes with 30 percent hydrogen peroxide. *Science* **1998,** *281*, 1646-1647.

(29) Leng, Y.; Wu, J.; Jiang, P.; Wang, J., Amphiphilic phosphotungstate-paired ionic copolymer as a highly efficient catalyst for triphase epoxidation of alkenes with H_2O_2. *Catal. Sci. Technol.* **2014,** *4*, 1293.

(30) Leng, Y.; Zhao, J.; Jiang, P.; Wang, J., Amphiphilic polyoxometalate-paired polymer coated Fe_3O_4: magnetically recyclable catalyst for epoxidation of bio-derived olefins with H_2O_2. *ACS Appl. Mater. Interfaces* **2014,** *6*, 5947-5954.

(31) Yamada, Y. M. A.; Guo, H. Q.; Uozumi, Y., Tightly convoluted polymeric phosphotungstate catalyst: An oxidative cyclization of alkenols and alkenoic acids. *Org. Lett.* **2007,** *9*, 1501-1504.

(32) Khlebnikova, T. B.; Pai, Z. P.; Fedoseeva, L. A.; Mattsat, Y. V., Catalytic oxidation of fatty acids. II. Epoxidation and oxidative cleavage of unsaturated fatty acid esters containing additional functional groups. *React. Kinet. Catal. Lett.* **2009,** *98*, 9-17.

(33) Abdullah, B. M.; Salimon, J., Epoxidation of vegetable oils and fatty acids: catalysts, methods and advantages. *J. Appl. Sci.* **2010,** *10*, 1545-1553.

(34) Dinda, S.; Patwardhan, A. V.; Goud, V. V.; Pradhan, N. C., Epoxidation of cottonseed oil by aqueous hydrogen peroxide catalysed by liquid inorganic acids. *Bioresour. Technol.* **2008,** *99*, 3737-3744.

(35) Goud, V. V.; Patwardhan, A. V.; Pradhan, N. C., Studies on the epoxidation of mahua oil (Madhumica indica) by hydrogen peroxide. *Bioresour. Technol.* **2006,** *97*, 1365-1371.

(36) Santacesaria, E.; Tesser, R.; Di Serio, M.; Turco, R.; Russo, V.; Verde, D., A biphasic model describing soybean oil epoxidation with H_2O_2 in a fed-batch reactor. *Chem. Eng. J.* **2011,** *173*, 198-209.

(37) Lane, B. S.; Vogt, M.; DeRose, V. J.; Burgess, K., Manganese-catalyzed epoxidations of alkenes in bicarbonate solutions. *J. Am. Chem. Soc.* **2002,** *124*, 11946-11954.

(38) Saedi, Z.; Tangestaninejad, S.; Moghadam, M.; Mirkhani, V.; Mohammadpoor-Baltork, I., MIL-101 metal-organic framework: A highly efficient heterogeneous catalyst for oxidative cleavage of alkenes with H_2O_2. *Catal. Commun.* **2012,** *17*, 18-22.

(39) Saedi, Z.; Tangestaninejad, S.; Moghadam, M.; Mirkhani, V.; Mohammadpoor-Baltork, I., The effect of encapsulated Zn-POM on the catalytic activity of MIL-101 in the oxidation of alkenes with hydrogen peroxide. *J. Coord. Chem.* **2012,** *65*, 463-473.

(40) Che, C. M.; Yip, W. P.; Yu, W. Y., Ruthenium-catalyzed oxidation of alkenes, alkynes, and alcohols to organic acids with aqueous hydrogen peroxide. *Chem. Asian J.* **2006,** *1*, 453-458.

(41) Vafaeezadeh, M.; Hashemi, M. M., Dual catalytic function of the task-specific ionic liquid: Green oxidation of cyclohexene to adipic acid using 30% H_2O_2. *Chem. Eng. J.* **2013,** *221*, 254-257.

(42) Rayati, S.; Abdolalian, P., Heterogenization of a molybdenum Schiff base complex as a magnetic nanocatalyst: An eco-friendly, efficient, selective and recyclable nanocatalyst for the oxidation of alkenes. *C. R. Chim.* **2013,** *16*, 814-820.

(43) Patil, H.; Waghmare, J., Catalyst for epoxidation of oils: a review. *Discovery* **2013,** *3*, 10-14.

(44) Lane, B. S.; Burgess, K., Metal-catalyzed epoxidations of alkenes with hydrogen peroxide. *Chem. Rev.* **2003,** *103*, 2457-2473.

(45) Borrás-Almenar, J. J., Polyoxometalate molecular science. *Kluwer Academic Publishers*, Dordrecht Boston, 2003.

(46) Te, M.; Fairbridge, C.; Ring, Z., Oxidation reactivities of dibenzothiophenes in polyoxometalate/H_2O_2 and formic acid/H_2O_2 systems. *Appl. Catal., A* **2001,** *219*, 267-280.

(47) Venturello, C.; Daloisio, R.; Bart, J. C. J.; Ricci, M., A New Peroxotungsten Heteropoly Anion with Special Oxidizing Properties: Synthesis and Structure of Tetrahexylammonium Tetra(Diperoxotungsto)Phosphate(3-). *J. Mol. Catal.* **1985,** *32*, 107-110.

(48) Yadav, G. D.; Pujari, A. A., Epoxidation of Styrene to Styrene Oxide: Synergism of Heteropoly Acid and Phase-Transfer Catalyst under Ishii-Venturello Mechanism. *Org. Process Res. Dev.* **2000,** *4*, 88-93.

(49) Chen, J. Z.; Hua, L.; Zhu, W. W.; Zhang, R.; Guo, L.; Chen, C.; Gan, H. M.; Song, B. N.; Hou, Z. S., Polyoxometalate anion-functionalized ionic liquid as a thermoregulated catalyst for the epoxidation of olefins. *Catal. Commun.* **2014,** *47*, 18-21.

(50) Ding, Y.; Zhao, W.; Hua, H.; Ma, B., $[\pi\text{-}C_5H_5N(CH_2)_{15}CH_3]_3[PW_4O_{32}]/H_2O_2$/ethyl acetate/alkenes: a recyclable and environmentally benign alkenes epoxidation catalytic system. *Green Chem.* **2008,** *10*, 910.

(51) Poli, E.; De Sousa, R.; Jerome, F.; Pouilloux, Y.; Clacens, J.-M., Catalytic epoxidation of styrene and methyl oleate over peroxophosphotungstate entrapped in mesoporous SBA-15. *Catal. Sci. Technol.* **2012,** *2*, 910-914.

(52) Auffan, M.; Rose, J.; Bottero, J. Y.; Lowry, G. V.; Jolivet, J. P.; Wiesner, M. R., Towards a definition of inorganic nanoparticles from an environmental, health and safety perspective. *Nat. Nanotechnol.* **2009,** *4*, 634-641.

(53) Reddy, K. M.; Manorama, S. V.; Reddy, A. R., Bandgap studies on anatase titanium dioxide nanoparticles. *Mater. Chem. Phys.* **2003,** *78*, 239-245.

(54) Sheng, H. W.; Ren, G.; Peng, L. M.; Hu, Z. Q.; Lu, K., Superheating and melting-point depression of Pb nanoparticles embedded in Al matrices. *Phil. Mag. Lett.* **1996,** *73*, 179-186.

(55) Zheng, X. G.; Xu, C. N.; Nishikubo, K.; Nishiyama, K.; Higemoto, W.; Moon, W. J.; Tanaka, E.; Otabe, E. S., Finite-size effect on Neel temperature in antiferromagnetic nanoparticles. *Phys. Rev. B* **2005,** *72*.

(56) Volokitin, Y.; Sinzig, J.; Jongh, L. J. d.; Schmidt, G.; Vargaftik, M. N.; Moiseev, I. I., Quantum-size effects in the thermodynamic properties of metallic nanoparticles. *Nature* **1996,** *384*, 621–623.

(57) Wu, Y.; Nordlander, P., Finite-Difference Time-Domain Modeling of the Optical Properties of Nanoparticles near Dielectric Substrates. *J. Phys. Chem.* **2010,** *114*, 7302–7307.

(58) Wang, X.; Zhuang, J.; Peng, Q.; Li, Y., A general strategy for nanocrystal synthesis. *Nature* **2005,** *437*, 121-124.

(59) Ndolomingo, M. J.; Bingwa, N.; Meijboom, R., Review of supported metal nanoparticles: synthesis methodologies, advantages and application as catalysts. *J. Mater. Sci.* **2020**, 6195–6241.

(60) Niu, Z.; Li, Y., Removal and Utilization of Capping Agents in Nanocatalysis. *Chem. Mater.* **2014**, 72-83.

(61) A.Quintanilla; V.C.L.Butselaar-Orthlieb; C.Kwakernaak; W.G.Sloof; M.T.Kreutzer; F.Kapteijn, Weakly bound capping agents on gold nanoparticles in catalysis: Surface poison? *J. Catal.* **2010,** *271*, 104-114.

(62) Ajitha, B.; Reddy, Y. A. K.; Reddy, P. S.; Jeon, H.-J.; Ahn, C. W., Role of capping agents in controlling silver nanoparticles size, antibacterial activity and potential application as optical hydrogen peroxide sensor. *RSC Adv.* **2016,** *6*, 36171–36179.

(63) Stankus, D. P.; Lohse, S. E.; Hutchison, J. E.; Nason, J. A., Interactions between Natural Organic Matter and Gold Nanoparticles Stabilized with Different Organic Capping Agents. *Environ. Sci. Technol.* **2011,** *45*, 3238–3244.

(64) Gelle, A.; Jin, T.; de la Garza, L.; Price, G. D.; Besteiro, L. V.; Moores, A., Applications of Plasmon-Enhanced Nanocatalysis to Organic Transformations. *Chem. Rev.* **2020,** *120*, 986-1041.

(65) Link, S.; Wang, Z. L.; El-Sayed, M. A., Alloy Formation of Gold−Silver Nanoparticles and the Dependence of the Plasmon Absorption on Their Composition. *J. Phys. Chem. B* **1999,** *103*, 3529-3533.

(66) He, R.; Wang, Y.-C.; Wang, X.; Wang, Z.; Liu, G.; Zhou, W.; Wen, L.; Li, Q.; Wang, X.; Chen, X., *et al.*, Facile synthesis of pentacle gold–copper alloy nanocrystals and their plasmonic and catalytic properties. *Nat. Commun.* **2014,** *5*, 4327.

(67) Xiao, Q.; Sarina, S.; Bo, A.; Jia, J.; Liu, H.; Arnold, D. P.; Huang, Y.; Wu, H.; Zhu, H., Visible Light-Driven Cross-Coupling Reactions at Lower Temperatures Using a Photocatalyst of Palladium and Gold Alloy Nanoparticles. *ACS Catal.* **2014,** *4*, 1725-1734.

(68) Swearer, D. F.; Leary, R. K.; Newell, R.; Yazdi, S.; Robatjazi, H.; Zhang, Y.; Renard, D.; Nordlander, P.; Midgley, P. A.; Halas, N. J., *et al.*, Transition-Metal Decorated Aluminum Nanocrystals. *ACS Nano* **2017,** *11*, 10281-10288.

(69) Ghosh Chaudhuri, R.; Paria, S., Core/shell nanoparticles: classes, properties, synthesis mechanisms, characterization, and applications. *Chem. Rev.* **2012,** *112*, 2373-2433.

(70) Kuhn, L. T.; Bojesen, A.; Timmermann, L.; Nielsen, M. M.; Mørup, S., Structural and magnetic properties of core-shell iron-iron oxide nanoparticles. *J. Phys.: Condens. Matter* **202,** *14*, 13551–13567.

(71) Nemati, Z.; Alonso, J.; Khurshid, H.; Phana, M. H.; Srikanth, H., Core/shell iron/iron oxide nanoparticles: are they promising for magnetic hyperthermia? *RSC Adv.* **2016,** *6*, 38697–38702.

(72) Knight, M. W.; King, N. S.; Liu, L.; Everitt, H. O.; Nordlander, P.; Halas, N. J., Aluminum for Plasmonics. *ACS Nano* **2014,** *8*, 834-840.

(73) Sambles, J. R.; Bradbery, G. W.; Yang, F. Z., Optical excitation of surface plasmons: An introduction. *Contemp. Phys.* **1991,** *32*, 173-183.

(74) Petryayeva, E.; Krull, U. J., Localized surface plasmon resonance: Nanostructures, bioassays and biosensing-A review. *Anal. Chim. Acta.* **2011,** *706*, 8-24.

(75) Herzog, J. B.; Knight, M. W.; Natelson, D., Thermoplasmonics: quantifying plasmonic heating in single nanowires. *Nano Lett.* **2014,** *14*, 499-503.

(76) Daniel, M.-C.; Astruc, D., Gold nanoparticles: assembly, supramolecular chemistry, quantum-size-related properties, and applications toward biology, catalysis, and nanotechnology. *Chem. Rev.* **2004,** *104*, 293-346.

(77) Rycenga, M.; Cobley, C. M.; Zeng, J.; Li, W.; Moran, C. H.; Zhang, Q.; Qin, D.; Xia, Y., Controlling the synthesis and assembly of silver nanostructures for plasmonic applications. *Chem. Rev.* **2011,** *111*, 3669-3712.

(78) Chan, G. H.; Zhao, J.; Hicks, E. M.; Schatz, G. C.; Van Duyne, R. P., Plasmonic Properties of Copper Nanoparticles Fabricated by Nanosphere Lithography. *Nano Lett.* **2007,** *7*, 1947-1952.

(79) Biggins, J. S.; Yazdi, S.; Ringe, E., Magnesium Nanoparticle Plasmonics. *Nano Lett.* **2018,** *18*, 3752-3758.

(80) Moscatelli, A., The aluminium rush. *Nat. Nanotechnol.* **2012,** *7*, 778.

(81) Baffou, G.; Quidant, R.; Girard, C., Heat generation in plasmonic nanostructures: Influence of morphology. *Appl. Phys. Lett.* **2009,** *94*, 153109.

(82) Govorov, A. O.; Richardson, H. H., Generating heat with metal nanoparticles. *Nano Today* **2007,** *2*, 30-38.

(83) Zhang, X.; Li, X. Q.; Reish, M. E.; Zhang, D.; Su, N. Q.; Gutierrez, Y.; Moreno, F.; Yang, W. T.; Everitt, H. O.; Liu, J., Plasmon-Enhanced Catalysis: Distinguishing Thermal and Nonthermal Effects. *Nano Lett.* **2018,** *18*, 1714-1723.

(84) Stamplecoskie, K. G.; Fasciani, C.; Scaiano, J. C., Dual-stage lithography from a light-driven, plasmon-assisted process: a hierarchical approach to subwavelength features. *Langmuir* **2012,** *28*, 10957-10961.

(85) Jain, P. K.; El-Sayed, I. H.; El-Sayed, M. A., Au nanoparticles target cancer. *Nano Today* **2007,** *2*, 18-29.

(86) Neumann, O.; Urban, A. S.; Day, J.; Lal, S.; Nordlander, P.; Halas, N. J., Solar vapor generation enabled by nanoparticles. *ACS Nano* **2012,** *7*, 42-49.

(87) Giannini, V.; Fernández-Domínguez, A. I.; Heck, S. C.; Maier, S. A., Plasmonic nanoantennas: fundamentals and their use in controlling the radiative properties of nanoemitters. *Chem. Rev.* **2011,** *111*, 3888-3912.

(88) Linic, S.; Christopher, P.; Ingram, D. B., Plasmonic-metal nanostructures for efficient conversion of solar to chemical energy. *Nat. Mater.* **2011,** *10*, 911-921.

(89) Mori, K.; Kawashima, M.; Che, M.; Yamashita, H., Enhancement of the Photoinduced Oxidation Activity of a Ruthenium(II) Complex Anchored on Silica-Coated Silver Nanoparticles by Localized Surface Plasmon Resonance. *Angew. Chem.* **2010,** *122*, 8780-8783.

(90) Zhang, X.; Du, A.; Zhu, H.; Jia, J.; Wang, J.; Ke, X., Surface plasmon-enhanced zeolite catalysis under light irradiation and its correlation with molecular polarity of reactants. *Chem. Commun.* **2014,** *50*, 13893-13895.

(91) Stamplecoskie, K. G.; Pacioni, N. L.; Larson, D.; Scaiano, J. C., Plasmon-mediated photopolymerization maps plasmon fields for silver nanoparticles. *J. Am. Chem. Soc.* **2011,** *133*, 9160-9163.

(92) Swearer, D. F.; Zhao, H. Q.; Zhou, L. N.; Zhang, C.; Robatjazi, H.; Martirez, J. M. P.; Krauter, C. M.; Yazdi, S.; McClain, M. J.; Ringe, E., *et al.*, Heterometallic antenna-reactor complexes for photocatalysis. *Proc. Natl. Acad. Sci. U.S.A.* **2016,** *113*, 8916-8920.

(93) Li, K.; Hogan, N. J.; Kale, M. J.; Halas, N. J.; Nordlander, P.; Christopher, P., Balancing near-field enhancement, absorption, and scattering for effective antenna–reactor plasmonic photocatalysis. *Nano Lett.* **2017,** *17*, 3710-3717.

(94) Dong, J.; Zhang, Z.; Zheng, H.; Sun, M., Recent Progress on Plasmon-Enhanced Fluorescence. In *Nanophotonics-Berlin*, 2015; Vol. 4, pp 472-490.

(95) Bauch, M.; Toma, K.; Toma, M.; Zhang, Q.; Dostalek, J., Plasmon-Enhanced Fluorescence Biosensors: a Review. *Plasmonics* **2014,** *9*, 781-799.

(96) Moskovits, M., Surface-enhanced Raman spectroscopy: a brief retrospective. *J. Raman Spectrosc.* **2005,** *36*, 485-496.

(97) Hartland, G. V.; Besteiro, L. V.; Johns, P.; Govorov, A. O., What's so hot about electrons in metal nanoparticles? *ACS Energy Lett.* **2017,** *2*, 1641-1653.

(98) Brongersma, M. L.; Halas, N. J.; Nordlander, P., Plasmon-induced hot carrier science and technology. *Nat. Nanotechnol.* **2015,** *10*, 25-34.

(99) Lee, S.-H.; Jo, J.-S.; Park, J. H.; Lee, S. W.; Jang, J.-W., A hot-electron-triggered catalytic oxidation reaction of plasmonic silver nanoparticles evidenced by surface potential mapping. *J. Mater. Chem. A* **2018,** *6*, 20939-20946.

(100) Sato, Y.; Naya, S.-i.; Tada, H., A new bimetallic plasmonic photocatalyst consisting of gold(core)-copper(shell) nanoparticle and titanium(IV) oxide support. *APL Mater.* **2015,** *3*, 104502.

(101) Wang, J.; Ando, R. A.; Camargo, P. H. C., Controlling the Selectivity of the Surface Plasmon Resonance Mediated Oxidation of p-Aminothiophenol on Au Nanoparticles by Charge Transfer from UV-excited TiO_2. *Angew. Chem.* **2015,** *127*, 7013-7016.

(102) Xiao, Q.; Sarina, S.; Jaatinen, E.; Jia, J.; Arnold, D. P.; Liu, H.; Zhu, H., Efficient photocatalytic Suzuki cross-coupling reactions on Au–Pd alloy nanoparticles under visible light irradiation. *Green Chem.* **2014,** *16*, 4272-4285.

(103) Trinh, T. T.; Sato, R.; Sakamoto, M.; Fujiyoshi, Y.; Haruta, M.; Kurata, H.; Teranishi, T., Visible to near-infrared plasmon-enhanced catalytic activity of Pd hexagonal nanoplates for the Suzuki coupling reaction. *Nanoscale* **2015,** *7*, 12435-12444.

(104) González-Béjar, M.; Peters, K.; Hallett-Tapley, G. L.; Grenier, M.; Scaiano, J. C., Rapid one-pot propargylamine synthesis by plasmon mediated catalysis with gold nanoparticles on ZnO under ambient conditions. *Chem. Commun.* **2013,** *49*, 1732-1734.

(105) Zhao, X. Y.; Long, R.; Liu, D.; Luo, B. B.; Xiong, Y. J., Pd-Ag alloy nanocages: integration of Ag plasmonic properties with Pd active sites for light-driven catalytic hydrogenation. *J. Mater. Chem. A* **2015,** *3*, 9390-9394.

(106) Quiroz, J.; Barbosa, E. C.; Araujo, T. P.; Fiorio, J. L.; Wang, Y.-C.; Zou, Y.-C.; Mou, T.; Alves, T. V.; de Oliveira, D. C.; Wang, B., *et al.*, Controlling Reaction Selectivity over Hybrid Plasmonic Nanocatalysts. *Nano Lett.* **2018,** *18*, 7289-7297.

(107) Gangishetty, M. K.; Fontes, A. M.; Malta, M.; Kelly, T. L.; Scott, R. W. J., Improving the rates of Pd-catalyzed reactions by exciting the surface plasmons of AuPd bimetallic nanotriangles. *RSC Adv.* **2017,** *7*, 40218-40226.

(108) Chase, P. A.; Welch, G. C.; Jurca, T.; Stephan, D. W., Metal-free catalytic hydrogenation. *Angew. Chem. Int. Ed.* **2007,** *46*, 8050-8053.

(109) Garnett, J. L.; Sollich-Baumgartner, W. A., π Complex Adsorption in Hydrogen Exchange on Group Vlll Transition Metal Catalysts. *Adv. Catal.* **1966,** *16*, 95-121.

(110) Mi, H. H.; Lee, W. J.; Chen, C. B.; Yang, H. H.; Wu, S. J., Effect of fuel aromatic content on PAH emission from a heavy-duty diesel engine. *Chemosphere* **2000,** *41*, 1783-1790.

(111) Ravindra, K.; Sokhi, R.; Grieken, R. V., Atmospheric polycyclic aromatic hydrocarbons: Source attribution, emission factors and regulation. *Atmos. Environ.* **2008,** *42*, 2895-2921.

(112) Sassykova, L. R., Development of Catalysts for the Hydrogenation of the Aromatic Ring in Gasolines. *Chem. Biochem. Eng. Q.* **2017,** *31*, 447-453.

(113) Schoenmaker-Stolk, M. C.; Verwijs, J. W.; Don, J. A.; Scholten, J. J. F., The catalytic hydrogenation of benzene over supported metal catalysts: I. Gas-phase hydrogenation of benzene over ruthenium-on-silica. *Appl. Catal.* **1987,** *29*, 73-90.

(114) Stanislaus, A.; Cooper, B. H., Aromatic Hydrogenation Catalysis: A Review. *Catal. Rev. Sci. Eng.* **1994,** *36*, 75-123.

(115) Dyson, P. J.; Ellis, D. J.; Welton, T.; Parker, D. G., Arene hydrogenation in a room-temperature ionic liquid using a ruthenium cluster catalyst. *Chem. Commun.* **1999**, 25-26.

(116) Bianchini, C.; Santo, V. D.; Meli, A.; Moneti, S.; Moreno, M.; Oberhauser, W.; Psaro, R.; Sordelli, L.; Vizza, F., A comparison between silica-immobilized ruthenium(II) single sites and silica-supported ruthenium nanoparticles in the catalytic hydrogenation of model hetero- and polyaromatics contained in raw oil materials. *J. Catal.* **2003,** *213*, 47-62.

(117) Rasero-Almansa, A. M.; Corma, A.; Iglesias, M.; Sánchez, F., Post-functionalized iridium-Zr-MOF as a promising recyclable catalyst for the hydrogenation of aromatics. *Green Chem.* **2014,** *16*, 3522–3527.

(118) Giustra, Z. X.; Ishibashi, J. S. A.; Liu, S.-Y., Homogeneous metal catalysis for conversion between aromatic and saturated compounds. *Coord. Chem. Rev.* **2016,** *314*, 134–181.

(119) Zahmakıran, M.; Tonbul, Y.; Özkar, S., Ruthenium(0) Nanoclusters Stabilized by a Nanozeolite Framework: Isolable, Reusable, and Green Catalyst for the Hydrogenation of Neat Aromatics under Mild Conditions with the Unprecedented Catalytic Activity and Lifetime. *J. Am. Chem. Soc.* **2010,** *132*, 6541-6549.

(120) Wang, D.-S.; Chen, Q.-A.; Lu, S.-M.; Zhou, Y.-G., Asymmetric hydrogenation of heteroarenes and arenes. *Chem. Rev.* **2012,** *112*, 2557-2590.

(121) Blasera, H.-U.; Honigb, H.; Studera, M.; Wedemeyer-Exl, C., Enantioselective synthesis of ethyl nipecotinate using cinchona modified heterogeneous catalysts. *J. Mol. Catal. A: Chem.* **1999,** *139*, 253–257.

(122) Studer, M.; Blaser, H.-U.; Exner, C., Enantioselective Hydrogenation Using Heterogeneous ModifiedCatalysts: An Update. *Adv. Synth. Catal.* **2003,** *345*, 45±46.

(123) Jacquin, M.; Jones, D. J.; Rozière, J.; Albertazzi, S.; Vaccari, A.; Lenarda, M.; Storaro, L.; Ganzerla, R., Novel supported Rh, Pt, Ir and Ru mesoporous alumino silicates as catalysts for the hydrogenation of naphthalene. *Appl. Catal. A* **2003,** *251*, 131-141.

(124) Zhou, G.; Jiang, L.; Dong, Y.; Li, R.; He, D., Engineering the exposed facets and open-coordinated sites of brookite TiO_2 to boost the loaded Ru nanoparticle efficiency in benzene selective hydrogenation. *Appl. Surf. Sci.* **2019,** *486*, 187-197.

(125) Alsalahi, W.; Tylus, W.; Trzeciak, A. M., Green Synthesis of Rhodium Nanoparticles that are Catalytically Active in Benzene Hydrogenation and 1-Hexene Hydroformylation. *ChemCatChem* **2018,** *10*, 2051-2058.

(126) Stuhl, L. S.; DuBois, M. R.; Flirsekorn, F. J.; Bleeke, J. R.; Stevens, A. E.; Muetterties, E. L., Catalytic homogeneous hydrogenation of arenes. 6. Reaction scope for the (eta3-2-propenyl) tris (trimethyl phosphite-P) cobalt catalyst. *J. Am. Chem. Soc.* **1978,** *100*, 2405-2410.

(127) Livingstone, S. E., The Chemistry of Ruthenium, Rhodium, Palladium, Osmium, Iridium and Platinum. *Pergamon Press*, 1973; Vol. 25.

(128) Hageluken, C., Markets for the catalyst metals platinum, palladium and rhodium. *Metall* **2006,** *60*, 31-42.

(129) Viniegra, M.; Gomez, R.; Gonzalez, R. D., The Role of Support in the Catalytic Hydrogenation of Benzene over Ruthenium Catalysts. *J. Catal.* **1988,** *111*, 429-432.

(130) Rossi, L. M.; Machado, G., Ruthenium nanoparticles prepared from ruthenium dioxide precursor: Highly active catalyst for hydrogenation of arenes under mild conditions. *J. Mol. Catal. A: Chem.* **2009,** *298*, 69-73.

(131) Rakers, L.; Martinez-Prieto, L. M.; Lopez-Vinasco, A. M.; Philippot, K.; Leeuwen, P. W. N. M. v.; Chaudret, B.; Glorius, F., Ruthenium nanoparticles ligated by cholesterol-derived NHCs and their application in the hydrogenation of arenes. *Chem. Commun.* **2018,** *54*, 7070--7073.

Following the need to improve the activity of heterogeneous catalysts for biomass valorization, the following chapter presents my research in development of phase transfer agents and synthetic methodology to achieve a highly active and recyclable peroxophosphotungstate catalyst for the epoxidation and cleavage of vegetable oils.

2. Epoxidation of fatty acids and esters

This chapter is adapted from a published article, with its corresponding citation below, which is reprinted with permission from the Royal Society of Chemistry and all co-authors.

Luis Carlos de la Garza, Karine De Oliveira Vigier, Gregory Chatel and Audrey Moores. "Amphiphilic dipyridinium-phosphotungstate as an efficient and recyclable catalyst for triphasic fatty ester epoxidation and oxidative cleavage with hydrogen peroxide" Green Chemistry, 2017, 19, 2855-2862.

2.1. Abstract

A novel amphiphilic dipyridinium peroxophosphotungstate ion pair was developed as a selective and recyclable catalyst for the triphasic epoxidation of fatty acids and esters with hydrogen peroxide. The synthesis of the catalyst was studied extensively by solid and liquid phase ^{31}P nuclear magnetic resonance (NMR). The oxidation of vegetable oils is of prime importance for the production of lubricants, plasticizers, polymer stabilizers and other olefinic compounds. Based on the oxidizing activity of peroxophosphotungstates, we designed a lipophilic phase transfer agent that renders the active complex insoluble in the reaction media, without having to support it on a matrix. This affords a catalyst combining the activity of homogeneous catalysts and the recyclability of heterogeneous systems. We show that this catalyst is able to fully epoxidize methyl oleate with excellent selectivity, with a turnover frequency of 149 h^{-1} at 60 °C, and can be easily recycled, to reach a record turn over number of 1868. A larger scale experiment on 13 grams and a scope including linoleic and ricinoleic acids were also demonstrated. The catalyst also shows excellent activity and selectivity for the oxidative cleavage of methyl oleate and the oxidation of small olefins.

2.2. Introduction

Biomass valorization constitutes a key instrument in the effort to mitigate global warming and its multiple environmental and economical consequences. Research in this area opens opportunities to address challenges such as the exploitation of non-edible resources and agricultural waste and transitioning out of fossil resources.[1] Among biomass sources, vegetable oils are the most important renewable raw material used in the chemical industry.[6] Vegetable oils consist of triglycerides with long lipophilic carbon chains, most of which feature one or several double bonds, depending on the oil source. These unsaturations can be oxidized to fabricate added-value products, such as epoxides, diols or carboxylic acids. Oxidized oil products are precursors for a variety of functional compounds such as lubricants, plasticizers, polymer stabilizers and other olefinic compounds.[132]

The most common industrial procedure to epoxidize oils is to use peroxyacids produced in situ from formic acid or acetic acid in the presence of hydrogen peroxide and sulfuric acid. While these reagents are cheap, they are used homogeneously and are corrosive and toxic, requiring special equipment and safety measures. The oxidation with peroxyacids is also highly exothermic ($\Delta H = 230$ kJ mol−1),[36] which makes temperature control difficult at industrial scales and imposes a slow addition of hydrogen peroxide and catalyst with long cooling times to avoid a runaway reaction.[36] The addition of a strong mineral acid as co-catalyst also limits selectivity, since lowering the pH promotes the epoxide's ring-opening reaction *via* hydrolysis.[133]

In search for more sustainable approaches, peroxophosphotungstate catalysts were initially found to be active for the epoxidation of double bonds with hydrogen peroxide as reported by Venturello *et al*.[47, 134] and triggered an important research effort thereafter. To overcome the immiscibility of the oxidant (aqueous hydrogen peroxide) with the substrate (a fatty acid, ester or triglyceride), the active peroxophosphotungstate species $(PO_4[W(O)(O_2)_2]_4)^{3-}$ trianion can be coupled with cationic phase transfer agents. This system prevents overheating hazards and efficiently affords epoxidized double bonds with higher selectivity and lower toxicity than peroxyacids. The oxidation method using peroxophosphotungstate species was further developed by Ishii *et al*. where they showed that it can also be used to fully cleave double bonds into carboxylic acids and that phosphotungstic acid can be used as a convenient precursor to the active species.[26] However, this system is currently not economically viable compared to peroxyacids, because the catalyst is homogeneously dispersed and thus unrecoverable. Research has thus shifted towards creating recyclable catalysts that can be both cost-effective and efficient.

In previous reports, the phase transfer agent was engineered so that the catalyst can be extracted,[135] or precipitated, either by cooling the medium,[49] or designing the catalyst to become insoluble once the hydrogen peroxide has been consumed.[136-137] Cationic supports have been shown to make the catalytic complex heterogeneous, such as polymers derived from ionic liquids,[29] functionalized silica,[138] or even magnetic iron oxide nanoparticles coated with either cationic polymers[30] or functionalized silica.[139-140] Another common method is to immobilize the neutral complex of peroxophosphotungstate and the phase transfer agent into a solid matrix, such as mesoporous silica,[51] amphiphilic copolymers grafted onto silica,[141] metal–organic frameworks,[142] or metallic supports.[25]

However, heterogeneous catalysts show reaction rates at least an order of magnitude lower than their best homogeneous counterparts (see Table 6 in appendix). While direct comparisons are often not possible to make due to widely different conditions such as substrate scope, catalyst loading, temperature and solvent, it is still clear that heterogeneous systems are significantly less active. In order to be economically viable as a replacement of peroxyacids, both activity and recyclability need to be optimized.

Herein we report a novel catalytic system, using a dipyridinium dication ($\mathbf{DP}^{2+}$) as the phase transfer agent paired with a peroxophosphotungstate trianion ($\mathbf{PPW}^{3-}$), active for the oxidation of vegetable oils with hydrogen peroxide that bridges the gap between the homogeneous and heterogeneous systems. Our catalyst ($[\mathbf{DP}^{2+}]_3[\mathbf{PPW}^{3-}]_2$) allows the reaction to function in a triphasic system–composed of an organic phase (the substrate), an aqueous phase (the oxidant) and a solid phase (the catalyst) – and shows reaction rates similar to reported homogeneous catalysts, while being easy to recycle through simple filtration and easy to synthesize from commercial reagents. The synthetic conditions for this well-defined complex were studied and characterization was performed by ^{31}P magic angle spinning nuclear magnetic resonance (^{31}P MAS NMR) as well as scanning electron microscopy (SEM). Leaching during catalytic experiments was very limited as established by inductively coupled plasma mass spectrometry (ICP-MS) and a hot filtration test proved a heterogeneous mechanism. Excellent results in terms of activity and selectivity were obtained for the epoxidation of methyl oleate, linoleic and ricinoleic acids, the oxidation of small alkenes to either the corresponding epoxide or diol and finally for the fully oxidative cleavage of methyl oleate. The recyclability of the system was also successfully tested.

2.3. Results and discussion

2.3.1. Optimization of the catalyst synthesis

Our aim in this study was to design a cationic transfer agent able to form a complex with the active **PPW**$^{3-}$, while being insoluble in both the aqueous and the oil phase to achieve recovery. It should nonetheless retain enough hydrophilic interactions to regenerate the active peroxophosphotungstate species with hydrogen peroxide, enough lipophilic affinity to react with the substrate and cause limited leaching of the catalyst by ionic dissociation. Commercial ammonium and pyridinium surfactants are water soluble, and the catalytic complexes obtained using those phase transfer agents are thus homogeneous in the reaction mixture and not recyclable. Conversely, excessively lipophilic polymers have been found to fully deactivate the catalyst by preventing catalyst regeneration in the aqueous phase.[29] Indeed such supports typically rearrange to expose only their hydrophobic alkyl chains. We decided to use dicationic or tricationic surfactants, to optimize ion pairing with the catalyst. We initially explored the triammonium based on pentamethyldiethylenetriamine to match the charge of the phosphotungstate, but the resulting complex was very unstable and degraded quickly. After testing several diamines and dipyridines, we settled on using 4,4′-trimethylenedipyridine. Notably, it was found during its synthesis to be stable at least up to 120 °C and insoluble in water below 80 °C. A similar type of pyridinium was already proven to be very stable for supporting phosphotungstates by Yamada et al.[31] Sufficient lipophilicity was introduced by functionalization of C14 carbon chains. Wu et al. showed that by increasing the length of the carbon chain on an alkylimidazolium, the activity towards the epoxidation of cyclohexene of the phosphotungstate-paired catalyst increased.[136] The synthesis of the dicationic phase transfer agent required only one step from commercially available substrates, followed by an ion exchange with PPW3−, produced in situ by mixing phosphotungstic acid with excess hydrogen peroxide (Scheme 10).

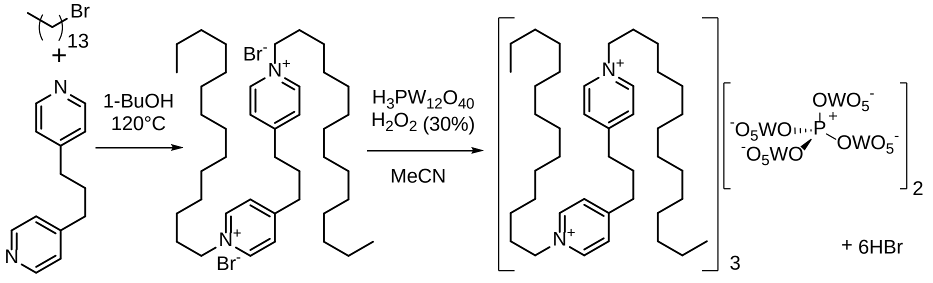

$[DP^{2+}]_3[PPW^{3-}]_2$

Scheme 10: Synthetic procedure to access the $[DP^{2+}]_3[PPW^{3-}]_2$ catalyst.

The oxidation of phosphotungstic acid into its activated peroxide prior to the ion exchange with 4,4′-trimethylenedipyridinium bromid was found to be crucial for obtaining an active catalyst. Although several reports in the literature showed that active catalysts can be obtained by directly performing the ion exchange with $H_3PW_{12}O_{40}$,[50, 136] or even mixing the surfactant and the phosphotungstate with the substrates in situ,[143] this scheme did not work in our hands using [**DP**$^{2+}$] as the phase transfer agent.

Both the synthesis of the active phosphotungstate catalytic species and the ion-pairing by phase transfer constitute a complex sequence of chemical equilibria and reactions (Scheme 11). It is generally accepted that the active species in the reaction is **PPW**$^{3-}$, *i.e.* $(PO_4[W(O)(O_2)_2]_4)^{3-}$, as described by Venturello et al.[47] This species is obtained by the complete oxidation of phosphotungstic acid with hydrogen peroxide. It precipitates out of the aqueous phase when paired with a lipophilic transfer agent. However, this oxidation reaction also affords tungstic acid (H_2WO_4), as a by-product which can be difficult to separate from the final product because they co-precipitate together under these conditions. Interestingly, it is also known that H_2WO_4 can be further oxidized by H_2O_2 to yield H_2WO_6, a strong acid which fully dissociates in water, and can pair with the cationic phase transfer agent.

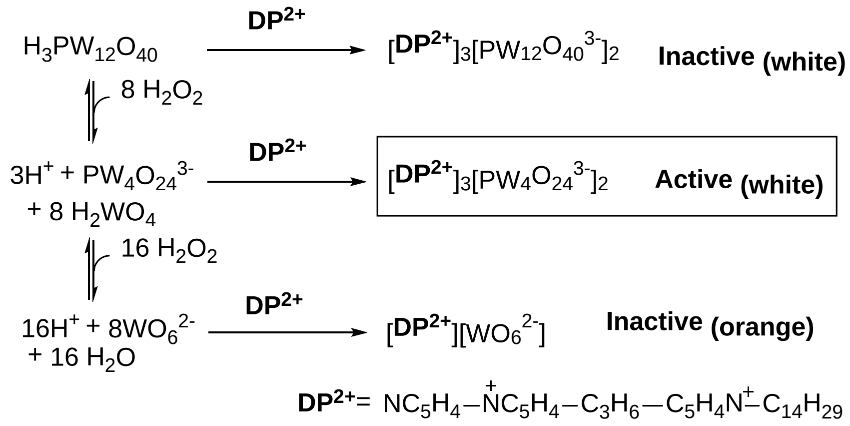

Scheme 11: Sequential oxidation of phosphotungstic acid by hydrogen peroxide and potential pairing with the amphiphilic dipyridinium (**DP**$^{2+}$). Stoichiometry is not provided on the right end side of the scheme for clarity.

In order to optimize the production of the active catalyst, [**DP**$^{2+}$]$_3$[**PPW**$^{3-}$]$_2$, we explored several parameters: the ratio of hydrogen peroxide to phosphotungstic acid, the ratio of dipyridinium to phosphotungstic acid, and the solvent used for synthesis. The catalysts obtained were evaluated for their activity in the epoxidation of methyl oleate using H_2O_2 as the oxidant at 60 °C with no solvent (Table 2).

Table 2: Optimization of catalyst synthetic conditions

	Catalyst synthetic conditions			Methyl Oleate epoxidation conditions and results[a]					
Entry	H_2O_2 / $H_3PW_{12}O_{40}$	**DP**$^{+2}$ / $H_3PW_{12}O_{40}$	Solvent	Catalyst Loading (mol%)	Time (h)	Conversion	Epoxide Selectivity	TON	TOF (h^{-1})
1	30:1	3:2	H_2O[b]	1.1	4	99%	58%	89	22
2	30:1	3:2	$CHCl_3$	1.1	4	97%	58%	88	22
3	30:1	3:2	MeOH	1.1	4	98%	84%	88	22
4	200:1	3:2	MeOH	1.1	4	95%	99%	85	22

5[c]	200:1	3:2	MeOH	1.1	2	71%	73%	64	32
6	200:1	5:1	MeOH	1.1	2	24%	96%	22	11
7	200:1	1:2	MeOH	0.22	4	88%	99%	400	100
8	200:1	1:2	H_2O*	0.22	4	89%	95%	404	101
9	200:1	1:2	MeCN	0.22	3	98%	96%	447	149

[a] Conditions for the epoxidation of methyl oleate: 500 mg of methyl oleate (1 eq.), 222 μL of H_2O_2 30% (1.32 eq.). Heated at 60 °C. No solvent. [b] H_2O needed to be heated above 80 °C to dissolve the dipyridinium bromide. [c] 50 mg of H_2WO_4 were added to the epoxidation of methyl oleate.

Catalysts prepared with 30 eq. of H_2O_2 (Table 2, entries 1 to 3) were tested for the epoxidation of methyl oleate and afforded good conversions. However, poor epoxide selectivity was observed when using catalysts that were prepared in water or chloroform. We reasoned that the expected release of H_2WO_4 under these conditions and its co-precipitation with the catalyst affected negatively the catalytic performances. Indeed, under catalytic epoxidation conditions where H_2O_2 is in large excess compared to the catalyst (60 °C, 1.1 mol% catalyst loading, 1.32 eq. of H_2O_2), H_2WO_4 readily oxidizes into H_2WO_6. This hypothesis was consistent with a measured pH between 0 and 1, indicative of the presence of the strong acid H_2WO_6.[144] It is known that mineral acids catalyze the hydrolysis of epoxides, which is bound to adversely affect selectivity.

Co-precipitation of tungstic acid could be prevented entirely by adding a large excess of hydrogen peroxide (200 : 1) to the phosphotungstic acid prior to the addition of the phase transfer agent (Table 2, entries 4 to 9). This causes full oxidation of the by-product into WO_6^{2-} during catalyst synthesis. Yet, since WO_6^{2-} is an anion, it can also partially bind to the phase transfer agent and co-precipitate with the desired catalyst. While this does not form adverse acid species, affecting catalyst selectivity, it does reduce its activity. Control experiments showed that directly using tungstic acid to form [**DP**$^{2+}$][WO_6^{2-}] yields an orange product that is inactive towards the epoxidation of methyl oleate (see the ESI†). The separation of [**DP**$^{2+}$][WO_6^{2-}] from

[**DP**$^{2+}$]$_3$[**PPW**$^{3-}$]$_2$ was resolved by careful solvent selection as explained below. In further tests, a ratio of 200 for $H_2O_2/H_3PW_{12}O_{40}$ was selected. Next the impact of the **DP**$^{+2}$/$H_3PW_{12}O_{40}$ ratio on catalytic performance was studied, using catalyst color as an indication of purity (see the ESI†).

The ratio of 3 : 2 was first tested as the "natural" choice to afford [**DP**$^{2+}$]$_3$[**PPW**$^{3-}$]$_2$ as a catalyst. When tested for epoxidation of methyl oleate, this catalyst afforded excellent conversion and selectivity of 95% and 99% respectively (Table 2, entry 4). Addition of H_2WO_4 to the catalyst under these conditions confirmed its adverse effect on both attributes (Table 2, entry 5). When excess of the transfer agent was added (Table 2, entry 6), the conversion dropped to 24%, likely because the transfer agent could precipitate a large amount of the inactive WO_6^{2-} by-product, thus contaminating the catalyst. Interestingly, when using an excess of phosphotungstic acid starting material (**DP**$^{2+}$/$H_3PW_{12}O_{40}$ ratio = 1 : 2, Table 2, entry 7), the catalytic activity was greatly enhanced and the catalyst loading could be reduced 5 fold, down from 1.1 mol% to 0.22 mol%. Under these conditions, excellent conversions and selectivity were obtained. Finally, methanol, water and acetonitrile solvents were screened and acetonitrile was found to be the best system with 98% conversion and 96% selectivity after 3 hours at 60 °C (Table 2, entries 7–9). Under the latter conditions, TON and TOF could be greatly enhanced to 447 and 149 h^{-1} respectively. Our experiments suggest that acetonitrile helps wash away the inactive, orange [**DP**$^{2+}$][WO_6^{2-}] by solubilizing this species. The effect of the solvent was studied by both liquid ^{31}P NMR (Figure 17 in appendix), prior to the ion exchange, and solid ^{31}P MAS NMR (Figure 18 in appendix) on the precipitated catalyst. The analysis showed that acetonitrile was the best solvent to promote the formation of highly peroxidized species, which is consistent with the higher activity observed.

2.3.2. Characterization of the catalyst

Since the catalyst was designed to be heterogeneous, it could not be dissolved in any common solvents for traditional analysis and characterization was performed by ^{31}P MAS NMR. As a standard for comparison, the inactive species [**DP**$^{2+}$]$_3$[$PW_{12}O_{40}^{3-}$]$_2$ was synthesized by simple ion exchange. It presented a chemical shift of −16.6 ppm, which is very similar to the chemical shift of phosphotungstic acid in water, −15.2 ppm (Figure 6a). The ^{31}P MAS NMR spectrum of [**DP**2^{+}]$_3$[**PPW**$^{3-}$]$_2$ synthesized under the conditions shown in Table 2, entry 9, reveals two peaks at 3.5 ppm and 1.5 ppm (Figure 6b). The chemical shift of $\mathrm{PW_4O_{24}}^{3-}$ species has been reported in the region between 0 and 1 ppm and is known to change when using different cationic surfactants.[26] Also, Duncan *et al.* had shown that by varying the amounts of $\mathrm{H_2O_2}$, peaks in the region −15 to 5 ppm could be observed by $_{31}$P NMR, attributed to fully or partially peroxidized species en route to $\mathrm{PW_4O_{24}}^{3-}$, but no formal characterization was reported.[27] This led us to believe that the peaks observed for our catalyst belong to either $\mathrm{PW_4O_{24}}^{3-}$ or highly peroxidized intermediates. However, despite exploring several reaction conditions and solvents, precipitated $[\mathbf{DP}^{2+}]_3[\mathbf{PPW}^{3-}]_2$ always presented itself as a mixture of several compounds in the 0–5 ppm region by ^{31}P MAS NMR (see Figure 18 in appendix). These results are in agreement with reports by Kozhevnikov et al. that showed activity towards the epoxidation of oleic acid with a mixture of phosphotungstate intermediates, as ascribed by ^{31}P NMR, suggesting that the Venturello anion may not be the only active species.[144]

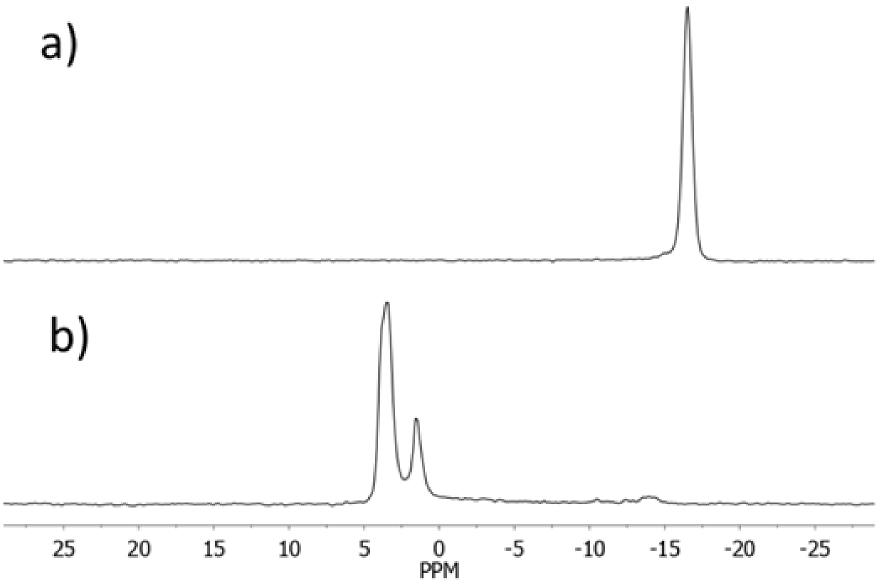

Figure 6: ^{31}P MAS NMR spectra of (a) $[\mathbf{DP}^{2+}]_3[\mathrm{PW_{12}O_{40}}^{3-}]_2$, (b) $[\mathbf{DP}^{2+}]_3[\mathbf{PPW}^{3-}]_2$ using conditions shown in Table 2 (entry 9).

The morphology of the catalyst was studied by SEM. The catalyst arranges itself in the shape of rectangular prisms with varying lengths between 2 and 50 μm, as well as width and height roughly between 0.5 and 5 μm. Some amorphous regions could also be observed, which is consistent with the ^{31}P MAS NMR study, revealing the fact that the catalysts are present as a mixture of closely related compounds (see Figure 19 in appendix).

2.3.3. Catalytic results

With an optimized catalyst synthesis in hand, we turned to catalytic reaction optimization. Epoxidation of methyl oleate was tested under neat conditions and with solvents (Table 2). In all cases but with methanol, the reaction took place in a triphasic mixture of a solid catalyst and two immiscible liquid phases, the aqueous phase containing hydrogen peroxide, and the organic phase containing methyl oleate. By design, the [**DP**$^{2+}$]$_3$[**PPW**$^{3-}$]$_2$ catalyst possesses amphiphilic properties,

with lipophilic long chains on the cation, combined with the hydrophilic properties of the peroxophosphotungstate moiety. Under neat conditions, good conversion (84%) with perfect selectivity was obtained at room temperature with 1 mol% of catalyst loading, while a fivefold loading reduction gave an excellent result of 98% conversion with 96% selectivity at 60 °C (entries 1 and 2). Overall, we observed that selectivity was perfect until 90% conversion, at which point, traces of the corresponding diols, hydroxyketones, aldehydes and carboxylic acids could be observed and selectivity dropped. The selectivity continued to drop when the reaction was left running past full conversion, as epoxides can slowly hydrolyse under these conditions.

Table 3: Epoxidation of methyl oleate

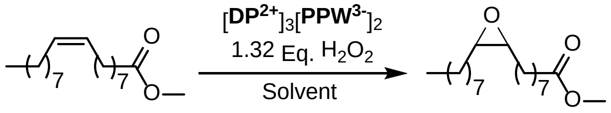

Entry	Catalyst (mol%)	Loading	Solvent (1 mL)	Time (h)	Temp (°C)	Conversion	Selectivity
1	1		neat	4	21	84%	100%
2	0.22		neat	3	60	98%	96%

3	0.22	Heptane	3	60	70%	100%
4	0.22	EtOAc	3	60	64%	100%
5	0.22	MeOH	3	60	96%	68%
6	0.22	MeCN	3	60	91%	98%
7	0.22	$CHCl_3$	3	60	87%	100%
8[a]	0.22	neat	2	60	93%	98%
9[b]	0.22	neat	3	60	2%	100%

Conditions for the epoxidation of methyl oleate: 500 mg of methyl oleate (1 eq.), 222 μL of H_2O_2 30% (1.32 eq.). Time and catalyst loading varied depending on activity observed. [a] Scaled up to 13.2 g of methyl oleate (1 eq.), 5.9 mL of H_2O_2 30% (1.32 eq.) and 200 mg of catalyst (0.0022 eq.). [b] Control test using [**DP**$^{2+}$]$_3$[$PW_{12}O_{40}{}^{3-}$]$_2$ as catalyst.

Using a solvent affected both conversion and selectivity. Lipophilic solvents (heptane, EtOAc and $CHCl_3$, entries 3–5) gave lower conversions likely because greater dilution of the oil limited the catalysis rate. Acetonitrile mixed with the aqueous phase (entry 6) gave results more similar to neat conditions with 91% conversion and 98% selectivity. Among the solvents tested, methanol was the only one able to dissolve both the aqueous and the organic phases into a single phase, thus allowing good mass transfer to reach 96% conversion. However, this solvent also facilitated the hydrolysis of the epoxide to form the diol, which reduces selectivity to 68% (entry 7). The catalyst [**DP**$^{2+}$]$_3$[**PPW**$^{3-}$]$_2$ was also tested on a larger scale, showing an excellent conversion of 93% and full selectivity upon epoxidizing 13 grams of methyl oleate (entry 8). A control experiment using the precursor [**DP**$^{2+}$]$_3$[$PW_{12}O_{40}{}^{3-}$]$_2$ showed almost no activity (entry 9), revealing the importance of pre-peroxidizing the catalyst prior to cation exchange (Scheme 11).

In an effort to expand the scope of the reaction, the epoxidation of two fatty acids, linoleic acid and ricinoleic acid, was tested with [**DP**$^{2+}$]$_3$[**PPW**$^{3-}$]$_2$, which proceeded with good conversions and selectivities (Scheme 12).

Cyclohexene, cyclooctene and styrene were also tested to verify if the catalyst, designed for large lipophilic substrates, would also epoxidize small alkenes effectively. Cyclooctene, in particular, is a commonly used substrate in the literature for epoxidation of phosphotungstate catalysts.[25, 29-30, 50, 136, 138-139, 141-143, 145]

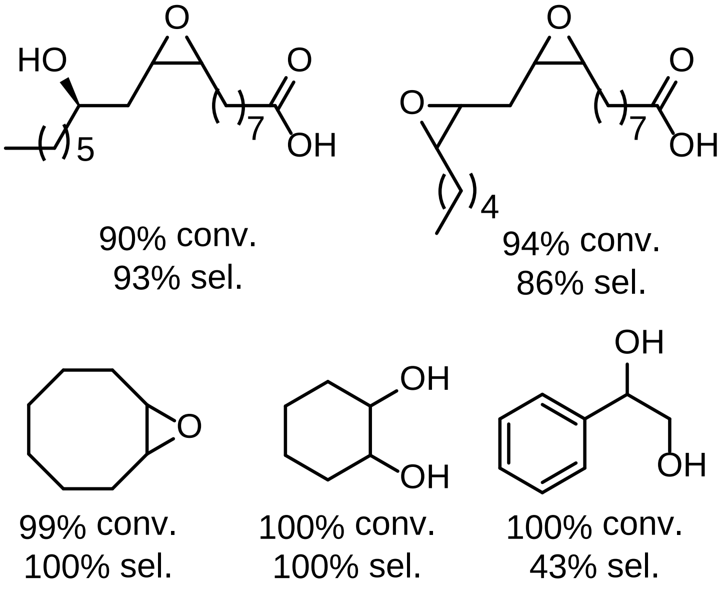

Scheme 12: Oxidation of alkenes with 0.22 mol% of [**DP**$^{2+}$]$_3$[**PPW**$^{3-}$]$_2$ as catalyst at 60 °C with no solvent. Conditions used for ricinoleic acid: 1 h, 1.32 eq. H_2O_2. Linoleic acid: 2 h, 2.2 eq. H_2O_2. Cyclohexene, cyclooctene and styrene: 3 h, 1.32 eq. H_2O_2.

The conversion and selectivity for the epoxidation of cyclooctene were in fact better than those obtained for methyl oleate, as shown in Scheme 12. 1,2-Epoxycyclooctene was obtained with full selectivity and 99% conversion in 3 h at 60 °C with 0.22 mol% of catalyst, which gives a TOF of 150 h^{-1}. To the best of our knowledge, this is the highest reported TOF for heterogeneous tungsten-based catalysts. Cyclohexene afforded full selectivity towards the diol instead of the epoxide, since 1,2-epoxycyclohexene quickly hydrolysed in the presence of [**DP**$^{2+}$]$_3$[**PPW**$^{3-}$]$_2$, even at room temperature. Styrene was found to be too reactive for this catalyst, leading to a complex mixture of aldehydes, carboxylic acids and styrene glycol.

A hot filtration test was performed with methyl oleate as the substrate to confirm the heterogeneous nature of the catalyst. In a standard epoxidation method, the solution was filtered after 30 minutes of the reaction at 60 °C, which showed 40.6% yield by GC-MS. The filtrate was stirred at 60 °C for 12 hours with an additional 1.32 eq. of H_2O_2 and a virtually unchanged yield of 42.4% was then measured. These results confirm that [**DP**$^{2+}$]$_3$[**PPW**$^{3-}$]$_2$ functions as a heterogeneous catalyst.

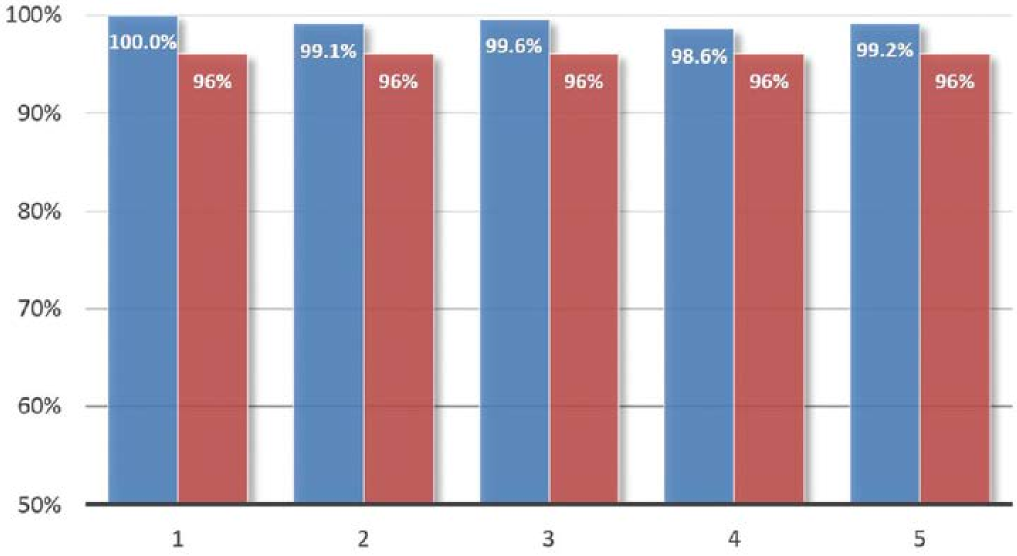

Figure 7: Conversion (blue, left bars) and selectivity (red, right bars) towards methyl 9,10-epoxystereate obtained as a function of cycle number for the epoxidation of methyl oleate with the recycled [**DP**$^{2+}$]$_3$[**PPW**$^{3-}$]$_2$ catalyst. Catalytic conditions: 1 h, 60 °C, 1 mol% catalyst loading.

Recycling tests were performed by diluting the mixture at the end of the reaction with ethyl acetate, centrifuging and removing both aqueous and organic supernatants with a pipette. The addition of an organic solvent was necessary to remove the product due to the high viscosity of the epoxidized methyl oleate at room temperature. The solid catalyst remained in the flask and was dried in air for 1 minute before reuse. When using 1 mol% catalyst loading, the catalyst performed very well over 5 cycles, with conversions ranging from 98.6 to 100% and selectivity remaining stable (Figure 7), thus affording a recyclable system. When employing an optimized loading of 0.22 mol%, a decrease in catalytic activity was observed after three cycles (see Table 7 in appendix). Pushing to 5 cycles under these conditions allowed achieving a record cumulated turnover number (TON) of 1868. The highest number of turnovers to date for Venturello-type catalyst has been reported by Khlebnikova et al.[32] with a value of 940 turnovers for a homogeneous catalysis loading at 0.01 mol%. The highest number of recycling cycles to date has been reported by Chen et al.[49] where 17 cycles at 3% catalyst loading amounted to 560 turnovers.

In order to study the stability of the catalyst, a leaching study was conducted. After filtering the solid catalyst, the aqueous filtrate from the 13 gram scale experiment was analysed by ICP-MS (using conditions of Table 2, entry 8). A limited leaching of 2.8% was measured. The product was recovered without contamination from the organic phase.

Previous reports by Duncan *et al.*[27] on quaternary ammonium paired peroxophosphotungstates investigated degradation of the Venturello catalyst. In their case, it was reported that the catalyst degraded after approximately 500 turnovers. Here [**DP**$^{2+}$]$_3$[**PPW**$^{3-}$]$_2$ starts to deactivate noticeably after 1300 turnovers (see Table 7 in appendix). Additional experiments were performed by preheating [**DP**$^{2+}$]$_3$[**PPW**$^{3-}$]$_2$ for 24 hours with methyl oleate at 60 °C before adding hydrogen peroxide, in order to exclude thermal degradation. The epoxide yield and selectivity were unchanged compared to the fresh batch of catalysts.

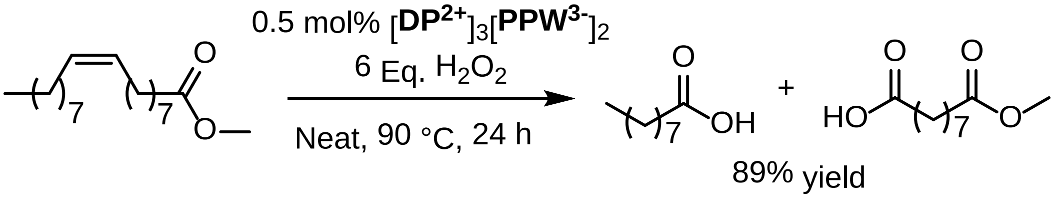

Scheme 13: Cleavage of methyl oleate with [**DP**$^{2+}$]$_3$[**PPW**$^{3-}$]$_2$ as catalyst.

Homogeneous Venturello-type catalysts have also been reported to cleave double bonds of fatty acids/esters and small organic molecules in order to form the corresponding carboxylic acids,[26, 28, 32] but no heterogeneous systems had proven successful for this reaction on the fatty molecules. The cleavage requires higher temperatures to promote the hydrolysis of the epoxide and a longer reaction time (Scheme 13). Since [**DP**$^{2+}$]$_3$[**PPW**$^{3-}$]$_2$ showed comparable activity for the epoxidation of methyl oleate to homogeneous systems, we tested the oxidative cleavage as well. The catalyst loading had to be increased to 0.5 mol% to support the four oxidation steps involved in the cleavage.[28] The catalyst successfully cleaved methyl oleate into its two corresponding carboxylic acids with a yield of 89% at 90 °C for 24 hours. The reaction afforded no side product, and no sign of transesterification or saponification was observed.

2.4. Conclusion

We have produced an active heterogeneous catalyst for the oxidation of olefins and vegetable oils, which is selective, recyclable and easy to synthesize. This phosphotungsten catalyst was rendered insoluble by tuning the lipophilicity and charge of the counter-cation, instead of supporting it to a solid structure. We optimized the synthetic conditions to access the catalyst and used liquid and solid state ^{31}P MAS NMR to support our findings. The resulting catalyst has shown excellent activity and selectivity for the epoxidation of methyl oleate, linoleic acid, ricinoleic acid and cyclooctene. It afforded clean diols with other small alkenes. Finally, changing the conditions gave access to excellent yields for the full oxidative cleavage of methyl oleate. It was also recyclable by simple centrifugation, at least 5 times. Very limited leaching was measured, while a large-scale experiment of 13 mg was successfully performed. In short, we have discovered a new counter anion providing excellent activity, selectivity, recyclability and versatility in alkene and unsaturated oil oxidation.

2.5. Experimental Section

All chemicals used were analytical grade except otherwise noted. Chemicals were all bought from Sigma Aldrich and used as received. The phosphotungstic acid hydrate water content was determined by thermogravimetric analysis (TGA). ^{1}H-NMR spectra were measured with a 500 MHz Bruker AVIIIHD spectrometer at ambient temperature in D_2O, MeOD or $CDCl_3$ using TMS as the internal reference. ^{31}P MAS NMR spectra were measured using a 400 MHz Varian VNMRS with 4 mm zirconia rotors spinning at 13 kHz at 25 °C using $(NH_4)_2HPO_4$ as the reference. Tungsten leaching was measured using a Thermo Scientific iCAP Q ICP-MS. The water content of phosphotungstic acid hydrate was determined by using a TGA Q500 instrument under N_2 at a rate of 10 °C min^{-1}. GC-MS spectra were measured using an Agilent 7890A gas chromatograph connected to an Agilent 5975C MS instrument with a triple-axis detector. The column used is an HP-5MS UI (length: 30 m, diameter 0.25 mm, film of 0.25 μm). SEM analysis was performed using a FEI Inspect F-50 FE-SEM.

2.5.1. Synthesis of 4,4′-(trimethylene)bis(1-tetradecylpyridinium) dibromide $C_{41}H_{72}N_2Br_2$

4,4′-Trimethylenedipyridinium (3.9652 g, 20 mmol, 1 eq.) and 1-bromotetradecane (16.6368 g, 60 mmol, 3 eq.) were dissolved in 1-butanol (40 mL) and stirred at 120 °C for 48 h. The product was precipitated by diluting in ethyl acetate, then filtered and washed with pentane. The solid was then recrystallized in water, filtered and washed with acetone. 11.5482 g of a white solid was recovered (77% yield). ^{1}H NMR (500 MHz, $CDCl_3$) δ (ppm) = 0.89 (t, 6H, CH_3), 1.25 (m, 44H, CH_2), 2.00 (m, 4H, CH_2), 2.33 (q, 2H, CH_2), 3.12 (t, 4H, Pyr–CH_2), 4.76 (4H, N^+–CH_2), 8.18 (d, 4H, CH), 9.02 (d, 4H, N^+–CH). m/z = 296.28560.

2.5.2. Synthesis of the catalyst $(C_{41}H_{72}N_2)_3(PW_4O_{24})_2$

Phosphotungstic acid hydrate ($H_3PW_4O_{24}\cdot16H_2O$) (2.496 g, 0.80 mmol, 2 eq.) is dissolved in 15.9 mL H_2O_2 30% (159 mmol, 200 eq.), stirred at room temperature for 10 minutes, and then the solution is diluted with 15 mL of acetonitrile. A solution of 4,4′-(trimethylene)bis(1-tetradecylpyridinium) dibromide (300 mg, 0.40 mmol, 1 eq.) in 50 mL of acetonitrile is slowly added dropwise to the first solution, during which the product precipitates in solution. The mixture is stirred for 2 h at room temperature. The solid is filtered and washed with 20 mL of water and then 20 mL of acetonitrile. 465 mg recovered (86% yield). ^{31}P MAS NMR (400 MHz, 13 kHz spinning, $(NH_4)H_2PO_4$ as the chemical shift reference at 0 ppm) δ (ppm) = 3.47 (s), 1.51 (s).

2.5.3. Catalytic epoxidation of methyl oleate

Methyl oleate (500 mg, 1.69 mmol, 1 eq.), $(C_{41}H_{72}N_2)_3(PW_4O_{24})_2$ (7.6 mg, 0.0037 mmol) and H_2O_2 30% (222 µL, 2.23 mmol, 1.32 eq.) were added to a 20 mL flask and heated to 60 °C under vigorous stirring for 3 h. After the reaction, the mixture was filtered to remove the catalyst. The organic phase was analyzed by GC-MS and ^{1}H NMR.

2.5.4. Catalyst recycling method

Methyl oleate (500 mg, 1.69 mmol, 1 eq.), $(C_{41}H_{72}N_2)_3(PW_4O_{24})_2$ (34.4 mg, 0.0168 mmol, 0.01 eq.) and H_2O_2 30% (222 µL, 2.23 mmol, 1.32 eq.) were added to a 20 mL flask and heated to 60 °C under vigorous stirring for 2 h. After the reaction, the mixture was diluted with 10 mL of ethyl acetate and centrifuged at 8000 rpm for 20 minutes. Then both the organic and aqueous supernatants were removed using a pipette. The organic phase was filtered using filter paper and analyzed by GC-MS. The solid remaining in the flask was dried in air for 1 minute, and then reused.

2.5.5. Catalytic cleavage of methyl oleate

Methyl oleate (500 mg, 1.69 mmol, 1 eq.), $(C_{41}H_{72}N_2)_3(PW_4O_{24})_2$ (17.2 mg, 0.0084 mmol, 0.005 eq.) and H_2O_2 30% (1.01 mL, 10.12 mmol, 6 eq.) were added to a 20 mL flask and heated to 90 °C under vigorous stirring for 24 h. After the reaction, the organic phase was diluted with 10 mL of ethyl acetate and filtered to remove the catalyst. The aqueous phase was saturated with NaCl and the product was extracted three times with 10 mL ethyl acetate, dried using $MgSO_4$ and filtered. The organic phase was analyzed by GC-MS.

2.6. References

(1) Tuck, C. O.; Perez, E.; Horvath, I. T.; Sheldon, R. A.; Poliakoff, M., Valorization of Biomass: Deriving More Value from Waste. *Science* **2012,** *337*, 695-699.

(6) Meier, M. A. R.; Metzger, J. O.; Schubert, U. S., Plant oil renewable resources as green alternatives in polymer science. *Chem. Soc. Rev.* **2007,** *36*, 1788-1802.

(25) Kamata, K.; Yonehara, K.; Sumida, Y.; Hirata, K.; Nojima, S.; Mizuno, N., Efficient heterogeneous epoxidation of alkenes by a supported tungsten oxide catalyst. *Angew. Chem. Int. Ed.* **2011,** *50*, 12062-12066.

(26) Ishii, Y.; Yamawaki, K.; Ura, T.; Yamada, H.; Yoshida, T.; Ogawa, M., Hydrogen-Peroxide Oxidation Catalyzed by Heteropoly Acids Combined with Cetylpyridinium Chloride - Epoxidation of Olefins and Allylic Alcohols, Ketonization of Alcohols and Diols, and Oxidative Cleavage of 1,2-Diols and Olefins. *J. Org. Chem.* **1988,** *53*, 3587-3593.

(27) Duncan, D. C.; Chambers, R. C.; Hecht, E.; Hill, C. L., Mechanism and Dynamics in the $H_3[PW_{12}O_{40}]$-Catalyzed Selective Epoxidation of Terminal Olefins by H_2O_2 - Formation, Reactivity, and Stability of $(PO_4[WO(O_2)_2]_4)^{3-}$. *J. Am. Chem. Soc.* **1995,** *117*, 681-691.

(28) Sato, K.; Aoki, M.; Noyori, R., A "green" route to adipic acid: Direct oxidation of cyclohexenes with 30 percent hydrogen peroxide. *Science* **1998,** *281*, 1646-1647.

(29) Leng, Y.; Wu, J.; Jiang, P.; Wang, J., Amphiphilic phosphotungstate-paired ionic copolymer as a highly efficient catalyst for triphase epoxidation of alkenes with H_2O_2. *Catal. Sci. Technol.* **2014,** *4*, 1293.

(30) Leng, Y.; Zhao, J.; Jiang, P.; Wang, J., Amphiphilic polyoxometalate-paired polymer coated Fe_3O_4: magnetically recyclable catalyst for epoxidation of bio-derived olefins with H_2O_2. *ACS Appl. Mater. Interfaces* **2014,** *6*, 5947-5954.

(31) Yamada, Y. M. A.; Guo, H. Q.; Uozumi, Y., Tightly convoluted polymeric phosphotungstate catalyst: An oxidative cyclization of alkenols and alkenoic acids. *Org. Lett.* **2007,** *9*, 1501-1504.

(32) Khlebnikova, T. B.; Pai, Z. P.; Fedoseeva, L. A.; Mattsat, Y. V., Catalytic oxidation of fatty acids. II. Epoxidation and oxidative cleavage of unsaturated fatty acid esters containing additional functional groups. *React. Kinet. Catal. Lett.* **2009,** *98*, 9-17.

(36) Santacesaria, E.; Tesser, R.; Di Serio, M.; Turco, R.; Russo, V.; Verde, D., A biphasic model describing soybean oil epoxidation with H_2O_2 in a fed-batch reactor. *Chem. Eng. J.* **2011,** *173*, 198-209.

(47) Venturello, C.; Daloisio, R.; Bart, J. C. J.; Ricci, M., A New Peroxotungsten Heteropoly Anion with Special Oxidizing Properties: Synthesis and Structure of Tetrahexylammonium Tetra(Diperoxotungsto)Phosphate(3-). *J. Mol. Catal.* **1985,** *32*, 107-110.

(49) Chen, J. Z.; Hua, L.; Zhu, W. W.; Zhang, R.; Guo, L.; Chen, C.; Gan, H. M.; Song, B. N.; Hou, Z. S., Polyoxometalate anion-functionalized ionic liquid as a thermoregulated catalyst for the epoxidation of olefins. *Catal. Commun.* **2014,** *47*, 18-21.

(50) Ding, Y.; Zhao, W.; Hua, H.; Ma, B., $[\pi\text{-}C_5H_5N(CH_2)_{15}CH_3]_3[PW_4O_{32}]/H_2O_2$/ethyl acetate/alkenes: a recyclable and environmentally benign alkenes epoxidation catalytic system. *Green Chem.* **2008,** *10*, 910.

(51) Poli, E.; De Sousa, R.; Jerome, F.; Pouilloux, Y.; Clacens, J.-M., Catalytic epoxidation of styrene and methyl oleate over peroxophosphotungstate entrapped in mesoporous SBA-15. *Catal. Sci. Technol.* **2012,** *2*, 910-914.

(132) Tayde, S.; Patnaik, M.; Bhagt, S. L.; Renge, V. C., Epoxidation of vegetable oils: a review. *Int. J. Adv. Res. Technol.* **2011,** *2*, 491-501.

(133) Campanella, A.; Baltanas, M. A., Degradation of the oxirane ring of epoxidized vegetable oils in liquid-liquid systems: II. Reactivity with solvated acetic and peracetic acids. *Lat. Am. Appl. Res.* **2005,** *35*, 211-216.

(134) Venturello, C.; Daloisio, R., Quaternary Ammonium Tetrakis(Diperoxotungsto)Phosphates(3-) as a New Class of Catalysts for Efficient Alkene Epoxidation with Hydrogen-Peroxide. *J. Org. Chem.* **1988,** *53*, 1553-1557.

(135) Plault, L.; Hauseler, A.; Nlate, S.; Astruc, D.; Ruiz, J.; Gatard, S.; Neumann, R., Synthesis of dendritic polyoxometalate complexes assembled by ionic bonding and their function as recoverable and reusable oxidation catalysts. *Angew. Chem. Int. Ed.* **2004,** *43*, 2924-2928.

(136) Wu, J. H.; Jiang, P. P.; Leng, Y.; Ye, Y. Y.; Qin, X. J., Synthesis of dicationic alkyl imidazolium peroxopolyoxotungsten-based phase transfer catalyst and its catalytic activity for olefin epoxidation. *Chin. J. Catal.* **2013,** *34*, 2236-2244.

(137) Chen, Y.; Tan, R.; Zheng, W.; Zhang, Y.; Zhao, G.; Yin, D., Dendritic phosphotungstate hybrids efficiently catalyze the selective oxidation of alcohols with H_2O_2. *Catal. Sci. Technol.* **2014,** *4*, 4084-4092.

(138) Yamaguchi, K.; Yoshida, C.; Uchida, S.; Mizuno, N., Peroxotungstate immobilized on ionic liquid-modified silica as a heterogeneous epoxidation catalyst with hydrogen peroxide. *J. Am. Chem. Soc.* **2005,** *127*, 530-531.

(139) Qiao, Y. X.; Li, H.; Hua, L.; Orzechowski, L.; Yan, K.; Feng, B.; Pan, Z. Y.; Theyssen, N.; Leitner, W.; Hou, Z. S., Peroxometalates Immobilized on Magnetically Recoverable Catalysts for Epoxidation. *ChemPlusChem* **2012,** *77*, 1128-1138.

(140) Zheng, X. X.; Zhang, L.; Li, J. Y.; Luo, S. Z.; Cheng, J. P., Magnetic nanoparticle supported polyoxometalates (POMs) via non-covalent interaction: reusable acid catalysts and catalyst supports for chiral amines. *Chem. Commun.* **2011,** *47*, 12325-12327.

(141) Neumann, R.; Cohen, M., Solvent-anchored supported liquid phase catalysis: Polyoxometalate-catalyzed oxidations. *Angew. Chem. Int. Ed.* **1997,** *36*, 1738-1740.

(142) Maksimchuk, N. V.; Kovalenko, K. A.; Arzumanov, S. S.; Chesalov, Y. A.; Melgunov, M. S.; Stepanov, A. G.; Fedin, V. P.; Kholdeeva, O. A., Hybrid polyoxotungstate/MIL-101 materials: synthesis, characterization, and catalysis of H_2O_2-based alkene epoxidation. *Inorg. Chem.* **2010,** *49*, 2920-2930.

(143) Grigoropoulou, G.; Clark, J. H.; Elings, J. A., Recent developments on the epoxidation of alkenes using hydrogen peroxide as an oxidant. *Green Chem.* **2003,** *5*, 1-7.

(144) Kozhevnikov, I. V.; Mulder, G. P.; Steverink-de Zoete, M. C.; Oostwal, M. G., Epoxidation of oleic acid catalyzed by peroxo phosphotungstate in a two-phase system. *J. Mol. Catal. A: Chem.* **1998,** *134*, 223-228.

(145) Vasylyev, M. V.; Astruc, D.; Neumann, R., Dendritic Phosphonates and thein situ Assembly of Polyperoxophosphotungstates: Synthesis and Catalytic Epoxidation of Alkenes with Hydrogen Peroxide. *Adv. Synth. Catal.* **2005,** *347*, 39-44.

In the previous chapter we synthesized a greener heterogeneous catalyst for the purpose of biomass valorization through oxidation of vegetable oils. Following the same goal of designing greener catalysts, the next chapter delves into the subject of hydrogenation. The focus of this research is to improve the activity of heterogeneous Ru-catalyzed hydrogenation of arenes by using LSPR. This method is very advantageous since light is a clean source of energy that can be harnessed towards catalytic activity via the LSPR. This increased activity will allow for milder reaction conditions and reduced catalyst loadings, which results in a much greener catalyst.

3. Plasmon-enhanced hydrogenation with ruthenium on gold nanoparticles

This chapter is adapted from an article accepted for publication, with its corresponding citation below, which is reproduced with permission from the American Chemical Society and all co-authors.

Luis Carlos de la Garza, Nicolas Brodusch, Raynald Gauvin and Audrey Moores, "Plasmon-Enhanced Hydrogenation of 1-Dodecene and Toluene Using Ruthenium-Coated Gold Nanoparticles" ACS Applied Nano Materials, 2021, DOI: 10.1021/acsanm.0c03077

3.1. Abstract

While a key reaction for oil upgrade, the hydrogenation of arene substrates remains a challenging one, requiring the use of transition metal catalysts and harsher reaction conditions than classic hydrogenation processes. We designed a photocatalyst by deposition of Ru clusters onto plasmonic Au nanoparticles to accelerate this reaction, as well as the hydrogenation of alkene. Light irradiation triggered an order of magnitude increase in the reaction rate for the hydrogenation of dodecene and toluene at room temperature and under atmospheric to mild H_2 pressures. The localized surface plasmon resonance featured by the supporting Au nanoparticles explains this interesting reactivity and was fully characterization by electron energy loss spectroscopy (EELS). A potential mechanism is proposed to explain this light-induced reactivity enhancement.

3.2. Introduction

Aromatic content in fuels is known to decrease the quality of vehicle emissions, leading to increased carbon monoxide, particulate matter and black carbon emissions upon combustion.[146] Yet, reducing the content of aromatics from gasoline and diesel has remained a challenge because refinery streams rich in aromatics were a traditional source of high octane molecules.[146] Driven by environmental concerns, regulations in many countries now limit the content of aromatic molecules in fuels.[111] A key method to reduce aromatic content in traditional fuels is by hydrogenation.[112] However, aromatic compounds are difficult to hydrogenate due to the stabilization of π bonds by resonance,[114] which results in reaction conditions that typically require high H_2 pressures, high temperatures and the use of catalysts based on noble metals such as Ir, Rh, Ru and Pt.[115, 123-125] These systems proceed via H_2 splitting on the catalyst surface to form metal hydrides and also surface binding of the π system of aromatics, which allows the hydride to react with the substrate and initiate reduction.[113] Therefore, in recent years, research in this topic has been focused on improving the activity of catalysts which can hydrogenate aromatics at a high rate under milder conditions. In particular, researchers have focused their attention on Ru, as it offers an excellent compromise between good activity for this reaction, and the cheapest price among the platinum series.[119, 127-128] Key to its catalytic reactivity is the ability to sustain Ru as small nanoparticles (NPs) under reaction conditions. Among the effective strategies to achieve this goal are the use of ionic liquids as solvent and nanoparticle (NP) stabilizer[147-148] or the deposition of metals or metal NPs onto supports designed to affect the electronic properties of the catalysts, such as nanozeolites,[119] cellulose nanocrystals,[149] or triazine-based frameworks.[150] Yet, there is the need to continue on improving on the performances of such catalysts in order to reduce the energy footprint of such transformations.

The recent development of plasmonic catalysis offers opportunities to boost the activity of catalysts using light in the presence of localized surface plasmon resonance (LSPR) active NPs.[64, 151-156] LSPR is a physical phenomenon exhibited by metal NPs involving the collective oscillation of their conductive electrons in resonance with an incident electromagnetic wave. For Ag and Au NPs, this phenomenon is typically observed in the visible range. The LSPR is known to locally produce an enhanced electric field, photothermal heating, and hot carriers.[64] This strategy has proven particularly effective for the activation of O_2 and H_2.[157-158] Some examples of LSPR-enhanced activation are summarized in Scheme 14. Linic reported that the Ag NPs catalyzed ethylene epoxidation with O_2 was enhanced under light irradiation, as the LSPR allowed for the generation of hot electrons improving the rate of O_2 dissociation, i.e. the rate-limiting step for this reaction.[159] The plasmon enhanced activation of H_2 has also been intensely researched and used in catalysis, since the first discovery by the Halas group that the H_2 molecule could be dissociated on the Au NP surface under light irradiation.[160] Our group previously reported the use of LSPR to enhance the activity of Ag nanocube-catalyzed hydrogenation of carbonyls irradiated with visible light, which allowed the reaction to proceed under 1 atm of H_2,[161] whereas this reaction typically requires pressures upwards of 10 atm in absence of light excitation.[162-163] Halas also reported using Pd NPs decorated Al nanodisks for the partial hydrogenation of acetylene, where the LSPR improved both the reaction rate and the selectivity towards ethylene.[92] This work demonstrated that the activity of Pd, which is not plasmonic under visible light, can be influenced by the LSPR of the Al nanodisks serving as antennas.[92] The Carter group further established a mechanism involving field enhancement favoring hydrogen desorption being key in the observed selectivity.[164] The latter system relies on the principle that a catalyst that is already active for a particular reaction (Pd) can be improved by depositing it on the surface of a plasmonic NP (Al),[92] a principle widely applied to plasmonic catalysis.[151] Similar effects have been observed using bimetallic alloys, such as PdAu NPs,[105, 107] and more complex heterometallic structures promoting LSPR.[106]

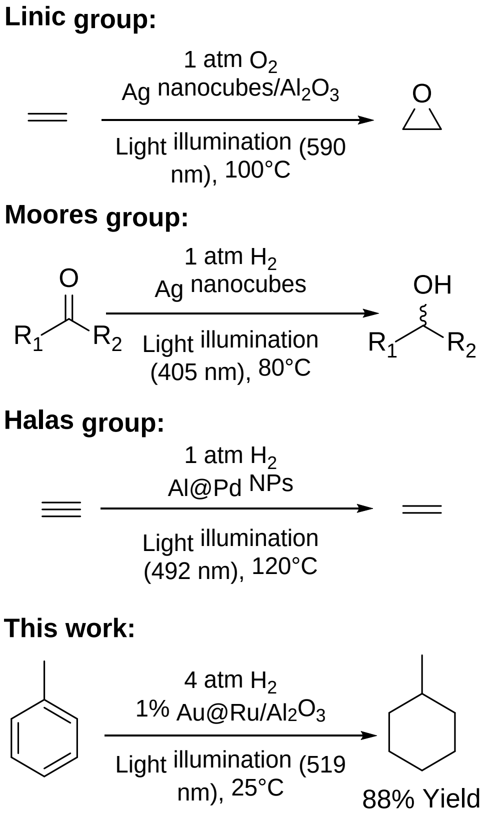

Scheme 14: Selected examples of LSPR-enhanced catalytic reactions.

With these precedents in mind, we developed a catalyst by combining non-plasmonic Ru with LSPR-active Au. Au was selected for its excellent stability and strong LSPR in the visible region. Ru on its front was chosen for its ability to catalyze effectively the difficult arene hydrogenation reaction. This system proved highly active for the hydrogenation of both arenes and alkenes under light irradiation with H_2 under mild conditions. While the system was active in darkness, its activity multiplied by a factor of 11 and 12 respectively for dodecene and toluene hydrogenation respectively, when irradiated by light centered on the plasmon band position of the nanocatalyst. We studied the plasmonic properties of the designed system using scanning transmission electron microscopy (STEM) – electron energy loss spectroscopy (EELS), which confirmed that LSPR influence is the most pronounced at the Au NPs surface and thus at the location of the Ru NPs. It serves as the first proof of concept for the use of LSPR activation in arene hydrogenation and for the use of Ru in a plasmonic catalysis scheme.

3.3. Results and discussion

3.3.1. Synthesis and characterization

For this project, we needed to access Au NPs able to absorb in the visible region in the 20-100 nm-diameter range and allow for the deposition of small Ru NPs in the <10 nm range. We tested a few synthetic strategies, including one step syntheses ones,[165] and selected the following multi-step method (Scheme 15), for its ability to form well-controlled nanomaterials with a narrow size range.

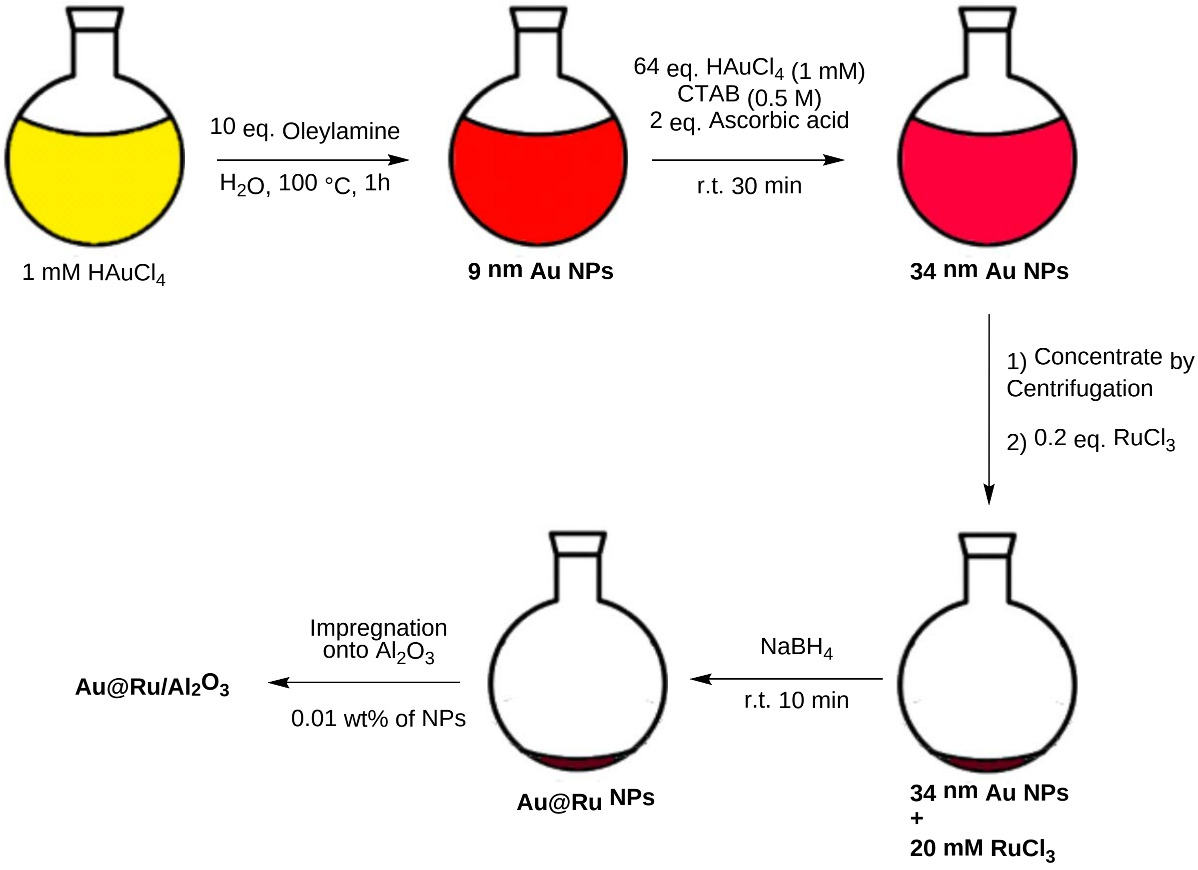

Scheme 15: Synthesis of $Au@Ru/Al_2O_3$.

Adapting known methodologies, we first accessed Au NP seeds by reducing $HAuCl_4$ with oleylamine in water at 100 °C.[166] Oleylamine performed a dual role as reductant and capping agent, which results in very uniform Au NPs of approximately 9 nm in diameter (see Figure 21 in appendix). The Au NPs were subsequently grown to roughly 34 nm in diameter by mixing the Au NP seeds with a growth solution composed of $HAuCl_4$ and hexadecyltrimethylammonium bromide (CTAB) then adding ascorbic acid as a reductant.[167] The resulting Au NP suspension was concentrated by centrifugation, in order to match the concentration requirements of the Ru deposition step. Indeed Ru deposition trials with high Au NPs dilutions failed in our hands to afford consistent Ru grown on Au surface. $RuCl_3$ was dissolved into the concentrated suspension of Au NPs with a 1:5 Ru:Au ratio. $RuCl_3$ was then reduced by adding an excess of $NaBH_4$. These NPs, named Au@Ru (core@shell), suspended very well in water. However both addition of water-miscible organic solvents or drying led to severe NPs aggregation. Aggregated Au NPs behave like bulk Au, which is not plasmonic, so it cannot be used for LSPR-enhanced catalysis.

Therefore, we supported the catalyst onto microparticulate Al_2O_3 by impregnation, thus immobilizing the catalyst and preventing aggregation during handling and catalytic tests. After screening several loadings and observing the results with TEM, we found that approximately 0.1 weight% of Au@Ru NPs to Al_2O_3 was the highest loading achievable without seeing the signs of Au@Ru NPs aggregation on the surface of the Al_2O_3. The resulting catalyst could be dried in vacuo and stored as a stable purple powder which could easily re-suspend in organic solvents, including hexane and methanol.

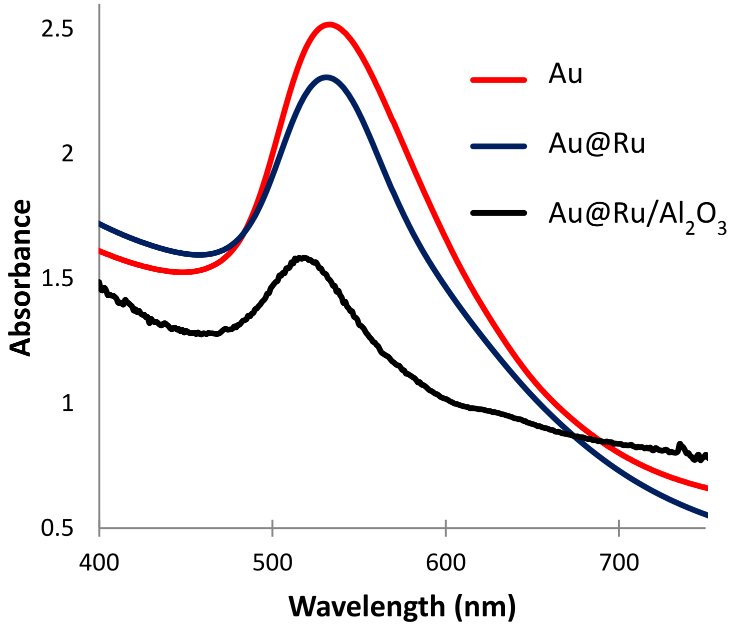

Figure 8: UV-Vis spectra of Au NPs, Au@Ru NPs and Au@Ru/Al_2O_3. Solid state UV-Vis of Au@Ru/Al_2O_3 was performed with a diffuse reflectance accessory and was scaled for visual clarity.

UV-vis spectroscopy of aqueous suspensions revealed that the synthesized Au@Ru NPs featured a strong LSPR band (Figure 8), as an absorbance peak at 535 nm, which is practically unchanged from the pristine Au NP absorbance peak at 537 nm. These numbers are comparable to the absorbances reported in the literature for Au NPs of similar sizes.[167] Once supported onto Al_2O_3, the peak was still clearly evident, although slightly shifted to 522 nm, as a consequence of the change in the dielectric medium of the environment caused by the presence of Al_2O_3.[168]

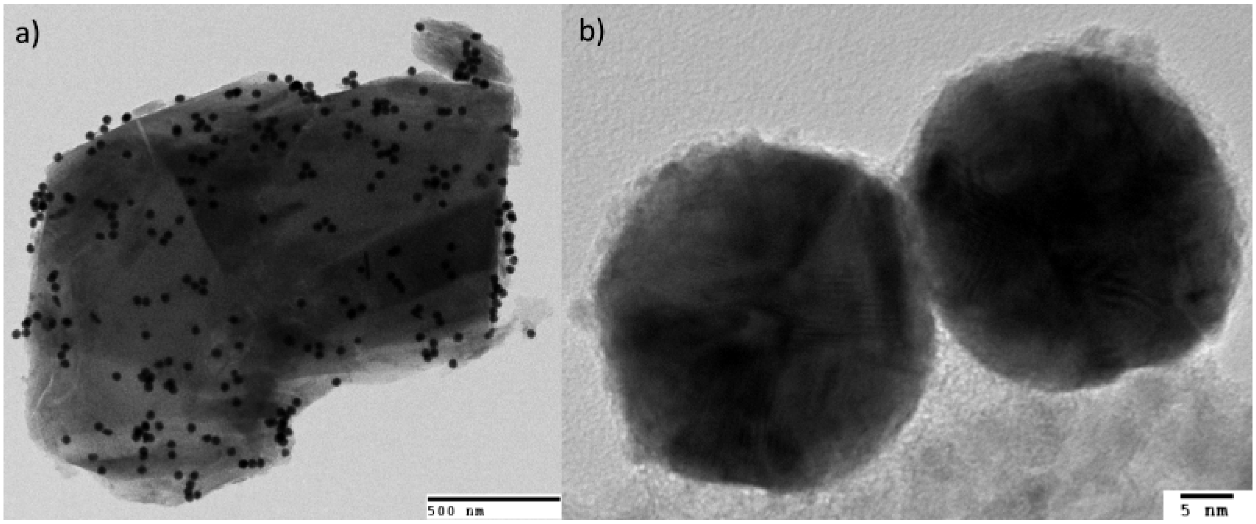

Figure 9: Bright-field TEM images of Au@Ru/Al_2O_3. a) Low magnification view showing Au@Ru NPs dispersed across Al_2O_3. b) High magnification view of Au@Ru NPs.

A transmission electron microscopy (TEM) study of Au@Ru/Al_2O_3 confirmed the formation of the desired NPs and their successful deposition onto Al_2O_3. The synthesized Au@Ru NPs had an average diameter of 34.3 nm with standard deviation of 1.8 nm (see Figure 22 in appendix) and the microparticulate Al_2O_3 was also in the expected size range of 150 mesh. As seen in Figure 9a, the Au@Ru NPs are well dispersed across the surface of the Al_2O_3, without any sign of NPs aggregation. Figure 9b features two Au@Ru NPs at high magnification, where the presence of Ru can be observed at the Au surface. Ru is present in the form of small clusters between 2 and 3 nm in diameter, seemingly fused together. Additional samples were prepared with a higher Ru loading of 1:2 Ru:Au to make the deposition more visually noticeable by TEM, (see Figure 23 in appendix). In these samples, the surface of the Au NPs is fully covered with Ru, with places where Ru grew away from the Au NP surface. The samples prepared at 1:2 Ru:Au loading were not tested for catalysis because the LSPR peak was significantly dampened.

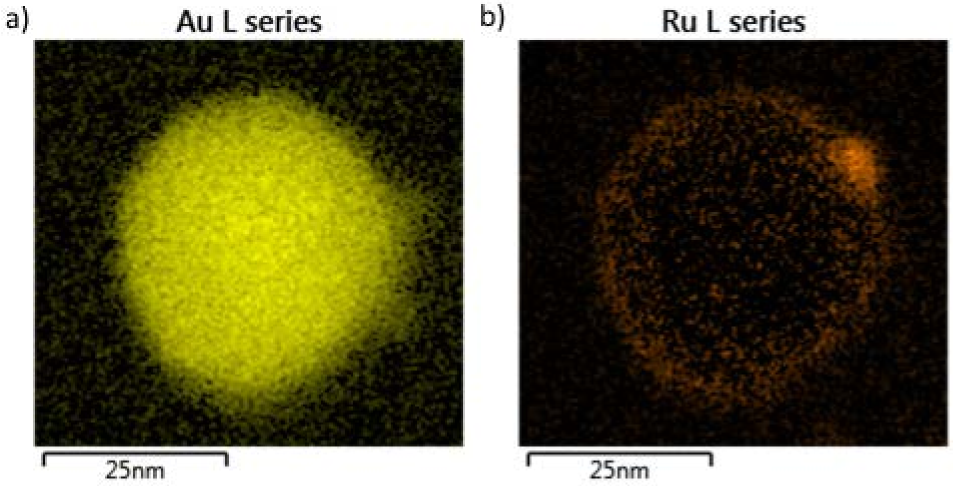

Figure 10: STEM-EDS images of Au@Ru NP. a) Au L signal b) Ru L signal.

In order to confirm that the layer observed at the surface of the Au NPs was indeed Ru, the catalyst Au@Ru/Al_2O_3 was also analyzed by low voltage STEM-energy dispersive spectroscopy (EDS). Figure 10 shows the EDS mapping across one Au@Ru NP. As seen in Figure 10a, the NP featured a uniformly strong signal for Au across the entire particle. Figure 10b shows that the Ru signal was also present on the entire particle, although with less intensity, as is expected for a surface-deposited material. A higher Ru intensity was observed at the edge of the particle indicating the presence of small Ru clusters on top of the Au NP. This confirmed that Ru was present on top of the Au NPs, and it was well distributed along the surface.

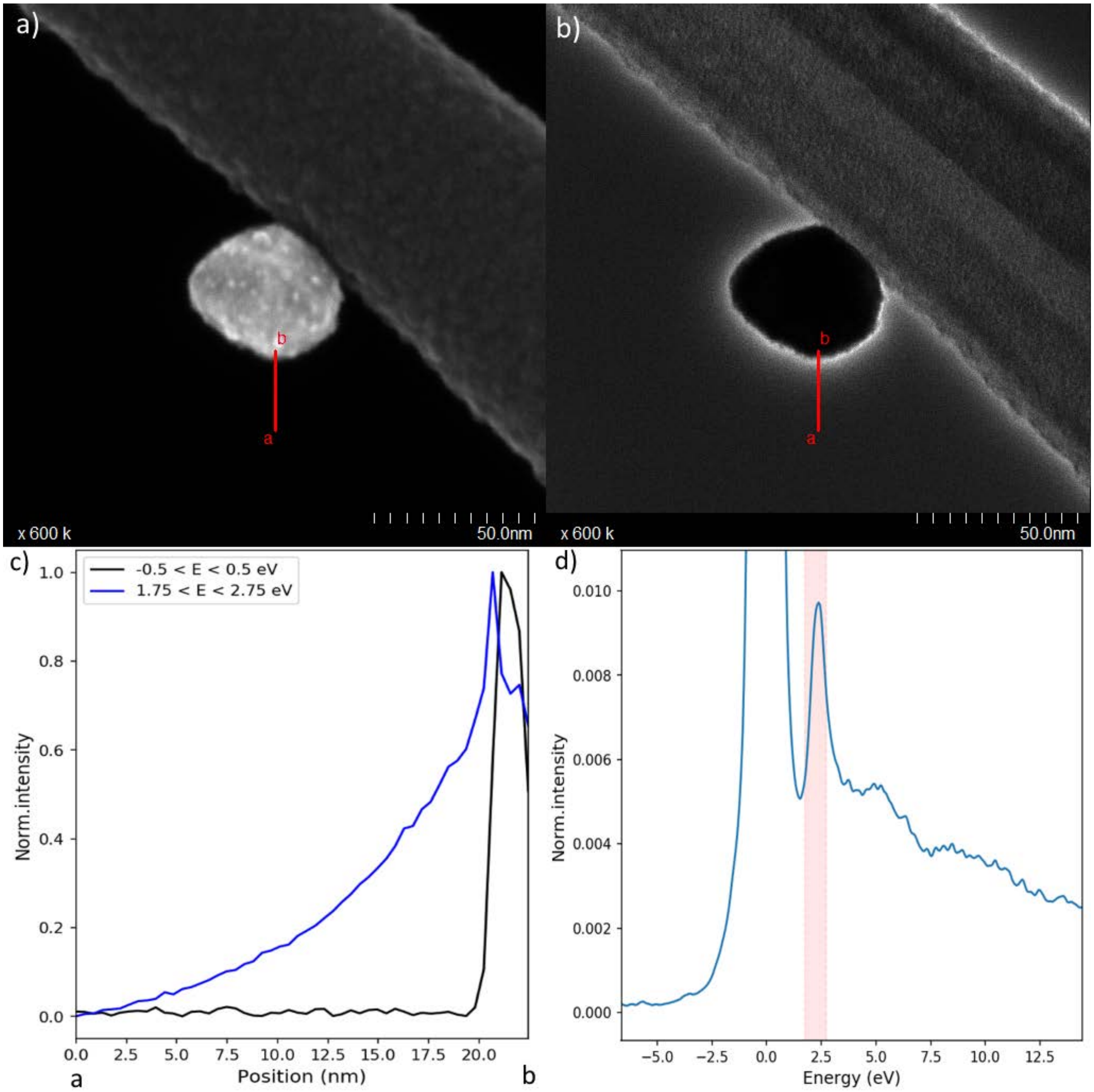

Figure 11: STEM-EELS analysis of Au@Ru/Al_2O_3. a) SE-SEM image of a Au@Ru NP onto Al_2O_3. b) Corresponding EF-STEM-EELS image of the same NP. Only electrons with energy at the Au LSPR position were collected (pink region in d). c) EELS line profile of 4a for the zero-loss peak (black) and the LSPR (blue). Points a and b in figure c are the position marked on images a) and b). d) Low-loss EELS spectrum at the surface of the Au@Ru NP, LSPR peak region centered on 2.36 eV is highlighted in red.

In order to gain further insight into the optical properties of Au@Ru/Al_2O_3 catalysts a STEM-EELS analysis was undergone. First the samples were analyzed by secondary electron SEM (SE-SEM, Figure 11a) revealing the granular surface of Au@Ru NP, as a result of the non-uniform deposition of Ru at the surface of Au, and consistent with STEM-EDS results. Comparatively pristine Au NPs featured a smooth surface (see Figure 24 in appendix). The same particle was then analyzed with energy-filtered STEM-EELS images (EF-STEM-EELS), whereby only electrons of the LSPR energy are collected (Figure 11b). The bright regions are the ones with the most intense LSPR field, and are right at the vicinity of the Au@Ru NP surface. Moving away from the surface, the LSPR intensity exponentially decays, as can be seen from the EELS line-scan in Figure 11c, blue line. Positions a and b in the graph's x-axis correspond to the a and b positions in Figure 11a and Figure 11b. The addition of Ru onto the Au NPs did not affect their LSPR properties, which is consistent with the UV-vis results (Figure 8). The EELS spectrum in Figure 11d taken at the surface of the NP showed a sharp peak at 2.36 eV, which is equivalent to 525 nm and corresponded to the LSPR of Au@Ru NPs and is in accordance with the absorbance peak at 522 nm measured by diffuse reflectance UV-vis. These results confirmed that the Ru NPs at the surface of Au NPs were located in a region of high LSPR intensity upon irradiation at the resonance wavelength.

3.3.2. Catalytic Results

The Au@Ru/Al_2O_3 catalyst was tested for the hydrogenation of alkenes and arenes at room temperature under mild pressures of H_2 (1 and 4 atm). 1-dodecene and toluene were used as model substrates. Photocatalytic tests were performed using green light-emitting diodes (LEDs) with emission at 519 nm (Figure 25 in appendix), a value close to the LSPR band of the catalyst measured at 522 nm.

Table 4: Hydrogenation of 1-dodecene.

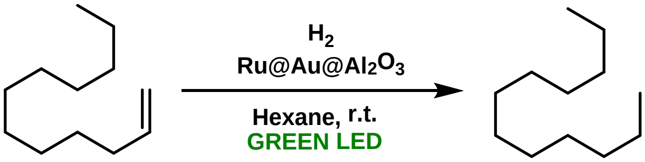

Entry	Ru load (mol%)	Pressure (atm)	Irradiation	Time (h)	Yield	TOF (h^{-1})
1	0.05	4	None	1	8.8%	176
2	0.05	4	Green LEDs	1	97%	1940
3	0.05	4	Red LEDs	1	9%	179
4	0.0025	4	Green LEDs	24	100%	1670
5	0.2	1	Green LEDs	1.5	98%	326
6	0[a]	4	Green LEDs	1	0%	0

Reaction conditions: 100 µL of 1-dodecene in 4 mL of hexane. 88 µL of decane used as internal standard.

[a] Control test using Au/Al_2O_3 without Ru.

The catalyst proved to be effective at hydrogenating 1-dodecene at 4 atm of H_2 and room temperature (Table 4). Control tests without irradiation were performed by wrapping the reaction flask with aluminium foil and keeping it in the dark. Under these conditions, a low conversion of 8.8% in 1 hour was observed (entry 1). However, when green light was applied, activity immediately increased by 11 fold (entry 2), to reach a conversion of 97% in 1 hour and a TOF of 1940. This proves that the LSPR definitely affects this reaction, improving the reaction rate. As seen in entry 3, irradiation with red-colored LEDs featuring an emission peak of 630 nm (Figure 26 in appendix), which does not overlap with the LSPR band at 522 nm, showed similar activity to the control test performed in the dark, which further corroborates that the increase in activity under green light is due to the LSPR. Entry 4 shows full conversion obtained after 24h with a loading of 0.0025 mol% Ru. The calculated TOF of 1670h^{-1}, corresponding to a TON of 40000 for a 24h runtime, revealed a high stability for the catalyst. Lastly, the catalyst was also able to hydrogenate 1-dodecene at 1 atm of H_2 and room temperature as seen in entry 5, albeit with a slower reaction rate due to the lower pressure, a highly appealing feature for this reaction. Control test with Au/Al_2O_3 resulted in no hydrogenation at all at 4 bars (entry 6). The lack of activity of Au/Al_2O_3 proves that Au is unable to perform the hydrogenation without Ru. UV-Vis characterization of Au/Al_2O_3 revealed an absorbance peak at 522 nm (Figure 27 in appendix). We also performed STEM-EELS measurements of Au NPs alone, and found that they featured plasmonic enhancement in the vicinity of the nanoparticle (Figure 28 in appendix), similarly to $Au@Ru/Al_2O_3$. Both results indicate the LSPR of the Au core is virtually is unaffected by the presence of Ru.Therefore, for the active catalyst $Au@Ru/Al_2O_3$, Au functions as an antenna to harness the LSPR, which enhances the activity of Ru.

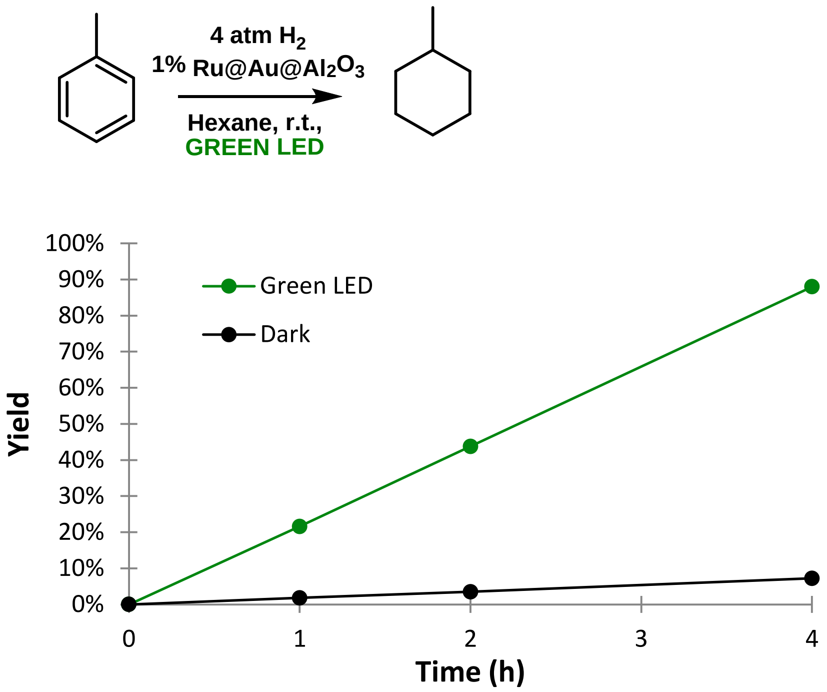

Figure 12: Toluene hydrogenation with and without light irradiation.

We then turned to aromatic hydrogenations under the mild pressure of 4 atm at room temperature. We observed good activity at 1 mol% Ru loading. Similar to the case with 1-dodecene, the exposure to green light increased the reaction rate of the hydrogenation of toluene by an order of magnitude (Figure 12). The hydrogenation of toluene showed a nearly constant TOF of 22 when irradiated with green LEDs, and a TOF of 1.8 in the dark, which is consistent with the zero-order rate with respect to the substrate, as expected of aromatic hydrogenations at room temperature.[113] GC-MS analysis of the product did not show any presence of methylcyclohexadienes or methylcyclohexene, and confirmed the catalyst was selective for the complete hydrogenation. This suggests that the LSPR increased the reaction rate of all the intermediate hydrogenation steps between toluene and methylcyclohexane, consistent with the increased reaction rate observed for 1-dodecene. Indeed once aromaticity is disrupted by the first hydrogenation, the subsequent reduction steps are easier to perform.

The reaction rate profile of Ru-catalyzed hydrogenation of arenes is known to change with increase in temperature, as higher temperatures weaken the chemisorption of substrates on the surface of Ru. Notably, above 100 °C the rate order of aromatics substrates is no longer zero.[113] The reaction rate profile of toluene hydrogenation under LSPR in our experiments was consistent with the rate profile observed in the dark, which suggests we do not have any photothermal effect. Indeed, if we did, we would expect local heating higher than 100 °C causing a rate order change. We also did not observe any photothermal collective heating,[169] as the reaction vessel remained at room temperature for the entire reaction. Since the reaction selectivity is unaffected by the LSPR effect, the rate of desorption of the substrates was not affected by light, unlike in other plasmonic systems.[164] Therefore the LSPR is likely to be enhancing the reaction rate by lowering the activation energy required for hydrogenation, either due to the enhanced electric field or by means of hot electrons, as previously reported.[160-161]

3.3. Conclusion

We have successfully deposited nanoparticulate metallic ruthenium on the surface of plasmonic gold NPs. The LSPR from the Au NPs was shown to improve the reaction rate of Ru-catalyzed hydrogenations of alkenes and arenes with H_2, allowing for the reaction to be performed at room temperature and low pressures. This system serves as a proof of concept for the developed of plasmon activated Ru-based catalysts.

3.4. Experimental Section

3.4.1. Materials

All chemicals used were analytical grade except otherwise noted. Chemicals were all bought from Sigma Aldrich and used as received.

3.4.2. Characterization techniques

GC-MS spectra were measured using an Agilent 7890A gas chromatography connected to an Agilent 5975C MS instrument with triple-axis detector. The column used is an HP-1MS UI (length: 30m, diameter 0.25 mm, film of 0.25μm). UV-Vis spectra were measured using a Cary 5000 UV-Vis-NIR spectrophotometer. For solid samples, UV-vis spectra were measured with a Praying Mantis Diffuse Reflectance accessory. LEDs used for photocatalysis were a 5 meter Laimante RGB LEDs strip with output of DC 12V/2.5A with 150 LEDs. Half of the strip was set in the inside of a bowl for a total of 75 LEDs aimed towards the reaction vessel. Emission spectrum of green and red light included in supporting information.

Bright-field TEM images were obtained using a Philips CM200 TEM with an accelerating voltage of 200 kV. SEM, STEM and EELS measurements were obtained using a Hitachi SU-9000 cold field emission SEM. The electron beam accelerating voltage was set to 30 kV. The SE image was obtained using the in-lens electron detector. The microscope has a commercial magnetic prism spectrometer for EELS detection provided by Hitachi (Hitachi High-Technologies, Japan) located below the high-angle annular dark-field (HAADF), bright-field (BF) STEM detectors. The spectrometer collection aperture was 5 mrad.

The EELS system consisted in a charge-coupled device (CCD) of 1024 (dispersion axis) × 256 pixels with pixel dimensions of 24 μm connected to an Yttrium Aluminum Garnet (YAG) scintillator to collect the energy dispersed scattered electrons permitting spectral imaging (SI) acquisitions. Energy-filtered images were collected via a “three-windows” detector[170] where the signal of each window was acquired with a single YAG scintillator. The dispersion used to acquire the EELS spectrum and energy-filtered images was 0.055 eV/channel. More information regarding the design of the integrated EELS system in the SU-9000 CFE-SEM was reported elsewhere.[171-172]

The EDS detector was an Extreme XMax silicon drift detector from Oxford Instrument installed on the Hitachi SU-9000 SEM/STEM. The nominal effective detector crystal collection area was 100 mm^2.

3.4.3. Synthesis of 9 nm Au NP seeds

This method was adapted from Aslam *et al.*[166] Chloroauric acid (63 mg, 0.18 mmol) was mixed with oleylamine (650 mg, 1.77 mmol) in 80 mL of deionized water and heated to 100 °C for 1h. The red suspension of Au NPs was sonicated and used as-is for the growth step.

3.4.4. Synthesis of 36 nm Au NPs

This method was adapted from Jana *et al.*[167] A growth solution was prepared by mixing chloroauric acid (50 mg, 0.14 mmol) with hexadecyltrimethyl ammonium bromide (500 mg, 1.37 mmol) in 100 mL of deionized water. A reductant solution was prepared separately by dissolving ascorbic acid (50 mg, 0.28 mmol) in 4 mL of deionized water. The growth was performed by 4 successive steps. 1 mL of the suspension of Au NP seeds was mixed with 25 mL of growth solution under stirring. Then 1 mL of the reductant solution was added and stirred for 5 minutes. The process was repeated 3 times by adding 25 mL of growth solution followed by 1 mL of reductant solution and stirred for 5 minutes each time. The resulting suspension was concentrated down to 3 mL via centrifugation and removal of the supernatant with a pipette.

3.4.5. Synthesis of Au@Ru NP

Ruthenium chloride monohydrate (6.5 mg, 0.029 mmol) was dissolved in 1 mL of deionized water. This solution was added to the 3 mL suspension of 36 nm Au NPs within the centrifuge tube and sonicated for 5 minutes. Sodium borohydride (10 mg, 0.27 mmol) was dissolved in 1 mL of deionized water and immediately added to the solution of $RuCl_3$ and Au NPs. The addition of $NaBH_4$ generates a large amount of foam, so the bottle was capped and vortexed for 10 minutes.

3.4.6. Synthesis of Au@Ru/Al_2O_3

The suspension of Au@Ru NPs was diluted to 10 mL by addition of deionized water and further sonicated. This solution was added drop by drop onto 46 g of Brockmann I basic Al_2O_3 on a 1 L beaker, distributing the suspension evenly across the solid. The mixture was stirred with a spatula until the powder looks evenly colored. Hexane was added to cover all the powder (approximately 50 mL) and subsequently acetone was added to remove the water from the alumina (approximately 50 mL) until the powder no longer clumps together. The product was then filtered, washed with a 1:1 mixture of acetone and hexane, and then dried under vacuum.

3.4.7. Hydrogenation of 1-dodecene

1-dodecene (100 μL, 0.45 mmol) was mixed with decane (88 μL, 0.45 mmol) as internal standard and 360 mg of $Au@Ru/Al_2O_3$ (0.0002 mmol Ru) in 4 mL of hexane into a thick-walled borosilicate glass round-bottom flask, connected to a pressurized hydrogen cylinder, equipped with a relief valve set to 4 atm (Figure 29 in appendix). The system was vacuumed for 20 seconds and then filled with 4 atm of H_2. The reaction was stirred at room temperature for 1 hour irradiated with green LEDs. The product was filtered and analyzed via GC-MS.

3.4.8. Hydrogenation of toluene

Toluene (500 μL, 4.7 mmol) was mixed with decane (500 μL, 2.4 mmol) as internal standard in 9 mL hexane to make a 0.47 M solution. 50 μL of this solution (0.024 mmol) was mixed with 377 mg of $Au@Ru/Al_2O_3$ (0.00024 mmol Ru) with 4 mL of hexane into a thick-walled borosilicate glass round-bottom flask, connected to a pressurized hydrogen cylinder, equipped with a relief valve set to 4 atm. The system was vacuumed for 20 seconds and then filled with 4 atm of H_2. The reaction was stirred at room temperature irradiated with green LEDs. The product was filtered and analyzed via GC-MS.

3.5. References

(64) Gelle, A.; Jin, T.; de la Garza, L.; Price, G. D.; Besteiro, L. V.; Moores, A., Applications of Plasmon-Enhanced Nanocatalysis to Organic Transformations. *Chem. Rev.* **2020,** *120*, 986-1041.

(92) Swearer, D. F.; Zhao, H. Q.; Zhou, L. N.; Zhang, C.; Robatjazi, H.; Martirez, J. M. P.; Krauter, C. M.; Yazdi, S.; McClain, M. J.; Ringe, E., *et al.*, Heterometallic antenna-reactor complexes for photocatalysis. *Proc. Natl. Acad. Sci. U.S.A.* **2016,** *113*, 8916-8920.

(105) Zhao, X. Y.; Long, R.; Liu, D.; Luo, B. B.; Xiong, Y. J., Pd-Ag alloy nanocages: integration of Ag plasmonic properties with Pd active sites for light-driven catalytic hydrogenation. *J. Mater. Chem. A* **2015,** *3*, 9390-9394.

(106) Quiroz, J.; Barbosa, E. C.; Araujo, T. P.; Fiorio, J. L.; Wang, Y.-C.; Zou, Y.-C.; Mou, T.; Alves, T. V.; de Oliveira, D. C.; Wang, B., *et al.*, Controlling Reaction Selectivity over Hybrid Plasmonic Nanocatalysts. *Nano Lett.* **2018,** *18*, 7289-7297.

(107) Gangishetty, M. K.; Fontes, A. M.; Malta, M.; Kelly, T. L.; Scott, R. W. J., Improving the rates of Pd-catalyzed reactions by exciting the surface plasmons of AuPd bimetallic nanotriangles. *RSC Adv.* **2017,** *7*, 40218-40226.

(111) Ravindra, K.; Sokhi, R.; Grieken, R. V., Atmospheric polycyclic aromatic hydrocarbons: Source attribution, emission factors and regulation. *Atmos. Environ.* **2008,** *42*, 2895-2921.

(112) Sassykova, L. R., Development of Catalysts for the Hydrogenation of the Aromatic Ring in Gasolines. *Chem. Biochem. Eng. Q.* **2017,** *31*, 447-453.

(113) Schoenmaker-Stolk, M. C.; Verwijs, J. W.; Don, J. A.; Scholten, J. J. F., The catalytic hydrogenation of benzene over supported metal catalysts: I. Gas-phase hydrogenation of benzene over ruthenium-on-silica. *Appl. Catal.* **1987,** *29*, 73-90.

(114) Stanislaus, A.; Cooper, B. H., Aromatic Hydrogenation Catalysis: A Review. *Catal. Rev. Sci. Eng.* **1994,** *36*, 75-123.

(115) Dyson, P. J.; Ellis, D. J.; Welton, T.; Parker, D. G., Arene hydrogenation in a room-temperature ionic liquid using a ruthenium cluster catalyst. *Chem. Commun.* **1999**, 25-26.

(119) Zahmakıran, M.; Tonbul, Y.; Özkar, S., Ruthenium(0) Nanoclusters Stabilized by a Nanozeolite Framework: Isolable, Reusable, and Green Catalyst for the Hydrogenation of Neat Aromatics under Mild Conditions with the Unprecedented Catalytic Activity and Lifetime. *J. Am. Chem. Soc.* **2010,** *132*, 6541-6549.

(123) Jacquin, M.; Jones, D. J.; Rozière, J.; Albertazzi, S.; Vaccari, A.; Lenarda, M.; Storaro, L.; Ganzerla, R., Novel supported Rh, Pt, Ir and Ru mesoporous alumino silicates as catalysts for the hydrogenation of naphthalene. *Appl. Catal. A* **2003,** *251*, 131-141.

(124) Zhou, G.; Jiang, L.; Dong, Y.; Li, R.; He, D., Engineering the exposed facets and open-coordinated sites of brookite TiO_2 to boost the loaded Ru nanoparticle efficiency in benzene selective hydrogenation. *Appl. Surf. Sci.* **2019,** *486*, 187-197.

(125) Alsalahi, W.; Tylus, W.; Trzeciak, A. M., Green Synthesis of Rhodium Nanoparticles that are Catalytically Active in Benzene Hydrogenation and 1-Hexene Hydroformylation. *ChemCatChem* **2018,** *10*, 2051-2058.

(127) Livingstone, S. E., The Chemistry of Ruthenium, Rhodium, Palladium, Osmium, Iridium and Platinum. *Pergamon Press*, 1973; Vol. 25.

(128) Hageluken, C., Markets for the catalyst metals platinum, palladium and rhodium. *Metall* **2006,** *60*, 31-42.

(146) Karavalakis, G.; Short, D.; Vu, D.; Russell, R.; Hajbabaei, M.; Asa-Awuku, A.; Durbin, T. D., Evaluating the Effects of Aromatics Content in Gasoline on Gaseous and Particulate Matter Emissions from SI-PFI and SIDI Vehicles. *Environ. Sci. Technol.* **2015,** *49*, 7021-7031.

(147) Silveira, E. T.; Umpierre, A. P.; Rossi, L. M.; Machado, G.; Morais, J.; Soares, G. V.; Baumvol, I. J.; Teixeira, S. R.; Fichtner, P. F.; Dupont, J., The partial hydrogenation of benzene to cyclohexene by nanoscale ruthenium catalysts in imidazolium ionic liquids. *Chem. Eur. J.* **2004,** *10*, 3734-3740.

(148) Dyson, P. J.; Ellis, D. J.; Henderson, W.; Laurenczy, G., A Comparison of Ruthenium-Catalysed Arene Hydrogenation Reactions in Water and 1-Alkyl-3-methylimidazolium Tetrafluoroborate Ionic Liquids. *Adv. Synth. Catal.* **2003,** *345*, 216-221.

(149) Kaushik, M.; Friedman, H. M.; Batemana, M.; Moores, A., Cellulose nanocrystals as non-innocent supports for the synthesis of ruthenium nanoparticles and their application to arene hydrogenation. *RSC Adv.* **2015,** *5*, 53207-53210.

(150) Siebels, M.; Schlüsener, C.; Thomas, J.; Xiao, Y.-X.; Yang, X.-Y.; Janiak, C., Rhodium nanoparticles supported on covalent triazine-based frameworks as re-usable catalyst for benzene hydrogenation and hydrogen evolution reaction. *J. Mater. Chem. A* **2019,** *7*, 11934-11943.

(151) Araujo, T. P.; Quiroz, J.; Barbosa, E. C. M.; Camargo, P. H. C., Understanding plasmonic catalysis with controlled nanomaterials based on catalytic and plasmonic metals. *Curr. Opin. Colloid Interface Sci.* **2019,** *39*, 110-122.

(152) Li, S.; Miao, P.; Zhang, Y.; Wu, J.; Zhang, B.; Du, Y.; Han, X.; Sun, J.; Xu, P., Recent Advances in Plasmonic Nanostructures for Enhanced Photocatalysis and Electrocatalysis. *Adv Mater* **2020**, 2000086.

(153) Zhan, C.; Moskovits, M.; Tian, Z.-Q., Recent Progress and Prospects in Plasmon-Mediated Chemical Reaction. *Matter* **2020,** *3*, 42-56.

(154) Liang, C.; Lu, Z.-A.; Wu, J.; Chen, M.-X.; Zhang, Y.; Zhang, B.; Gao, G.-L.; Li, S.; Xu, a. P., Recent Advances in Plasmon-Promoted Organic Transformations Using Silver-Based Catalysts. *ACS Appl. Mater. Interfaces* **2020,** *12*, 54266–54284.

(155) Meng, L.; Chen, Z.; Ma, Z.; He, S.; Hou, Y.; Li, H.-H.; Yuan, R.; Huang, X.-H.; Wang, X.; Wang, X., *et al.*, Gold plasmon-induced photocatalytic dehydrogenative coupling of methane to ethane on polar oxide surfaces. *Energy Environ. Sci.* **2018,** *11*, 294-298.

(156) Zhao, J.; Liu, B.; Meng, L.; He, S.; Yuan, R.; Hou, Y.; Ding, Z.; Lin, H.; Zhang, Z.; Wang, X., *et al.*, Plasmonic control of solar-driven CO_2 conversion at the metal/ZnO interfaces. *Appl. Catal. B* **2019,** *256*, 117823.

(157) Silva, A. G. M. d.; Rodrigues, T. S.; Correia, V. G.; Alves, T. V.; Alves, R. S.; Ando, R. A.; Ornellas, F. R.; Wang, J.; Andrade, L. H.; Camargo, P. H. C., Plasmonic Nanorattles as Next-Generation Catalysts for Surface Plasmon Resonance-Mediated Oxidations Promoted by Activated Oxygen. *Angew. Chem. Int. Ed.* **2016,** *55*, 7111-7115.

(158) Barbosa, E. C. M.; Fiorio, J. L.; Mou, T.; Wang, B.; Rossi, L. M.; Camargo, P. H. C., Reaction Pathway Dependence in Plasmonic Catalysis: Hydrogenation as a Model Molecular Transformation. *Chem. Eur. J.* **2018,** *24*, 12330-12339.

(159) Christopher, P.; Xin, H.; Marimuthu, A.; Linic, S., Singular characteristics and unique chemical bond activation mechanisms of photocatalytic reactions on plasmonic nanostructures. *Nat. Mater.* **2012,** *11*, 1044-1050.

(160) Mukherjee, S.; Libisch, F.; Large, N.; Neumann, O.; Brown, L. V.; Cheng, J.; Lassiter, J. B.; Carter, E. A.; Nordlander, P.; Halas, N. J., Hot Electrons Do the Impossible: Plasmon-Induced Dissociation of H_2 on Au. *Nano Lett.* **2013,** *13*, 240-247.

(161) Landry, M. J.; Gellé, A.; Meng, B. Y.; Barrett, C. J.; Moores, A., Surface-Plasmon-Mediated Hydrogenation of Carbonyls Catalyzed by Silver Nanocubes under Visible Light. *ACS Catal.* **2017,** *7*, 6128-6133.

(162) Li, A. Y.; Kaushik, M.; Li, C.-J.; Moores, A., Microwave-Assisted Synthesis of Magnetic Carboxymethyl Cellulose-Embedded Ag-Fe_3O_4 Nanocatalysts for Selective Carbonyl Hydrogenation. *ACS Sustain. Chem. Eng.* **2016,** *4*, 965-973.

(163) Claus, P., Selective hydrogenation of alpha,beta-unsaturated aldehydes and other C=O and C=C bonds containing compounds. *Top. Catal.* **1998,** *5*, 51-62.

(164) Spata, V. A.; Carter, E. A., Mechanistic insights into photocatalyzed hydrogen desorption from palladium surfaces assisted by localized surface plasmon resonances. *ACS Nano* **2018,** *12*, 3512-3522.

(165) Hou, P. F.; Liu, H.; Li, J. L.; Yang, J., One-pot synthesis of noble metal nanoparticles with a core-shell construction. *CrystEngComm* **2015,** *17*, 1826-1832.

(166) Aslam, M.; Fu, L.; Su, M.; Vijayamohanan, K.; Dravid, V. P., Novel one-step synthesis of amine-stabilized aqueous colloidal gold nanoparticles. *J. Mater. Chem.* **2004,** *14*, 1795-1797.

(167) Jana, N. R.; Gearheart, L.; Murphy, C. J., Seeding growth for size control of 5-40 nm diameter gold nanoparticles. *Langmuir* **2001,** *17*, 6782-6786.

(168) Moores, A.; Goettmann, F., The plasmon band in noble metal nanoparticles: an introduction to theory and applications. *New J. Chem.* **2006,** *30*, 1121-1132.

(169) Baffou, G.; Bordacchini, I.; Baldi, A.; Quidant, R., Simple experimental procedures to distinguish photothermal from hot-carrier processes in plasmonics. *Light Sci. Appl.* **2020,** *9*, 1-16.

(170) Williams, D. B.; Carter, B., Transmission Electron Microscopy: Diffraction, Imaging, and Spectroscopy. *Springer*, 2016.

(171) Yamazawa, Y.; Okada, S.; Yasenjiang, Z.; Sunaoshi, T.; Kaji, K., The First Results of the Low Voltage Cold-FE SEM/STEM System Equipped With EELS. *Microsc. Microanal.* **2016,** *22*, 50-51.

(172) Brodusch, N.; Demers, H.; Gellé, A.; Moores, A.; Gauvin, R., Electron energy-loss spectroscopy (EELS) with a cold-field emission scanning electron microscope at low accelerating voltage in transmission mode. *Ultramicroscopy* **2018,** *203*, 21-36.

In the previous chapter we successfully applied LSPR to enhance the catalytic activity of Ru-catalyzed hydrogenations of alkenes and arenes. The design of the catalyst used Au NPs as an antenna to harness the LSPR effect onto the active catalyst Ru, which was grown at the surface of the plasmonic NPs. Now that this application for LSPR has been validated, we intend to further improve this catalyst by replacing Au with Al, which can also form plasmonic NPs. With Al being the most abundant metal on Earth, and therefore much cheaper and more sustainable than Au, we intend to produce a greener catalyst.

4. Plasmon-enhanced hydrogenation with ruthenium on aluminium nanoparticles

This chapter is adapted from an article in preparation.

Luis Carlos de la Garza, Nicolas Brodusch, Raynald Gauvin and Audrey Moores, "Plasmon-enhanced hydrogenation of alkenes and arenes using ruthenium-decorated aluminium nanoparticles", (manuscript in preparation).

4.1. Abstract

The hydrogenation of aromatic compounds is a challenging reaction which requires transition metal catalysts as well as high temperatures and pressures of H_2. We synthesized a new photocatalyst by deposition of Ru clusters onto plasmonic Al NPs with the intent to make a greener catalyst for this reaction. Ru decorations were grown onto Al NPs with sizes ranging between 170 nm and 230 nm in diameter and tested for hydrogenation of styrene under light irradiation. Unfortunately, our catalyst did not exhibit rate-enhancement towards hydrogenation when irradiating the catalyst with visible light. Characterization done by EELS revealed that the LSPR of our Al NPs was below wavelength of 200 nm, which was unsuitable for aromatic hydrogenations. This highly energetic LSPR was not in accordance with literature reports of Al NPs synthesized with the same methodology, as well as similar size, shape and capping agents. Further research tuning the LSPR absorbance of Al NPs will be required before they can be applied for aromatic hydrogenations.

4.2. Introduction

Hydrogenation reactions are an important class of chemical transformations with wide variety of applications from fine chemicals, pharmaceutical synthesis and industrial applications, be it by direct reaction with gaseous H_2 or via transfer hydrogenation.[173] In particular, hydrogenation has a massive economic and environmental impact as a method used to decrease aromatic content of fuels, since aromatics have been reported to decrease the quality of vehicle emissions which has led to aromatic content in fuels being regulated.[111, 146]

Direct hydrogenation of aromatic molecules is typically performed using noble metal catalysts such as Ir, Rh, Ru and Pt, and commonly require high temperatures and H_2 pressures to be effective.[115, 123-125] Ru in particular has received attention because it offers great catalytic activity while being the cheapest metal of the platinum series.[119, 127-128] To make these reactions more favorable there are several strategies aimed at increasing the reactivity of the active catalytic species in order to reduce the amount of catalyst necessary, as well as performing the reaction under milder conditions. One strategy is to utilize Localized Surface Plasmon Resonance (LSPR) to enhance the activity of Ru deposited at the surface of a plasmonic nanoparticle, which acts like an antenna. LSPR is a characteristic of metal nanoparticles that generates a collective oscillation of the conductive electrons at their surface when irradiated with an electromagnetic wave at a specific resonant wavelength, which depends on the material, morphology and size of the nanoparticles.[64] The plasmonic nanoparticles show a strong absorption of light at their resonant wavelength and produce an enhanced electric field at the surface, which can be harnessed by nearby molecules.

We recently reported that LSPR was effective at enhancing the reaction rate of Ru-based hydrogenations of alkenes and arenes by depositing Ru onto Au nanoparticles, supported on Al_2O_3.[174] In this paper we intend to extend this application by replacing gold with aluminium in order to make a potentially greener catalyst, due to the advantage of Al being the most abundant metal on Earth. Research of earth abundant metals that are effective at sustaining LSPR has been recently become more prevalent, with Al receiving the most attention, although other metals like Cu and Mg are also worth studying.[79] Aluminium nanoparticles have been reported to be viable LSPR antennae, with nanoparticles below 100 nm in diameter typically having their LSPR in the UV while nanoparticles larger than 100 nm have their LSPR peak within the visible range.[72, 175] Aluminium nanoparticles coated with Pd and Cu_2O have both been reported to be able to harness the LSPR towards catalytic reactions using visible light.[92, 176]

4.3. Results and discussion

4.3.1. Synthesis and characterization

Aluminium nanoparticles were synthesized following a published method[177] consisting of a thermal decomposition of N,N-dimethylethylamine alane under air-free conditions in a

THF/dioxane mixture using titanium tetraisopropoxide as a catalyst. The size of the nanoparticles was controlled between 80 ±6 and 300 ±20 nm in diameter by changing the amount of catalyst used and THF/dioxane ratio in the solvent. This method does not require any capping agents to control the nucleation and growth of the nanoparticles, and results in well-dispersed particles that are fairly uniform. Since the reaction is performed without air, the nanoparticles produced are pure Al(0).

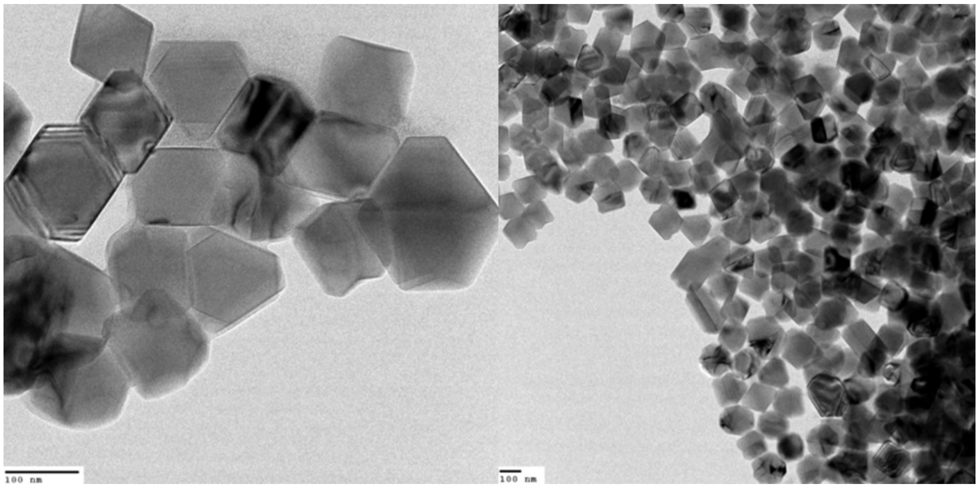

Figure 13: TEM images of Al NPs capped with oleic acid.

It is well known that aluminium will always form a thin layer of aluminium oxide when exposed to air, typically between 3 and 7 nm thick. Therefore, nanoparticles that are larger than 10 nm in diameter will form a core-shell composite with a thin layer of aluminium oxide at the surface and pure aluminium at the core. This layer of aluminium oxide prevents further oxidation of the aluminium underneath, effectively passivating the surface. Therefore, it has been reported that aluminium nanoparticles can be exposed to air without any further protection. However, in all of the experiments we carried out, we found this passivating layer to be insufficient to properly protect the aluminium nanoparticles. Upon exposure to air, all of our uncapped nanoparticles would oxidize almost entirely, with the majority of the sample becoming an agglomerated oxide, and only a few nanoparticles left, surrounded by uneven amounts of oxide (see Figure 30 in appendix).

Although exposure to air should only generate a self-passivating oxide shell around the Al NPs, aluminium also reacts violently with water.[178] Therefore, for the sake of making a stable product that we could handle outside of a glove-box we chose to add capping agents our aluminium nanoparticles to protect them from any moisture present in the air or solvents used in subsequent reactions. We were able to successfully produce aluminium nanoparticles capped with oleic acid, and the TEM images of the resulting nanoparticles are in accordance with the results observed in the literature (Figure 13).[177] We also did a subsequent ligand exchange with citric acid to improve the dispersion of these nanoparticles, since oleic acid capped nanoparticles would only disperse well in oily solvents such as hexadecane, whereas citric acid capped nanoparticles dispersed well in multiple solvents such as ethanol, ethylene glycol and ethyl acetate, which facilitated the deposition of ruthenium onto the Al NPs and subsequent hydrogenation reactions.

Ruthenium was deposited onto the surface of the aluminium nanoparticles by polyol reduction of ruthenium chloride, following a procedure published by Halas and coworkers.[68] As seen in Figure 14, the ruthenium grows preferably on the surface of the aluminium nanoparticles. Importantly, the amount of ruthenium added needed to be controlled to obtain a uniform layer, as otherwise Ru continues to grow onto itself. So we kept the ruthenium loading at 2 mol% with respect to aluminium, which results in very little aggregation.

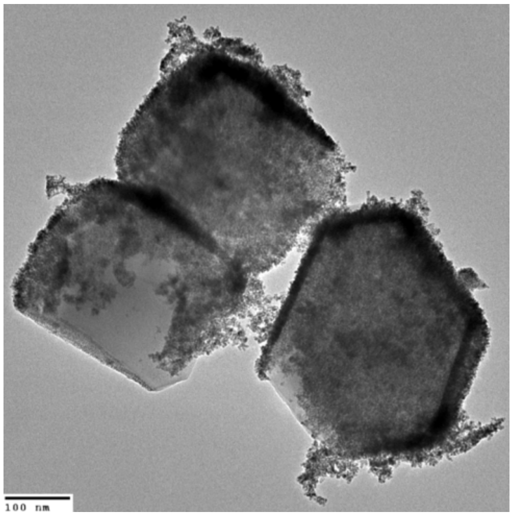

Figure 14: TEM image of Ru@Al NPs.

UV-vis characterization was performed on several samples of Al NPs, as shown in Figure 15. Three samples were selected with average sizes of 172 nm, 217 nm and 232 nm, as they appeared to have some small peaks in the visible spectrum.

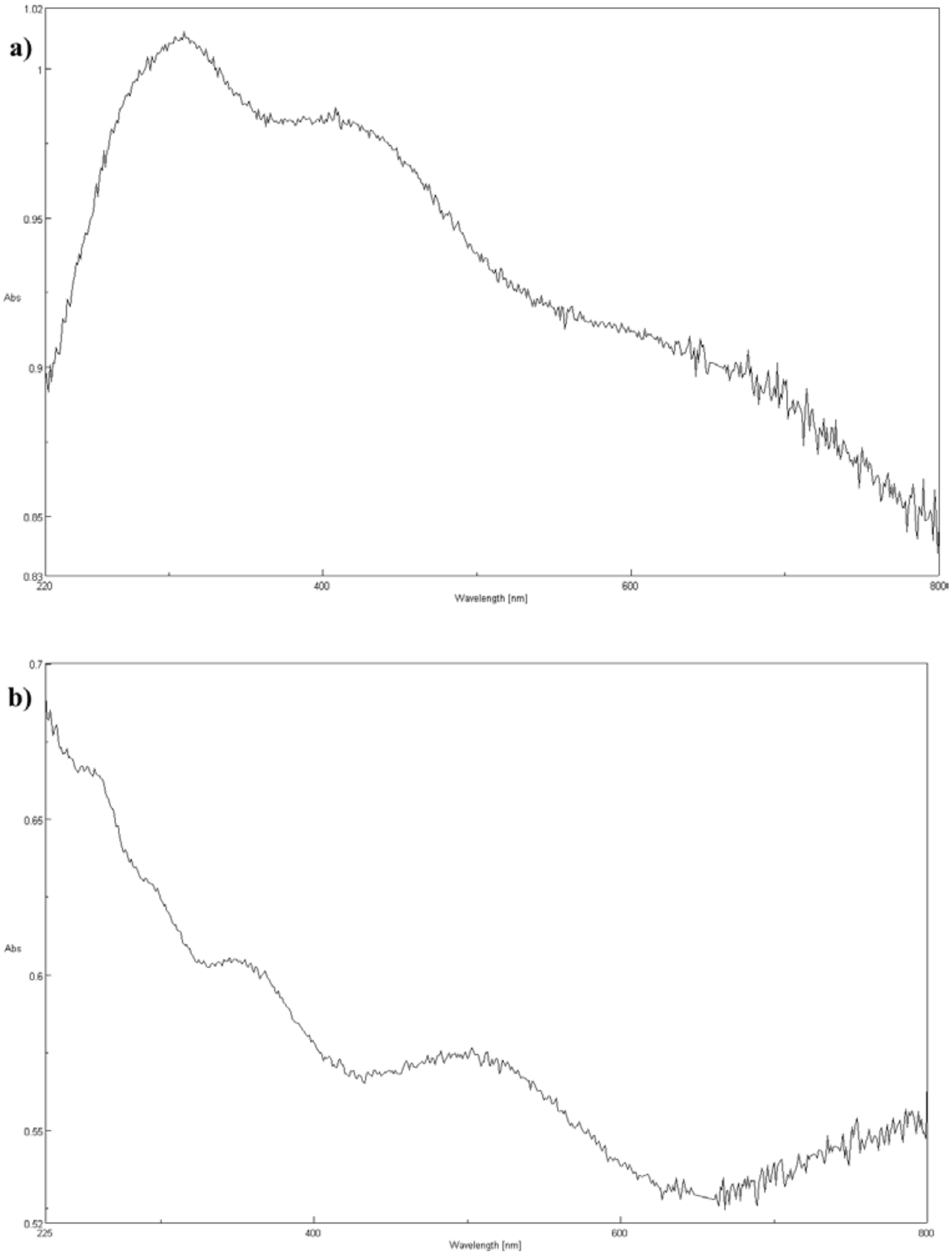

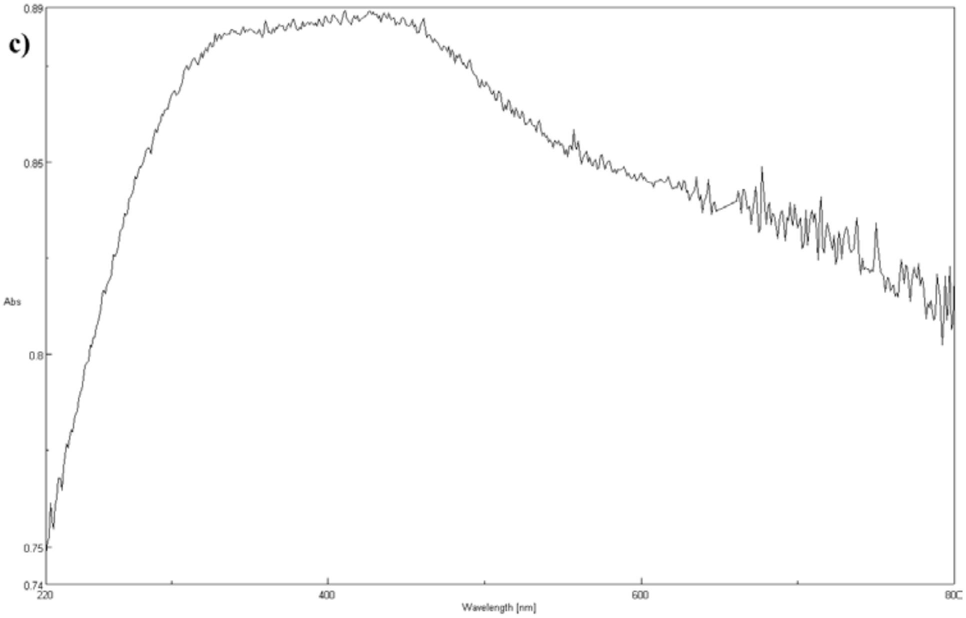

Figure 15: UV-vis analysis of Al NPs with average sizes of a) 172 nm, b) 217 nm, c) 232 nm.

Al NPs were also characterized by electron energy loss spectroscopy (EELS), as seen in Figure 16. Energy-filtered EELS spectra show that the LSPR is definitely present. EELS mapping at the edge and corner show the LSPR of aluminium nanoparticles with diameter of 153 nm to be present between 6.4 and 7.5 eV, which translates to an absorbance of wavelengths between 165 and 194 nm.

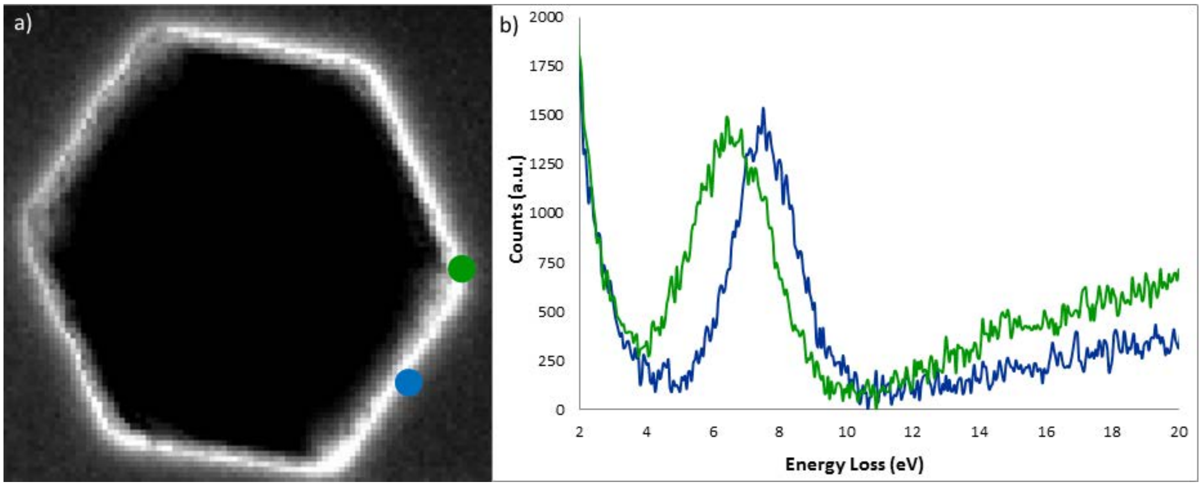

Figure 16: EELS images of Al NP. a) Energy-filtered EELS image showing the LSPR of an Al NP, highlighting a spot at the edge of the NP and a spot at the side of the NP. b) EELS spectrum of the surface of the Al NP. Green line corresponds to the edge (green point in 3a). Blue line corresponds to the side (blue point in 3a).

4.3.2. Catalytic results

Based on literature reports, Al NPs above 100 nm in diameter were expected to have an LSPR at wavelengths between 400 nm and 500 nm, and the LSPR should be red-shifted with larger NP size.[72, 177] Therefore, preliminary catalytic tests were carried out using a Kessil PR-160 blue colored lamp with an emission centered at 427 nm to irradiate the Ru@Al NPs during the hydrogenation of styrene.

Table 5: Hydrogenation of styrene

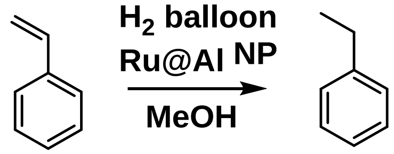

Catalyst	NP Size (nm)	T (°C)	Time (min)	Ru (%mol)	Irradiation (400 nm)	Yield
1	172	30	30	0.5	No	32%
					Yes	37%
2	217	50	20	0.2	No	6%
					Yes	8%
3	232	50	20	3.5	No	76%
					Yes	89%

Three different catalysts were tested with different diameters and Ru loadings in an attempt to optimize the parameters for this reaction. The size of the catalysts used for catalysis were purposely larger than 150 nm since it is known that the LSPR red-shifts with larger NP sizes.[72] The Ru@Al NP catalysts were all able to hydrogenate the double bond of styrene to form ethylbenzene, but the aromatic ring was not hydrogenated under these conditions. As shown in Table 5, all three samples showed a marginal increase in catalytic activity when exposed to light. However, based on results previously obtained with Ru@Au NPs,[174] such a small increase in activity cannot be attributed to LSPR-enhancement, and is most likely due to a small increase in temperature of the reaction flask from the heat generated by the lamp itself. There was also no activity observed when using Al NPs without Ru.

Based on the results obtained from EELS, it’s clear that the samples of Ru@Al NPs produced for these tests have LSPR absorbance below the wavelengths of visible light, even at Al NP diameters above 200 nm. The lack of LSPR enhancement is simply due to the irradiation light not lining up with the absorbance peak. However, since aromatic molecules have absorptions within the entire UV range,[179] these type of LSPR-enhanced photocatalysts need to have absorbance in the visible range to be effective, so performing the hydrogenation with a UV lamp is not viable. Therefore, more research is required in order to tune the LSPR absorption peak of the Al NPs.

4.4. Conclusion

Aluminium nanoparticles decorated with ruthenium were successfully synthesized and tested for alkene and aromatic hydrogenation. However, none of our catalyst samples showed LSPR within the expected range of wavelengths and we were unable to use the LSPR to improve the activity of Ru-based hydrogenations with these samples.

4.5. Experimental Section

All chemicals used were analytical grade except otherwise noted. Chemicals were all bought from Sigma Aldrich and used as received. GC-MS spectra were measured using an Agilent 7890A gas chromatography connected to an Agilent 5975C MS instrument with triple-axis detector. The column used is an HP-1MS UI (length: 30m, diameter 0.25 mm, film of 0.25μm). UV-Vis spectra were measured using a Cary 5000 UV-Vis-NIR spectrophotometer.

4.5.1. Synthesis of aluminium nanoparticles

6.5 mL of a 0.5M toluene solution of N,N-dimethylethylamine alane (3.25 mmol) was added to a schlenk flask under argon with 25 mL of degassed THF. 4 mL of a 1.22M solution of titanium isopropoxide in toluene was quickly injected and stirred at room temperature for 16 hours. Then 1 g of oleic acid in 5 mL of degassed THF was injected into the flask, stirred for 5 minutes, then centrifuged. The product was re-dispersed in 20 mL of THF with 500 mg of anhydrous citric acid and stirred for 2 minutes, then centrifuged and washed twice with THF. Product was analyzed by TEM.

4.5.2. Synthesis of Ru@Al NPs

44 mg of Al NPs were mixed with 17 mg of $RuCl_3$ (0.08 mmol) in 40 mL of ethylene glycol under argon and heated to 160°C for 1 hour. The product was centrifuged and washed with ethanol three times.

4.5.3. Hydrogenation of styrene with Ru@Al NPs

320 mg of styrene (3.07 mmol) were mixed with 10 mg of Ru@Al NPs (0.0154 mmol of Ru) and 5 mL of ethanol in a sealed flask. The flask was degassed and refilled with H_2 using a balloon filled with H_2 and stirred for 30 minutes at 30°C. The solution was filtered and analyzed by GC-MS.

4.6. References

(64) Gelle, A.; Jin, T.; de la Garza, L.; Price, G. D.; Besteiro, L. V.; Moores, A., Applications of Plasmon-Enhanced Nanocatalysis to Organic Transformations. *Chem. Rev.* **2020,** *120,* 986-1041.

(68) Swearer, D. F.; Leary, R. K.; Newell, R.; Yazdi, S.; Robatjazi, H.; Zhang, Y.; Renard, D.; Nordlander, P.; Midgley, P. A.; Halas, N. J., *et al.*, Transition-Metal Decorated Aluminum Nanocrystals. *ACS Nano* **2017,** *11,* 10281-10288.

(72) Knight, M. W.; King, N. S.; Liu, L.; Everitt, H. O.; Nordlander, P.; Halas, N. J., Aluminum for Plasmonics. *ACS Nano* **2014,** *8*, 834-840.

(79) Biggins, J. S.; Yazdi, S.; Ringe, E., Magnesium Nanoparticle Plasmonics. *Nano Lett.* **2018,** *18*, 3752-3758.

(92) Swearer, D. F.; Zhao, H. Q.; Zhou, L. N.; Zhang, C.; Robatjazi, H.; Martirez, J. M. P.; Krauter, C. M.; Yazdi, S.; McClain, M. J.; Ringe, E., *et al.*, Heterometallic antenna-reactor complexes for photocatalysis. *Proc. Natl. Acad. Sci. U.S.A.* **2016,** *113*, 8916-8920.

(111) Ravindra, K.; Sokhi, R.; Grieken, R. V., Atmospheric polycyclic aromatic hydrocarbons: Source attribution, emission factors and regulation. *Atmos. Environ.* **2008,** *42*, 2895-2921.

(115) Dyson, P. J.; Ellis, D. J.; Welton, T.; Parker, D. G., Arene hydrogenation in a room-temperature ionic liquid using a ruthenium cluster catalyst. *Chem. Commun.* **1999**, 25-26.

(119) Zahmakıran, M.; Tonbul, Y.; Özkar, S., Ruthenium(0) Nanoclusters Stabilized by a Nanozeolite Framework: Isolable, Reusable, and Green Catalyst for the Hydrogenation of Neat Aromatics under Mild Conditions with the Unprecedented Catalytic Activity and Lifetime. *J. Am. Chem. Soc.* **2010,** *132*, 6541-6549.

(123) Jacquin, M.; Jones, D. J.; Rozière, J.; Albertazzi, S.; Vaccari, A.; Lenarda, M.; Storaro, L.; Ganzerla, R., Novel supported Rh, Pt, Ir and Ru mesoporous alumino silicates as catalysts for the hydrogenation of naphthalene. *Appl. Catal. A* **2003,** *251*, 131-141.

(124) Zhou, G.; Jiang, L.; Dong, Y.; Li, R.; He, D., Engineering the exposed facets and open-coordinated sites of brookite TiO_2 to boost the loaded Ru nanoparticle efficiency in benzene selective hydrogenation. *Appl. Surf. Sci.* **2019,** *486*, 187-197.

(125) Alsalahi, W.; Tylus, W.; Trzeciak, A. M., Green Synthesis of Rhodium Nanoparticles that are Catalytically Active in Benzene Hydrogenation and 1-Hexene Hydroformylation. *ChemCatChem* **2018,** *10*, 2051-2058.

(127) Livingstone, S. E., The Chemistry of Ruthenium, Rhodium, Palladium, Osmium, Iridium and Platinum. *Pergamon Press*, 1973; Vol. 25.

(128) Hageluken, C., Markets for the catalyst metals platinum, palladium and rhodium. *Metall* **2006,** *60*, 31-42.

(146) Karavalakis, G.; Short, D.; Vu, D.; Russell, R.; Hajbabaei, M.; Asa-Awuku, A.; Durbin, T. D., Evaluating the Effects of Aromatics Content in Gasoline on Gaseous and Particulate Matter Emissions from SI-PFI and SIDI Vehicles. *Environ. Sci. Technol.* **2015,** *49*, 7021-7031.

(173) Wang, D.; Astruc, D., The Golden Age of Transfer Hydrogenation. *Chem. Rev.* **2015,** *115*, 6621-6686.

(174) Garza, L. C. d. l.; Brodusch, N.; Gauvin, R.; Moores, A., Plasmon-enhanced hydrogenation of alkenes and arenes using Ruthenium-coated Gold nanoparticles. *ACS Appl. Nano.* **2020**, Submitted.

(175) Honda, M.; Kumamoto, Y.; Taguchi, A.; Saito, Y.; Kawata, S., Efficient UV photocatalysis assisted by densely distributed aluminum nanoparticles. *J. Phys. D: Appl. Phys.* **2015,** *48*, 1-6.

(176) Robatjazi, H.; Zhao, H.; Swearer, D. F.; Hogan, N. J.; Zhou, L.; Alabastri, A.; McClain, M. J.; Nordlander, P.; Halas, N. J., Plasmon-induced selective carbon dioxide conversion on earth-abundant aluminum-cuprous oxide antenna-reactor nanoparticles. *Nat. Commun.* **2017,** *8*, 27.

(177) McClain, M. J.; Schlather, A. E.; Ringe, E.; King, N. S.; Liu, L.; Manjavacas, A.; Knight, M. W.; Kumar, I.; Whitmire, K. H.; Everitt, H. O., *et al.*, Aluminum Nanocrystals. *Nano Lett.* **2015,** *15*, 2751-2755.

(178) Bunker, C. E.; Smith, M. J.; Fernando, K. A. S.; Harruff, B. A.; Lewis, W. K.; Gord, J. R.; Guliants, E. A.; Phelps, D. K., Spontaneous Hydrogen Generation from Organic-Capped Al Nanoparticles and Water. *ACS Appl. Mater. Inter*. **2010,** *2*, 11-14.

(179) Jones, R. N., The ultraviolet absorption spectra of aromatic hydrocarbons. *Chem. Rev.* **1942,** *1*, 1-46.

5. Conclusions and Future Work

Our attempts to make greener catalysts were successful both for vegetable oil oxidation and LSPR-enhanced hydrogenation.

The goal of the research presented in chapter 2 was to develop a recyclable heterogeneous catalyst for the selective epoxidation of fatty acids that retained the activity of homogeneous peroxophosphotungstates. Our catalyst was able to perform the epoxidation under fairly mild conditions and be recycled to obtain record TON numbers. Our catalyst was also able to cleave fatty acids by increasing the temperature without any other modifications. First, the analysis performed using ^{31}P MAS NMR allowed us to identify the reason why heterogeneous catalysts across the literature showed lower activity than homogeneous catalysts. Namely, the immobilization of the phosphotungstates prevents the formation of the fully peroxidized phosphotungstate *in situ*. Therefore, Venturello's catalyst needs to be formed prior to immobilization to obtain the most active catalyst. Second, we were able to optimize the synthesis method to ensure the formation of highly peroxidized species, resulting in a highly active heterogeneous catalyst. Most notably, using MeCN as co-solvent with an excess of aqueous H_2O_2 was a crucial step in improving the degree of peroxidation of the catalyst, compared to MeOH, $CHCl_3$ and H_2O. A slow addition of the phase transfer agent was absolutely necessary as well, in order to minimize the formation of inactive tungstate species $(C_{41}H_{72}N_2)(WO_6)$, which can be tracked qualitatively by color, since this species was bright orange whereas the active catalyst was white. These improvements in characterization and synthesis can also be applied to other types of heterogeneous peroxophosphotungstates and should be very useful for the development of the field.

The goal of the research presented in chapter 3 was to employ the LSPR to enhance the activity of Ru-based hydrogenation of arenes, which was successful. First, we were able to develop a method to support Ru on Au NPs by modifying reported procedures to support Pd and Pt on Au NPs. In particular, the suspension needed to be concentrated significantly before the Ru precursor was reduced; otherwise the Ru would not grow on the surface of the Au NPs. Second, we were able to enhance the reaction rate of hydrogenations by irradiating the catalyst with green-colored light, with the irradiation wavelength set to overlap with the LSPR peak of the Au

NPs. Reaction rates under LED irradiation were approximately 11 times higher than the reaction rates observed in the dark. This proves that using the antenna-reactor couple can harness light via LSPR to augment Ru hydrogenations. The reaction rate of arene hydrogenation remained zero order both in the dark and under light irradiation, which suggests that the rate enhancement via LSPR is not related to a change in the substrate's chemisorption or due to localized heating. So we hypothesize that the LSPR lowers the activation energy required for hydrogenation. However, we were not able to confirm if this effect is due to the enhanced electric field or the influence of hot electrons.

The goal of the research presented in chapter 4 was to extend the applicability of LSPR enhanced hydrogenations by switching Au NPs for Al NPs. Indeed Al is both the most abundant metal on Earth and an LSPR active metal, which makes it a good candidate for greener and cheaper antenna-reactor systems. We were successful at supporting Ru on Al NPs, but we were not successful in harnessing the LSPR of Al NPs, which led to negative catalytic results. According to our EELS characterization, all of the Al NPs we synthesized appeared to have LSPR absorption peaks below 200 nm. Although it may be possible to perform plasmon-enhanced hydrogenations under UV light, wavelengths below 200 nm are too energetic for many organic substrates, which can result in substrates degrading to the exposure of UV light. Aromatics in particular are known for absorbing UV light, which would cause interference for the NPs to absorb the light. More research is clearly needed to tune the wavelength of the LSPR peak towards the visible light, or at least near-UV. Since the LSPR of Al NPs is known to red-shift when the proportion of oxide increases, a possible avenue to tune the LSPR is to increase the thickness of the oxide shell. Several literature reports on Al NPs with features similar to ours report absorbance peaks in the visible range, so this research might also be continued in collaboration with other researchers working in the field of Al NP synthesis.

On the topic of peroxophosphotungstate catalysts, there is still a very important issue that demands further research before this type of catalyst can be considered to be really superior to peroxyacids. Since the purpose of making the catalyst recyclable is to lower the production costs of the reaction, the long-term stability of the peroxophosphotungstate species needs to be addressed. In our experiments, we were able to notice a clear decline in the efficiency of the catalyst after 1300 turnovers, independently from the number of times the catalyst was recycled.

We were also unable to find literature reports showing higher TON either with homogeneous or heterogeneous peroxophosphotungstates, which leads us to believe that the catalyst may be degrading after that threshold. Therefore, further research is necessary to figure out exactly how and why the catalyst activity drops in order to establish some solutions to regenerate the catalyst or prevent its degradation. In that vein, there are reports of non-peroxidized phosphotungstate catalysts made by immobilizing phosphotungstic acid directly which show higher stability and TONs, but the activity is several orders of magnitude lower, which currently only allows for epoxidation reactions of highly active substrates like allylic alcohols.[31] Based on our current results, we hypothesize that the Keggin-structured phosphotungstic acid is more stable than the fully peroxidized Venturello's catalyst. If the stability really decreases with the degree of peroxidation that can be determined by testing catalysts at varying degrees of peroxidation, which may provide useful information for future research to make these heterogeneous catalysts more stable.

The Ru-based catalyst faced similar issues. Although we were able to carry out reactions with very low catalyst loadings to reach TONs up to 40000, we were not able to reuse the catalyst in any of the experiments. This may be due to side reactions degrading the catalyst when the Ru hydrides are exposed to air, or perhaps the lack of an adequate washing procedure to ensure catalyst does not degrade. Further research is needed to establish a proper methodology to recycle the catalyst, as well as more characterization on the catalyst after the reaction is over, to verify what happens to the Ru species at the surface of the NPs. We were also able to observe that catalyst samples stored under air would oxidize slowly over time and then exhibit a different response to the irradiation with green LEDs, but the activity of those samples didn't match with the catalysts that were used for hydrogenation and recycled. So the effects of oxidation also need further research, as well as proper storage conditions to prevent degradation of the catalyst. Although the plasmon-enhancement was successful towards hydrogenation, and mechanistic considerations were provided, further research is required to fully elucidate the mechanism in which LSPR affects the reaction.

There is also plenty of room for further research to expand the scope of plasmonic catalysts. Ru has been used for hydrogenation of ketones, as well as transfer hydrogenations.[180-181] Research from our group has shown plasmon-enhanced hydrogenation of carbonyls using Ag nanocubes.[161] So extending the application of LSPR to other types of hydrogenations using our Ru@Au@Al_2O_3 catalyst is worth investigating.

6. References

(1) Tuck, C. O.; Perez, E.; Horvath, I. T.; Sheldon, R. A.; Poliakoff, M., Valorization of Biomass: Deriving More Value from Waste. *Science* **2012,** *337*, 695-699.

(2) Simmons, B. A.; Loque, D.; Blanch, H. W., Next-generation biomass feedstocks for biofuel production. *Genome Biol.* **2008,** *9*.

(3) Williams, P. J. L.; Laurens, L. M. L., Microalgae as biodiesel & biomass feedstocks: Review & analysis of the biochemistry, energetics & economics. *Energy Environ. Sci.* **2010,** *3*, 554-590.

(4) Rulkens, W., Sewage sludge as a biomass resource for the production of energy: Overview and assessment of the various options. *Energy Fuels* **2008,** *22*, 9-15.

(5) Mirabella, N.; Castellani, V.; Sala, S., Current options for the valorization of food manufacturing waste: a review. *J. Clean. Prod.* **2014,** *65*, 28-41.

(6) Meier, M. A. R.; Metzger, J. O.; Schubert, U. S., Plant oil renewable resources as green alternatives in polymer science. *Chem. Soc. Rev.* **2007,** *36*, 1788-1802.

(7) Corma, A.; Iborra, S.; Velty, A., Chemical routes for the transformation of biomass into chemicals. *Chem. Rev.* **2007,** *107*, 2411-2502.

(8) Alam, M.; Akra, D.; Sharmin, E.; Zafar, F.; Ahmad, S., Vegetable oil based eco-friendly coating materials: A review article. *Arab. J. Chem.* **2014,** *7*, 469-479.

(9) Rahmat, N.; Abdullah, A. Z.; Mohamed, A. R., Recent progress on innovative and potential technologies for glycerol transformation into fuel additives: A critical review. *Renew. Sust. Energy Rev.* **2010,** *14*, 987-1000.

(10) Clark, J.; Deswarte, F., Introduction to Chemicals from Biomass. *Wiley*, 2014.

(11) Frazer, A. C.; Sammons, H. G., The formation of mono- and di-glycerides during the hydrolysis of triglyceride by pancreatic lipase. *Biochem. J.* **1945,** *39*, 122-128.

(12) Orsavova, J.; Misurcova, L.; Ambrozova, J. V.; Vicha, R.; Mlcek, J., Fatty Acids Composition of Vegetable Oils and Its Contribution to Dietary Energy Intake and Dependence of Cardiovascular Mortality on Dietary Intake of Fatty Acids. *Int. J. Mol. Sci.* **2015,** *16*, 12871-12890.

(13) Andrikopoulos, N. K., Triglyceride species compositions of common edible vegetable oils and methods used for their identification and quantification. *Food Rev. Int.* **2002,** *18*, 71-102.

(14) Albright, L. F.; Wisniak, J., Selectivity and Isomerization During Partial Hydrogenation of Cottonseed Oil and Methyl Oleate: Effect of Operating Variables. *J. Am. Oil Chem. Soc.* **1962,** *39*.

(15) Company, T. C. ChemFlexx Epoxidized Soybean Oil (ESO). https://thechemco.com/chemical/epoxidized-soybean-oil/ (accessed August 2020).

(16) Omonov, T. S.; Curtis, J. M., 7 - Plant Oil-Based Epoxy Intermediates for Polymers. In Bio-Based Plant Oil Polymers and Composites, *Elsevier*, 2016; pp 99-125.

(17) Sieber, M. A.; Hegel, J. K., Azelaic acid: Properties and mode of action. *Skin Pharmacol. Physiol.* **2014,** *27 Suppl 1*, 9-17.

(18) Schuster, M.; Blechert, S., Olefin Metathesis in Organic Chemistry. *Angew. Chem. Int. Ed.* **1997,** *36*, 2037-2056.

(19) Ivin, K. J., Some recent applications of olefin metathesis in organicsynthesis: A review. *J. Mol. Catal. A: Chem.* **1998,** *133*, 1-16.

(20) Patel, J.; Mujcinovic, S.; Jackson, W. R.; Robinson, A. J.; Serelis, A. K.; Such, C., High conversion and productive catalyst turnovers in cross-metathesis reactions of natural oils with 2-butene. *Green Chem.* **2006,** *8*, 450-454.

(21) De, C.; Saha, R.; Ghosh, S. K.; Ghosh, A.; Mukherjee, K.; Bhattacharyya, S. S.; Saha, B., A review of biphasic hydroformylation for long chain substrates. *Res. Chem. Intermed.* **2013,** *39*, 3463–3474.

(22) Hydrogen Peroxide (H_2O_2) Safety and Handling Guidelines. https://www.h2o2.com/technical-library/default.aspx?pid=66&name=Safety-amp-Handling (accessed August 2020).

(23) Mizuno, N.; Yamaguchi, K.; Kamata, K., Epoxidation of olefins with hydrogen peroxide catalyzed by polyoxometalates. *Coord. Chem. Rev.* **2005,** *249*, 1944-1956.

(24) Kamata, K.; Yonehara, K.; Sumida, Y.; Yamaguchi, K.; Hikichi, S.; Mizuno, N., Efficient epoxidation of olefins with >= 99% selectivity and use of hydrogen peroxide. *Science* **2003,** *300*, 964-966.

(25) Kamata, K.; Yonehara, K.; Sumida, Y.; Hirata, K.; Nojima, S.; Mizuno, N., Efficient heterogeneous epoxidation of alkenes by a supported tungsten oxide catalyst. *Angew. Chem. Int. Ed.* **2011,** *50*, 12062-12066.

(26) Ishii, Y.; Yamawaki, K.; Ura, T.; Yamada, H.; Yoshida, T.; Ogawa, M., Hydrogen-Peroxide Oxidation Catalyzed by Heteropoly Acids Combined with Cetylpyridinium Chloride - Epoxidation of Olefins and Allylic Alcohols, Ketonization of Alcohols and Diols, and Oxidative Cleavage of 1,2-Diols and Olefins. *J. Org. Chem.* **1988,** *53*, 3587-3593.

(27) Duncan, D. C.; Chambers, R. C.; Hecht, E.; Hill, C. L., Mechanism and Dynamics in the $H_3[PW_{12}O_{40}]$-Catalyzed Selective Epoxidation of Terminal Olefins by H_2O_2 - Formation, Reactivity, and Stability of $(PO_4[WO(O_2)_2]_4)^{3-}$. *J. Am. Chem. Soc.* **1995,** *117*, 681-691.

(28) Sato, K.; Aoki, M.; Noyori, R., A "green" route to adipic acid: Direct oxidation of cyclohexenes with 30 percent hydrogen peroxide. *Science* **1998,** *281*, 1646-1647.

(29) Leng, Y.; Wu, J.; Jiang, P.; Wang, J., Amphiphilic phosphotungstate-paired ionic copolymer as a highly efficient catalyst for triphase epoxidation of alkenes with H_2O_2. *Catal. Sci. Technol.* **2014,** *4*, 1293.

(30) Leng, Y.; Zhao, J.; Jiang, P.; Wang, J., Amphiphilic polyoxometalate-paired polymer coated Fe_3O_4: magnetically recyclable catalyst for epoxidation of bio-derived olefins with H_2O_2. *ACS Appl. Mater. Interfaces* **2014,** *6*, 5947-5954.

(31) Yamada, Y. M. A.; Guo, H. Q.; Uozumi, Y., Tightly convoluted polymeric phosphotungstate catalyst: An oxidative cyclization of alkenols and alkenoic acids. *Org. Lett.* **2007,** *9*, 1501-1504.

(32) Khlebnikova, T. B.; Pai, Z. P.; Fedoseeva, L. A.; Mattsat, Y. V., Catalytic oxidation of fatty acids. II. Epoxidation and oxidative cleavage of unsaturated fatty acid esters containing additional functional groups. *React. Kinet. Catal. Lett.* **2009,** *98*, 9-17.

(33) Abdullah, B. M.; Salimon, J., Epoxidation of vegetable oils and fatty acids: catalysts, methods and advantages. *J. Appl. Sci.* **2010,** *10*, 1545-1553.

(34) Dinda, S.; Patwardhan, A. V.; Goud, V. V.; Pradhan, N. C., Epoxidation of cottonseed oil by aqueous hydrogen peroxide catalysed by liquid inorganic acids. *Bioresour. Technol.* **2008,** *99*, 3737-3744.

(35) Goud, V. V.; Patwardhan, A. V.; Pradhan, N. C., Studies on the epoxidation of mahua oil (Madhumica indica) by hydrogen peroxide. *Bioresour. Technol.* **2006,** *97*, 1365-1371.

(36) Santacesaria, E.; Tesser, R.; Di Serio, M.; Turco, R.; Russo, V.; Verde, D., A biphasic model describing soybean oil epoxidation with H_2O_2 in a fed-batch reactor. *Chem. Eng. J.* **2011,** *173*, 198-209.

(37) Lane, B. S.; Vogt, M.; DeRose, V. J.; Burgess, K., Manganese-catalyzed epoxidations of alkenes in bicarbonate solutions. *J. Am. Chem. Soc.* **2002,** *124*, 11946-11954.

(38) Saedi, Z.; Tangestaninejad, S.; Moghadam, M.; Mirkhani, V.; Mohammadpoor-Baltork, I., MIL-101 metal-organic framework: A highly efficient heterogeneous catalyst for oxidative cleavage of alkenes with H_2O_2. *Catal. Commun.* **2012,** *17*, 18-22.

(39) Saedi, Z.; Tangestaninejad, S.; Moghadam, M.; Mirkhani, V.; Mohammadpoor-Baltork, I., The effect of encapsulated Zn-POM on the catalytic activity of MIL-101 in the oxidation of alkenes with hydrogen peroxide. *J. Coord. Chem.* **2012,** *65*, 463-473.

(40) Che, C. M.; Yip, W. P.; Yu, W. Y., Ruthenium-catalyzed oxidation of alkenes, alkynes, and alcohols to organic acids with aqueous hydrogen peroxide. *Chem. Asian J.* **2006,** *1*, 453-458.

(41) Vafaeezadeh, M.; Hashemi, M. M., Dual catalytic function of the task-specific ionic liquid: Green oxidation of cyclohexene to adipic acid using 30% H_2O_2. *Chem. Eng. J.* **2013,** *221*, 254-257.

(42) Rayati, S.; Abdolalian, P., Heterogenization of a molybdenum Schiff base complex as a magnetic nanocatalyst: An eco-friendly, efficient, selective and recyclable nanocatalyst for the oxidation of alkenes. *C. R. Chim.* **2013,** *16*, 814-820.

(43) Patil, H.; Waghmare, J., Catalyst for epoxidation of oils: a review. *Discovery* **2013,** *3*, 10-14.

(44) Lane, B. S.; Burgess, K., Metal-catalyzed epoxidations of alkenes with hydrogen peroxide. *Chem. Rev.* **2003,** *103*, 2457-2473.

(45) Borrás-Almenar, J. J., Polyoxometalate molecular science. *Kluwer Academic Publishers*, Dordrecht Boston, 2003.

(46) Te, M.; Fairbridge, C.; Ring, Z., Oxidation reactivities of dibenzothiophenes in polyoxometalate/H_2O_2 and formic acid/H_2O_2 systems. *Appl. Catal., A* **2001,** *219*, 267-280.

(47) Venturello, C.; Daloisio, R.; Bart, J. C. J.; Ricci, M., A New Peroxotungsten Heteropoly Anion with Special Oxidizing Properties: Synthesis and Structure of Tetrahexylammonium Tetra(Diperoxotungsto)Phosphate(3-). *J. Mol. Catal.* **1985,** *32*, 107-110.

(48) Yadav, G. D.; Pujari, A. A., Epoxidation of Styrene to Styrene Oxide: Synergism of Heteropoly Acid and Phase-Transfer Catalyst under Ishii-Venturello Mechanism. *Org. Process Res. Dev.* **2000,** *4*, 88-93.

(49) Chen, J. Z.; Hua, L.; Zhu, W. W.; Zhang, R.; Guo, L.; Chen, C.; Gan, H. M.; Song, B. N.; Hou, Z. S., Polyoxometalate anion-functionalized ionic liquid as a thermoregulated catalyst for the epoxidation of olefins. *Catal. Commun.* **2014,** *47*, 18-21.

(50) Ding, Y.; Zhao, W.; Hua, H.; Ma, B., [π-$C_5H_5N(CH_2)_{15}CH_3]_3[PW_4O_{32}]/H_2O_2$/ethyl acetate/alkenes: a recyclable and environmentally benign alkenes epoxidation catalytic system. *Green Chem.* **2008,** *10*, 910.

(51) Poli, E.; De Sousa, R.; Jerome, F.; Pouilloux, Y.; Clacens, J.-M., Catalytic epoxidation of styrene and methyl oleate over peroxophosphotungstate entrapped in mesoporous SBA-15. *Catal. Sci. Technol.* **2012,** *2*, 910-914.

(52) Auffan, M.; Rose, J.; Bottero, J. Y.; Lowry, G. V.; Jolivet, J. P.; Wiesner, M. R., Towards a definition of inorganic nanoparticles from an environmental, health and safety perspective. *Nat. Nanotechnol.* **2009,** *4*, 634-641.

(53) Reddy, K. M.; Manorama, S. V.; Reddy, A. R., Bandgap studies on anatase titanium dioxide nanoparticles. *Mater. Chem. Phys.* **2003,** *78*, 239-245.

(54) Sheng, H. W.; Ren, G.; Peng, L. M.; Hu, Z. Q.; Lu, K., Superheating and melting-point depression of Pb nanoparticles embedded in Al matrices. *Phil. Mag. Lett.* **1996,** *73*, 179-186.

(55) Zheng, X. G.; Xu, C. N.; Nishikubo, K.; Nishiyama, K.; Higemoto, W.; Moon, W. J.; Tanaka, E.; Otabe, E. S., Finite-size effect on Neel temperature in antiferromagnetic nanoparticles. *Phys. Rev. B* **2005,** *72*.

(56) Volokitin, Y.; Sinzig, J.; Jongh, L. J. d.; Schmidt, G.; Vargaftik, M. N.; Moiseev, I. I., Quantum-size effects in the thermodynamic properties of metallic nanoparticles. *Nature* **1996,** *384*, 621–623.

(57) Wu, Y.; Nordlander, P., Finite-Difference Time-Domain Modeling of the Optical Properties of Nanoparticles near Dielectric Substrates. *J. Phys. Chem.* **2010,** *114*, 7302–7307.

(58) Wang, X.; Zhuang, J.; Peng, Q.; Li, Y., A general strategy for nanocrystal synthesis. *Nature* **2005,** *437*, 121-124.

(59) Ndolomingo, M. J.; Bingwa, N.; Meijboom, R., Review of supported metal nanoparticles: synthesis methodologies, advantages and application as catalysts. *J. Mater. Sci.* **2020**, 6195–6241.

(60) Niu, Z.; Li, Y., Removal and Utilization of Capping Agents in Nanocatalysis. *Chem. Mater.* **2014**, 72-83.

(61) A.Quintanilla; V.C.L.Butselaar-Orthlieb; C.Kwakernaak; W.G.Sloof; M.T.Kreutzer; F.Kapteijn, Weakly bound capping agents on gold nanoparticles in catalysis: Surface poison? *J. Catal.* **2010,** *271*, 104-114.

(62) Ajitha, B.; Reddy, Y. A. K.; Reddy, P. S.; Jeon, H.-J.; Ahn, C. W., Role of capping agents in controlling silver nanoparticles size, antibacterial activity and potential application as optical hydrogen peroxide sensor. *RSC Adv.* **2016,** *6,* 36171–36179.

(63) Stankus, D. P.; Lohse, S. E.; Hutchison, J. E.; Nason, J. A., Interactions between Natural Organic Matter and Gold Nanoparticles Stabilized with Different Organic Capping Agents. *Environ. Sci. Technol.* **2011,** *45*, 3238–3244.

(64) Gelle, A.; Jin, T.; de la Garza, L.; Price, G. D.; Besteiro, L. V.; Moores, A., Applications of Plasmon-Enhanced Nanocatalysis to Organic Transformations. *Chem. Rev.* **2020,** *120*, 986-1041.

(65) Link, S.; Wang, Z. L.; El-Sayed, M. A., Alloy Formation of Gold−Silver Nanoparticles and the Dependence of the Plasmon Absorption on Their Composition. *J. Phys. Chem. B* **1999,** *103*, 3529-3533.

(66) He, R.; Wang, Y.-C.; Wang, X.; Wang, Z.; Liu, G.; Zhou, W.; Wen, L.; Li, Q.; Wang, X.; Chen, X., *et al.*, Facile synthesis of pentacle gold–copper alloy nanocrystals and their plasmonic and catalytic properties. *Nat. Commun.* **2014,** *5*, 4327.

(67) Xiao, Q.; Sarina, S.; Bo, A.; Jia, J.; Liu, H.; Arnold, D. P.; Huang, Y.; Wu, H.; Zhu, H., Visible Light-Driven Cross-Coupling Reactions at Lower Temperatures Using a Photocatalyst of Palladium and Gold Alloy Nanoparticles. *ACS Catal.* **2014,** *4*, 1725-1734.

(68) Swearer, D. F.; Leary, R. K.; Newell, R.; Yazdi, S.; Robatjazi, H.; Zhang, Y.; Renard, D.; Nordlander, P.; Midgley, P. A.; Halas, N. J., *et al.*, Transition-Metal Decorated Aluminum Nanocrystals. *ACS Nano* **2017,** *11*, 10281-10288.

(69) Ghosh Chaudhuri, R.; Paria, S., Core/shell nanoparticles: classes, properties, synthesis mechanisms, characterization, and applications. *Chem. Rev.* **2012,** *112*, 2373-2433.

(70) Kuhn, L. T.; Bojesen, A.; Timmermann, L.; Nielsen, M. M.; Mørup, S., Structural and magnetic properties of core-shell iron-iron oxide nanoparticles. *J. Phys.: Condens. Matter* **202,** *14*, 13551–13567.

(71) Nemati, Z.; Alonso, J.; Khurshid, H.; Phana, M. H.; Srikanth, H., Core/shell iron/iron oxide nanoparticles: are they promising for magnetic hyperthermia? *RSC Adv.* **2016,** *6*, 38697–38702.

(72) Knight, M. W.; King, N. S.; Liu, L.; Everitt, H. O.; Nordlander, P.; Halas, N. J., Aluminum for Plasmonics. *ACS Nano* **2014,** *8*, 834-840.

(73) Sambles, J. R.; Bradbery, G. W.; Yang, F. Z., Optical excitation of surface plasmons: An introduction. *Contemp. Phys.* **1991,** *32*, 173-183.

(74) Petryayeva, E.; Krull, U. J., Localized surface plasmon resonance: Nanostructures, bioassays and biosensing-A review. *Anal. Chim. Acta.* **2011,** *706*, 8-24.

(75) Herzog, J. B.; Knight, M. W.; Natelson, D., Thermoplasmonics: quantifying plasmonic heating in single nanowires. *Nano Lett.* **2014,** *14*, 499-503.

(76) Daniel, M.-C.; Astruc, D., Gold nanoparticles: assembly, supramolecular chemistry, quantum-size-related properties, and applications toward biology, catalysis, and nanotechnology. *Chem. Rev.* **2004,** *104*, 293-346.

(77) Rycenga, M.; Cobley, C. M.; Zeng, J.; Li, W.; Moran, C. H.; Zhang, Q.; Qin, D.; Xia, Y., Controlling the synthesis and assembly of silver nanostructures for plasmonic applications. *Chem. Rev.* **2011,** *111*, 3669-3712.

(78) Chan, G. H.; Zhao, J.; Hicks, E. M.; Schatz, G. C.; Van Duyne, R. P., Plasmonic Properties of Copper Nanoparticles Fabricated by Nanosphere Lithography. *Nano Lett.* **2007,** *7*, 1947-1952.

(79) Biggins, J. S.; Yazdi, S.; Ringe, E., Magnesium Nanoparticle Plasmonics. *Nano Lett.* **2018,** *18*, 3752-3758.

(80) Moscatelli, A., The aluminium rush. *Nat. Nanotechnol.* **2012,** *7*, 778.

(81) Baffou, G.; Quidant, R.; Girard, C., Heat generation in plasmonic nanostructures: Influence of morphology. *Appl. Phys. Lett.* **2009,** *94*, 153109.

(82) Govorov, A. O.; Richardson, H. H., Generating heat with metal nanoparticles. *Nano Today* **2007,** *2*, 30-38.

(83) Zhang, X.; Li, X. Q.; Reish, M. E.; Zhang, D.; Su, N. Q.; Gutierrez, Y.; Moreno, F.; Yang, W. T.; Everitt, H. O.; Liu, J., Plasmon-Enhanced Catalysis: Distinguishing Thermal and Nonthermal Effects. *Nano Lett.* **2018,** *18*, 1714-1723.

(84) Stamplecoskie, K. G.; Fasciani, C.; Scaiano, J. C., Dual-stage lithography from a light-driven, plasmon-assisted process: a hierarchical approach to subwavelength features. *Langmuir* **2012,** *28*, 10957-10961.

(85) Jain, P. K.; El-Sayed, I. H.; El-Sayed, M. A., Au nanoparticles target cancer. *Nano Today* **2007,** *2*, 18-29.

(86) Neumann, O.; Urban, A. S.; Day, J.; Lal, S.; Nordlander, P.; Halas, N. J., Solar vapor generation enabled by nanoparticles. *ACS Nano* **2012,** *7*, 42-49.

(87) Giannini, V.; Fernández-Domínguez, A. I.; Heck, S. C.; Maier, S. A., Plasmonic nanoantennas: fundamentals and their use in controlling the radiative properties of nanoemitters. *Chem. Rev.* **2011,** *111*, 3888-3912.

(88) Linic, S.; Christopher, P.; Ingram, D. B., Plasmonic-metal nanostructures for efficient conversion of solar to chemical energy. *Nat. Mater.* **2011,** *10*, 911-921.

(89) Mori, K.; Kawashima, M.; Che, M.; Yamashita, H., Enhancement of the Photoinduced Oxidation Activity of a Ruthenium(II) Complex Anchored on Silica-Coated Silver Nanoparticles by Localized Surface Plasmon Resonance. *Angew. Chem.* **2010,** *122*, 8780-8783.

(90) Zhang, X.; Du, A.; Zhu, H.; Jia, J.; Wang, J.; Ke, X., Surface plasmon-enhanced zeolite catalysis under light irradiation and its correlation with molecular polarity of reactants. *Chem. Commun.* **2014,** *50*, 13893-13895.

(91) Stamplecoskie, K. G.; Pacioni, N. L.; Larson, D.; Scaiano, J. C., Plasmon-mediated photopolymerization maps plasmon fields for silver nanoparticles. *J. Am. Chem. Soc.* **2011,** *133*, 9160-9163.

(92) Swearer, D. F.; Zhao, H. Q.; Zhou, L. N.; Zhang, C.; Robatjazi, H.; Martirez, J. M. P.; Krauter, C. M.; Yazdi, S.; McClain, M. J.; Ringe, E., *et al.*, Heterometallic antenna-reactor complexes for photocatalysis. *Proc. Natl. Acad. Sci. U.S.A.* **2016,** *113*, 8916-8920.

(93) Li, K.; Hogan, N. J.; Kale, M. J.; Halas, N. J.; Nordlander, P.; Christopher, P., Balancing near-field enhancement, absorption, and scattering for effective antenna–reactor plasmonic photocatalysis. *Nano Lett.* **2017,** *17*, 3710-3717.

(94) Dong, J.; Zhang, Z.; Zheng, H.; Sun, M., Recent Progress on Plasmon-Enhanced Fluorescence. In *Nanophotonics-Berlin*, 2015; Vol. 4, pp 472-490.

(95) Bauch, M.; Toma, K.; Toma, M.; Zhang, Q.; Dostalek, J., Plasmon-Enhanced Fluorescence Biosensors: a Review. *Plasmonics* **2014,** *9*, 781-799.

(96) Moskovits, M., Surface-enhanced Raman spectroscopy: a brief retrospective. *J. Raman Spectrosc.* **2005,** *36*, 485-496.

(97) Hartland, G. V.; Besteiro, L. V.; Johns, P.; Govorov, A. O., What's so hot about electrons in metal nanoparticles? *ACS Energy Lett.* **2017,** *2*, 1641-1653.

(98) Brongersma, M. L.; Halas, N. J.; Nordlander, P., Plasmon-induced hot carrier science and technology. *Nat. Nanotechnol.* **2015,** *10*, 25-34.

(99) Lee, S.-H.; Jo, J.-S.; Park, J. H.; Lee, S. W.; Jang, J.-W., A hot-electron-triggered catalytic oxidation reaction of plasmonic silver nanoparticles evidenced by surface potential mapping. *J. Mater. Chem. A* **2018,** *6*, 20939-20946.

(100) Sato, Y.; Naya, S.-i.; Tada, H., A new bimetallic plasmonic photocatalyst consisting of gold(core)-copper(shell) nanoparticle and titanium(IV) oxide support. *APL Mater.* **2015,** *3*, 104502.

(101) Wang, J.; Ando, R. A.; Camargo, P. H. C., Controlling the Selectivity of the Surface Plasmon Resonance Mediated Oxidation of p-Aminothiophenol on Au Nanoparticles by Charge Transfer from UV-excited TiO_2. *Angew. Chem.* **2015,** *127*, 7013-7016.

(102) Xiao, Q.; Sarina, S.; Jaatinen, E.; Jia, J.; Arnold, D. P.; Liu, H.; Zhu, H., Efficient photocatalytic Suzuki cross-coupling reactions on Au–Pd alloy nanoparticles under visible light irradiation. *Green Chem.* **2014,** *16*, 4272-4285.

(103) Trinh, T. T.; Sato, R.; Sakamoto, M.; Fujiyoshi, Y.; Haruta, M.; Kurata, H.; Teranishi, T., Visible to near-infrared plasmon-enhanced catalytic activity of Pd hexagonal nanoplates for the Suzuki coupling reaction. *Nanoscale* **2015,** *7*, 12435-12444.

(104) González-Béjar, M.; Peters, K.; Hallett-Tapley, G. L.; Grenier, M.; Scaiano, J. C., Rapid one-pot propargylamine synthesis by plasmon mediated catalysis with gold nanoparticles on ZnO under ambient conditions. *Chem. Commun.* **2013,** *49*, 1732-1734.

(105) Zhao, X. Y.; Long, R.; Liu, D.; Luo, B. B.; Xiong, Y. J., Pd-Ag alloy nanocages: integration of Ag plasmonic properties with Pd active sites for light-driven catalytic hydrogenation. *J. Mater. Chem. A* **2015,** *3*, 9390-9394.

(106) Quiroz, J.; Barbosa, E. C.; Araujo, T. P.; Fiorio, J. L.; Wang, Y.-C.; Zou, Y.-C.; Mou, T.; Alves, T. V.; de Oliveira, D. C.; Wang, B., *et al.*, Controlling Reaction Selectivity over Hybrid Plasmonic Nanocatalysts. *Nano Lett.* **2018,** *18*, 7289-7297.

(107) Gangishetty, M. K.; Fontes, A. M.; Malta, M.; Kelly, T. L.; Scott, R. W. J., Improving the rates of Pd-catalyzed reactions by exciting the surface plasmons of AuPd bimetallic nanotriangles. *RSC Adv.* **2017,** *7*, 40218-40226.

(108) Chase, P. A.; Welch, G. C.; Jurca, T.; Stephan, D. W., Metal-free catalytic hydrogenation. *Angew. Chem. Int. Ed.* **2007,** *46*, 8050-8053.

(109) Garnett, J. L.; Sollich-Baumgartner, W. A., π Complex Adsorption in Hydrogen Exchange on Group Vlll Transition Metal Catalysts. *Adv. Catal.* **1966,** *16*, 95-121.

(110) Mi, H. H.; Lee, W. J.; Chen, C. B.; Yang, H. H.; Wu, S. J., Effect of fuel aromatic content on PAH emission from a heavy-duty diesel engine. *Chemosphere* **2000,** *41*, 1783-1790.

(111) Ravindra, K.; Sokhi, R.; Grieken, R. V., Atmospheric polycyclic aromatic hydrocarbons: Source attribution, emission factors and regulation. *Atmos. Environ.* **2008,** *42*, 2895-2921.

(112) Sassykova, L. R., Development of Catalysts for the Hydrogenation of the Aromatic Ring in Gasolines. *Chem. Biochem. Eng. Q.* **2017,** *31*, 447-453.

(113) Schoenmaker-Stolk, M. C.; Verwijs, J. W.; Don, J. A.; Scholten, J. J. F., The catalytic hydrogenation of benzene over supported metal catalysts: I. Gas-phase hydrogenation of benzene over ruthenium-on-silica. *Appl. Catal.* **1987,** *29*, 73-90.

(114) Stanislaus, A.; Cooper, B. H., Aromatic Hydrogenation Catalysis: A Review. *Catal. Rev. Sci. Eng.* **1994,** *36*, 75-123.

(115) Dyson, P. J.; Ellis, D. J.; Welton, T.; Parker, D. G., Arene hydrogenation in a room-temperature ionic liquid using a ruthenium cluster catalyst. *Chem. Commun.* **1999**, 25-26.

(116) Bianchini, C.; Santo, V. D.; Meli, A.; Moneti, S.; Moreno, M.; Oberhauser, W.; Psaro, R.; Sordelli, L.; Vizza, F., A comparison between silica-immobilized ruthenium(II) single sites and silica-supported ruthenium nanoparticles in the catalytic hydrogenation of model hetero- and polyaromatics contained in raw oil materials. *J. Catal.* **2003,** *213*, 47-62.

(117) Rasero-Almansa, A. M.; Corma, A.; Iglesias, M.; Sánchez, F., Post-functionalized iridium-Zr-MOF as a promising recyclable catalyst for the hydrogenation of aromatics. *Green Chem.* **2014,** *16*, 3522–3527.

(118) Giustra, Z. X.; Ishibashi, J. S. A.; Liu, S.-Y., Homogeneous metal catalysis for conversion between aromatic and saturated compounds. *Coord. Chem. Rev.* **2016,** *314*, 134–181.

(119) Zahmakıran, M.; Tonbul, Y.; Özkar, S., Ruthenium(0) Nanoclusters Stabilized by a Nanozeolite Framework: Isolable, Reusable, and Green Catalyst for the Hydrogenation of Neat

Aromatics under Mild Conditions with the Unprecedented Catalytic Activity and Lifetime. *J. Am. Chem. Soc.* **2010,** *132*, 6541-6549.

(120) Wang, D.-S.; Chen, Q.-A.; Lu, S.-M.; Zhou, Y.-G., Asymmetric hydrogenation of heteroarenes and arenes. *Chem. Rev.* **2012,** *112*, 2557-2590.

(121) Blasera, H.-U.; Honigb, H.; Studera, M.; Wedemeyer-Exl, C., Enantioselective synthesis of ethyl nipecotinate using cinchona modified heterogeneous catalysts. *J. Mol. Catal. A: Chem.* **1999,** *139*, 253–257.

(122) Studer, M.; Blaser, H.-U.; Exner, C., Enantioselective Hydrogenation Using Heterogeneous ModifiedCatalysts: An Update. *Adv. Synth. Catal.* **2003,** *345*, 45±46.

(123) Jacquin, M.; Jones, D. J.; Rozière, J.; Albertazzi, S.; Vaccari, A.; Lenarda, M.; Storaro, L.; Ganzerla, R., Novel supported Rh, Pt, Ir and Ru mesoporous alumino silicates as catalysts for the hydrogenation of naphthalene. *Appl. Catal. A* **2003,** *251*, 131-141.

(124) Zhou, G.; Jiang, L.; Dong, Y.; Li, R.; He, D., Engineering the exposed facets and open-coordinated sites of brookite TiO_2 to boost the loaded Ru nanoparticle efficiency in benzene selective hydrogenation. *Appl. Surf. Sci.* **2019,** *486*, 187-197.

(125) Alsalahi, W.; Tylus, W.; Trzeciak, A. M., Green Synthesis of Rhodium Nanoparticles that are Catalytically Active in Benzene Hydrogenation and 1-Hexene Hydroformylation. *ChemCatChem* **2018,** *10*, 2051-2058.

(126) Stuhl, L. S.; DuBois, M. R.; Flirsekorn, F. J.; Bleeke, J. R.; Stevens, A. E.; Muetterties, E. L., Catalytic homogeneous hydrogenation of arenes. 6. Reaction scope for the (eta3-2-propenyl) tris (trimethyl phosphite-P) cobalt catalyst. *J. Am. Chem. Soc.* **1978,** *100*, 2405-2410.

(127) Livingstone, S. E., The Chemistry of Ruthenium, Rhodium, Palladium, Osmium, Iridium and Platinum. *Pergamon Press*, 1973; Vol. 25.

(128) Hageluken, C., Markets for the catalyst metals platinum, palladium and rhodium. *Metall* **2006,** *60*, 31-42.

(129) Viniegra, M.; Gomez, R.; Gonzalez, R. D., The Role of Support in the Catalytic Hydrogenation of Benzene over Ruthenium Catalysts. *J. Catal.* **1988,** *111*, 429-432.

(130) Rossi, L. M.; Machado, G., Ruthenium nanoparticles prepared from ruthenium dioxide precursor: Highly active catalyst for hydrogenation of arenes under mild conditions. *J. Mol. Catal. A: Chem.* **2009,** *298*, 69-73.

(131) Rakers, L.; Martinez-Prieto, L. M.; Lopez-Vinasco, A. M.; Philippot, K.; Leeuwen, P. W. N. M. v.; Chaudret, B.; Glorius, F., Ruthenium nanoparticles ligated by cholesterol-derived NHCs and their application in the hydrogenation of arenes. *Chem. Commun.* **2018,** *54*, 7070--7073.

(132) Tayde, S.; Patnaik, M.; Bhagt, S. L.; Renge, V. C., Epoxidation of vegetable oils: a review. *Int. J. Adv. Res. Technol.* **2011,** *2*, 491-501.

(133) Campanella, A.; Baltanas, M. A., Degradation of the oxirane ring of epoxidized vegetable oils in liquid-liquid systems: II. Reactivity with solvated acetic and peracetic acids. *Lat. Am. Appl. Res.* **2005,** *35*, 211-216.

(134) Venturello, C.; Daloisio, R., Quaternary Ammonium Tetrakis(Diperoxotungsto)Phosphates(3-) as a New Class of Catalysts for Efficient Alkene Epoxidation with Hydrogen-Peroxide. *J. Org. Chem.* **1988,** *53*, 1553-1557.

(135) Plault, L.; Hauseler, A.; Nlate, S.; Astruc, D.; Ruiz, J.; Gatard, S.; Neumann, R., Synthesis of dendritic polyoxometalate complexes assembled by ionic bonding and their function as recoverable and reusable oxidation catalysts. *Angew. Chem. Int. Ed.* **2004,** *43*, 2924-2928.

(136) Wu, J. H.; Jiang, P. P.; Leng, Y.; Ye, Y. Y.; Qin, X. J., Synthesis of dicationic alkyl imidazolium peroxopolyoxotungsten-based phase transfer catalyst and its catalytic activity for olefin epoxidation. *Chin. J. Catal.* **2013,** *34*, 2236-2244.

(137) Chen, Y.; Tan, R.; Zheng, W.; Zhang, Y.; Zhao, G.; Yin, D., Dendritic phosphotungstate hybrids efficiently catalyze the selective oxidation of alcohols with H_2O_2. *Catal. Sci. Technol.* **2014,** *4*, 4084-4092.

(138) Yamaguchi, K.; Yoshida, C.; Uchida, S.; Mizuno, N., Peroxotungstate immobilized on ionic liquid-modified silica as a heterogeneous epoxidation catalyst with hydrogen peroxide. *J. Am. Chem. Soc.* **2005,** *127*, 530-531.

(139) Qiao, Y. X.; Li, H.; Hua, L.; Orzechowski, L.; Yan, K.; Feng, B.; Pan, Z. Y.; Theyssen, N.; Leitner, W.; Hou, Z. S., Peroxometalates Immobilized on Magnetically Recoverable Catalysts for Epoxidation. *ChemPlusChem* **2012,** *77*, 1128-1138.

(140) Zheng, X. X.; Zhang, L.; Li, J. Y.; Luo, S. Z.; Cheng, J. P., Magnetic nanoparticle supported polyoxometalates (POMs) via non-covalent interaction: reusable acid catalysts and catalyst supports for chiral amines. *Chem. Commun.* **2011,** *47*, 12325-12327.

(141) Neumann, R.; Cohen, M., Solvent-anchored supported liquid phase catalysis: Polyoxometalate-catalyzed oxidations. *Angew. Chem. Int. Ed.* **1997,** *36*, 1738-1740.

(142) Maksimchuk, N. V.; Kovalenko, K. A.; Arzumanov, S. S.; Chesalov, Y. A.; Melgunov, M. S.; Stepanov, A. G.; Fedin, V. P.; Kholdeeva, O. A., Hybrid polyoxotungstate/MIL-101 materials: synthesis, characterization, and catalysis of H_2O_2-based alkene epoxidation. *Inorg. Chem.* **2010,** *49*, 2920-2930.

(143) Grigoropoulou, G.; Clark, J. H.; Elings, J. A., Recent developments on the epoxidation of alkenes using hydrogen peroxide as an oxidant. *Green Chem.* **2003,** *5*, 1-7.

(144) Kozhevnikov, I. V.; Mulder, G. P.; Steverink-de Zoete, M. C.; Oostwal, M. G., Epoxidation of oleic acid catalyzed by peroxo phosphotungstate in a two-phase system. *J. Mol. Catal. A: Chem.* **1998,** *134*, 223-228.

(145) Vasylyev, M. V.; Astruc, D.; Neumann, R., Dendritic Phosphonates and thein situ Assembly of Polyperoxophosphotungstates: Synthesis and Catalytic Epoxidation of Alkenes with Hydrogen Peroxide. *Adv. Synth. Catal.* **2005,** *347*, 39-44.

(146) Karavalakis, G.; Short, D.; Vu, D.; Russell, R.; Hajbabaei, M.; Asa-Awuku, A.; Durbin, T. D., Evaluating the Effects of Aromatics Content in Gasoline on Gaseous and Particulate Matter Emissions from SI-PFI and SIDI Vehicles. *Environ. Sci. Technol.* **2015,** *49*, 7021-7031.

(147) Silveira, E. T.; Umpierre, A. P.; Rossi, L. M.; Machado, G.; Morais, J.; Soares, G. V.; Baumvol, I. J.; Teixeira, S. R.; Fichtner, P. F.; Dupont, J., The partial hydrogenation of benzene to cyclohexene by nanoscale ruthenium catalysts in imidazolium ionic liquids. *Chem. Eur. J.* **2004,** *10*, 3734-3740.

(148) Dyson, P. J.; Ellis, D. J.; Henderson, W.; Laurenczy, G., A Comparison of Ruthenium-Catalysed Arene Hydrogenation Reactions in Water and 1-Alkyl-3-methylimidazolium Tetrafluoroborate Ionic Liquids. *Adv. Synth. Catal.* **2003,** *345*, 216-221.

(149) Kaushik, M.; Friedman, H. M.; Batemana, M.; Moores, A., Cellulose nanocrystals as non-innocent supports for the synthesis of ruthenium nanoparticles and their application to arene hydrogenation. *RSC Adv.* **2015,** *5*, 53207-53210.

(150) Siebels, M.; Schlüsener, C.; Thomas, J.; Xiao, Y.-X.; Yang, X.-Y.; Janiak, C., Rhodium nanoparticles supported on covalent triazine-based frameworks as re-usable catalyst for benzene hydrogenation and hydrogen evolution reaction. *J. Mater. Chem. A* **2019,** *7*, 11934-11943.

(151) Araujo, T. P.; Quiroz, J.; Barbosa, E. C. M.; Camargo, P. H. C., Understanding plasmonic catalysis with controlled nanomaterials based on catalytic and plasmonic metals. *Curr. Opin. Colloid Interface Sci.* **2019,** *39*, 110-122.

(152) Li, S.; Miao, P.; Zhang, Y.; Wu, J.; Zhang, B.; Du, Y.; Han, X.; Sun, J.; Xu, P., Recent Advances in Plasmonic Nanostructures for Enhanced Photocatalysis and Electrocatalysis. *Adv Mater* **2020**, 2000086.

(153) Zhan, C.; Moskovits, M.; Tian, Z.-Q., Recent Progress and Prospects in Plasmon-Mediated Chemical Reaction. *Matter* **2020,** *3*, 42-56.

(154) Liang, C.; Lu, Z.-A.; Wu, J.; Chen, M.-X.; Zhang, Y.; Zhang, B.; Gao, G.-L.; Li, S.; Xu, a. P., Recent Advances in Plasmon-Promoted Organic Transformations Using Silver-Based Catalysts. *ACS Appl. Mater. Interfaces* **2020,** *12*, 54266–54284.

(155) Meng, L.; Chen, Z.; Ma, Z.; He, S.; Hou, Y.; Li, H.-H.; Yuan, R.; Huang, X.-H.; Wang, X.; Wang, X., *et al.*, Gold plasmon-induced photocatalytic dehydrogenative coupling of methane to ethane on polar oxide surfaces. *Energy Environ. Sci.* **2018,** *11*, 294-298.

(156) Zhao, J.; Liu, B.; Meng, L.; He, S.; Yuan, R.; Hou, Y.; Ding, Z.; Lin, H.; Zhang, Z.; Wang, X., *et al.*, Plasmonic control of solar-driven CO_2 conversion at the metal/ZnO interfaces. *Appl. Catal. B* **2019,** *256*, 117823.

(157) Silva, A. G. M. d.; Rodrigues, T. S.; Correia, V. G.; Alves, T. V.; Alves, R. S.; Ando, R. A.; Ornellas, F. R.; Wang, J.; Andrade, L. H.; Camargo, P. H. C., Plasmonic Nanorattles as Next-Generation Catalysts for Surface Plasmon Resonance-Mediated Oxidations Promoted by Activated Oxygen. *Angew. Chem. Int. Ed.* **2016,** *55*, 7111-7115.

(158) Barbosa, E. C. M.; Fiorio, J. L.; Mou, T.; Wang, B.; Rossi, L. M.; Camargo, P. H. C., Reaction Pathway Dependence in Plasmonic Catalysis: Hydrogenation as a Model Molecular Transformation. *Chem. Eur. J.* **2018,** *24*, 12330-12339.

(159) Christopher, P.; Xin, H.; Marimuthu, A.; Linic, S., Singular characteristics and unique chemical bond activation mechanisms of photocatalytic reactions on plasmonic nanostructures. *Nat. Mater.* **2012,** *11*, 1044-1050.

(160) Mukherjee, S.; Libisch, F.; Large, N.; Neumann, O.; Brown, L. V.; Cheng, J.; Lassiter, J. B.; Carter, E. A.; Nordlander, P.; Halas, N. J., Hot Electrons Do the Impossible: Plasmon-Induced Dissociation of H_2 on Au. *Nano Lett.* **2013,** *13*, 240-247.

(161) Landry, M. J.; Gellé, A.; Meng, B. Y.; Barrett, C. J.; Moores, A., Surface-Plasmon-Mediated Hydrogenation of Carbonyls Catalyzed by Silver Nanocubes under Visible Light. *ACS Catal.* **2017,** *7*, 6128-6133.

(162) Li, A. Y.; Kaushik, M.; Li, C.-J.; Moores, A., Microwave-Assisted Synthesis of Magnetic Carboxymethyl Cellulose-Embedded Ag-Fe_3O_4 Nanocatalysts for Selective Carbonyl Hydrogenation. *ACS Sustain. Chem. Eng.* **2016,** *4*, 965-973.

(163) Claus, P., Selective hydrogenation of alpha,beta-unsaturated aldehydes and other C=O and C=C bonds containing compounds. *Top. Catal.* **1998,** *5*, 51-62.

(164) Spata, V. A.; Carter, E. A., Mechanistic insights into photocatalyzed hydrogen desorption from palladium surfaces assisted by localized surface plasmon resonances. *ACS Nano* **2018,** *12*, 3512-3522.

(165) Hou, P. F.; Liu, H.; Li, J. L.; Yang, J., One-pot synthesis of noble metal nanoparticles with a core-shell construction. *CrystEngComm* **2015,** *17*, 1826-1832.

(166) Aslam, M.; Fu, L.; Su, M.; Vijayamohanan, K.; Dravid, V. P., Novel one-step synthesis of amine-stabilized aqueous colloidal gold nanoparticles. *J. Mater. Chem.* **2004,** *14*, 1795-1797.

(167) Jana, N. R.; Gearheart, L.; Murphy, C. J., Seeding growth for size control of 5-40 nm diameter gold nanoparticles. *Langmuir* **2001,** *17*, 6782-6786.

(168) Moores, A.; Goettmann, F., The plasmon band in noble metal nanoparticles: an introduction to theory and applications. *New J. Chem.* **2006,** *30*, 1121-1132.

(169) Baffou, G.; Bordacchini, I.; Baldi, A.; Quidant, R., Simple experimental procedures to distinguish photothermal from hot-carrier processes in plasmonics. *Light Sci. Appl.* **2020,** *9*, 1-16.

(170) Williams, D. B.; Carter, B., Transmission Electron Microscopy: Diffraction, Imaging, and Spectroscopy. *Springer*, 2016.

(171) Yamazawa, Y.; Okada, S.; Yasenjiang, Z.; Sunaoshi, T.; Kaji, K., The First Results of the Low Voltage Cold-FE SEM/STEM System Equipped With EELS. *Microsc. Microanal.* **2016,** *22*, 50-51.

(172) Brodusch, N.; Demers, H.; Gellé, A.; Moores, A.; Gauvin, R., Electron energy-loss spectroscopy (EELS) with a cold-field emission scanning electron microscope at low accelerating voltage in transmission mode. *Ultramicroscopy* **2018,** *203*, 21-36.

(173) Wang, D.; Astruc, D., The Golden Age of Transfer Hydrogenation. *Chem. Rev.* **2015,** *115*, 6621-6686.

(174) Garza, L. C. d. l.; Brodusch, N.; Gauvin, R.; Moores, A., Plasmon-enhanced hydrogenation of alkenes and arenes using Ruthenium-coated Gold nanoparticles. *ACS Appl. Nano.* **2020**, Submitted.

(175) Honda, M.; Kumamoto, Y.; Taguchi, A.; Saito, Y.; Kawata, S., Efficient UV photocatalysis assisted by densely distributed aluminum nanoparticles. *J. Phys. D: Appl. Phys.* **2015,** *48*, 1-6.

(176) Robatjazi, H.; Zhao, H.; Swearer, D. F.; Hogan, N. J.; Zhou, L.; Alabastri, A.; McClain, M. J.; Nordlander, P.; Halas, N. J., Plasmon-induced selective carbon dioxide conversion on earth-abundant aluminum-cuprous oxide antenna-reactor nanoparticles. *Nat. Commun.* **2017,** *8*, 27.

(177) McClain, M. J.; Schlather, A. E.; Ringe, E.; King, N. S.; Liu, L.; Manjavacas, A.; Knight, M. W.; Kumar, I.; Whitmire, K. H.; Everitt, H. O., *et al.*, Aluminum Nanocrystals. *Nano Lett.* **2015,** *15*, 2751-2755.

(178) Bunker, C. E.; Smith, M. J.; Fernando, K. A. S.; Harruff, B. A.; Lewis, W. K.; Gord, J. R.; Guliants, E. A.; Phelps, D. K., Spontaneous Hydrogen Generation from Organic-Capped Al Nanoparticles and Water. *ACS Appl. Mater. Inter.* **2010,** *2*, 11-14.

(179) Jones, R. N., The ultraviolet absorption spectra of aromatic hydrocarbons. *Chem. Rev.* **1942,** *1*, 1-46.

(180) Clapham, S. E.; Hadzovic, A.; Morris, R. H., Mechanisms of the H_2-hydrogenation and transfer hydrogenation of polar bonds catalyzed by ruthenium hydride complexes. *Coord. Chem. Rev.* **2004,** *248*, 2201–2237.

(181) Baig, R. B. N.; Varma, R. S., Magnetic Silica-Supported Ruthenium Nanoparticles: An Efficient Catalyst for Transfer Hydrogenation of Carbonyl Compounds. *ACS Sustainable Chem. Eng.* **2013,** *1*, 805−809.

7. Appendices

7.1. Appendix I: Supporting information for chapter 2

Table 6: Reported activities of selected, best performing tungstate catalysts for the epoxidation of methyl oleate or olefins, and comparison with my research.

Catalyst	**Substrate**	**Eq. H_2O_2**	**Solvent**	**Temp (°C)**	**Time (h)**	**Conv.**[a]	**Sel.**	**TON**	**TOF (h^{-1})**	**TON**	**REF**
$[DP^{2+}]_3[PPW^{3-}]_2$	Methyl oleate	1.32	Neat	60	3	98%	96%	447	149	1868 5 cycles	This work
$[Me(n\text{-}C_8H_{17})_3N]_3$ $[PO_4[WO(O_2)_2]_4]$	Methyl oleate	2	Neat	60	5	94%	95%	940	188	940 not recyclable	[32]
Fe@PILPW-AM	Methyl oleate	0.4	MeCN	70	6	37%	95%	124	21	375[b] 3 cycles	[30]
DIM-CIM-PW	Cyclooctene	1.2	EtOAc	60	6	100%	100%	167	28	830 5 cycles	[29]
$(Bu_4N)_4$ $(SiW_{10}O_{34}(H_2O)_2)$	Cyclooctene	0.2	MeCN	32	2	20%	99%	124	62	620 5 cycles	[24]
W-Zn/SnO_2	Cyclooctene	2[c]	DMC	60	4	99%	99%	30	8	149 5 cycles	[25]
Poly(dipyridinium) $PW_{12}O_{40}$	4-decen-1-ol	2.5	Neat	50	24	92%	100%	460	19	2885 6 cycles	[31]

[a] Conversions in this table are shown respective to the alkene. Entries with low conversions used H_2O_2 as limiting reagent.

[b] Recycling tests performed with DL-Limonene, not methyl oleate.

[c] H_2O_2 60% was used in this case, which increases the reaction rate. Most of the literature uses 30% or 35%.

7.1.1. Complimentary Experimental Section

Synthesis of $(C_{41}H_{72}N_2)(WO_6)$

$(C_{41}H_{72}N_2)(WO_6)$ was recognized as a possible side product during the synthesis of $(C_{41}H_{72}N_2)_3(PW_4O_{24})_2$. Therefore $(C_{41}H_{72}N_2)(WO_6)$ was purposely synthesized and tested for the epoxidation of methyl oleate as a control experiment to determine the detrimental effects of this side product.

Tungstic acid (100 mg, 0.4 mmol, 1 eq.) is suspended in 8 mL of H_2O_2 30% (79.7 mmol, 200 eq.). The suspension is heated to 60 °C for 10 minutes, until the solid has dissolved and the solution becomes transparent. The solution is then diluted with 10 mL of methanol. A solution of 4,4’-(trimethylene)bis(1-tetradecylpyridinium) dibromide (300 mg, 0.4 mmol, 1 eq.) in 10 mL of methanol is slowly added to the first solution over 10 minutes, during which the product precipitates in solution as a bright orange solid. The mixture is left to cool down to room temperature and stirred for 1 h. The solid is filtered and washed with water and acetonitrile. 288 mg recovered (83% yield).

Catalytic epoxidation of methyl oleate using $(C_{41}H_{72}N_2)(WO_6)$ as catalyst

Methyl oleate (500 mg, 1.69 mmol, 1 eq.), $(C_{41}H_{72}N_2)(WO_6)$ (16.2 mg, 0.02 mmol, 0.01 eq.) and H_2O_2 30% (222 μL, 2.23 mmol, 1.32 eq.) were added to a 20 mL flask and stirred at room temperature for 20 h. After the reaction, the mixture was diluted with 10 mL of ethyl acetate. A sample of the organic phase was removed, filtered and analysed by GC-MS.

Analysis showed 3% conversion with 94% selectivity for the epoxidation using $(C_{41}H_{72}N_2)(WO_6)$. In comparison, the active catalyst $(C_{41}H_{72}N_2)_3(PW_4O_{24})_2$ achieved 84%

conversion and 100% selectivity in only 4 hours at room temperature, using the same catalyst loading (0.01 eq.). Therefore, the production of the side product $(C_{41}H_{72}N_2)(WO_6)$ is significantly detrimental to the activity of the catalyst and must be avoided.

Catalytic epoxidation of linoleic acid using $(C_{41}H_{72}N_2)_3(PW_4O_{24})_2$ as catalyst

Linoleic acid (500 mg, 1.78 mmol, 1 eq.), $(C_{41}H_{72}N_2)_3(PW_4O_{24})_2$ (8.00 mg, 0.0039 mmol, 0.0022 eq.) and H_2O_2 30% (427 μL, 4.28 mmol, 2.4 eq.) were added to a 20 mL flask and stirred at 60 °C for 2 h. After the reaction, a sample of the organic phase was diluted with $CDCl_3$ and analysed by ^1H NMR.

Catalytic epoxidation of ricinoleic acid using $(C_{41}H_{72}N_2)_3(PW_4O_{24})_2$ as catalyst

Ricinoleic acid (500 mg, 1.68 mmol, 1 eq.), $(C_{41}H_{72}N_2)_3(PW_4O_{24})_2$ (7.52 mg, 0.0036 mmol, 0.0022 eq.) and H_2O_2 30% (221 μL, 2.21 mmol, 1.32 eq.) were added to a 20 mL flask and stirred at 60 °C for 2 h. After the reaction, a sample of the organic phase was diluted with $CDCl_3$ and analysed by ^1H NMR.

Catalytic epoxidation of cyclooctene using $(C_{41}H_{72}N_2)_3(PW_4O_{24})_2$ as catalyst

Cyclooctene (591 μL, 4.54 mmol, 1 eq.), $(C_{41}H_{72}N_2)_3(PW_4O_{24})_2$ (18.5 mg, 0.009 mmol, 0.0022 eq.) and H_2O_2 30% (598 μL, 5.99 mmol, 1.32 eq.) were added to a 20 mL flask and stirred at 60 °C for 3 h. After the reaction, the mixture was diluted with 10 mL of ethyl acetate. A sample of the organic phase was removed, filtered and analysed by GC-MS.

Catalytic epoxidation of cyclohexene using $(C_{41}H_{72}N_2)_3(PW_4O_{24})_2$ as catalyst

Cyclohexene (247 μL, 2.43 mmol, 1 eq.), $(C_{41}H_{72}N_2)_3(PW_4O_{24})_2$ (10.93 mg, 0.005 mmol, 0.0022 eq.) and H_2O_2 30% (321 μL, 3.21 mmol, 1.32 eq.) were added to a 20 mL flask and stirred at 60 °C for 3 h. After the reaction, the mixture was diluted with 10 mL of ethyl acetate. A sample of the organic phase was removed, filtered and analysed by GC-MS.

Catalytic epoxidation of styrene using $(C_{41}H_{72}N_2)_3(PW_4O_{24})_2$ as catalyst

Styrene (275 µL, 2.40 mmol, 1 eq.), $(C_{41}H_{72}N_2)_3(PW_4O_{24})_2$ (10.77 mg, 0.005 mmol, 0.0022 eq.) and H_2O_2 30% (276 µL, 2.76 mmol, 1.32 eq.) were added to a 20 mL flask and stirred at 60 °C for 3 h. After the reaction, the mixture was diluted with 10 mL of ethyl acetate. A sample of the organic phase was removed, filtered and analysed by GC-MS.

7.1.2. Colorimetric analysis

The inactive species $(C_{41}H_{72}N_2)(WO_6)$ showed a bright orange color that could be used to determine its presence during the catalyst optimization experiments (Table 2), compared to the white color of $(C_{41}H_{72}N_2)_3(PW_{12}O_{40})_2$ and $(C_{41}H_{72}N_2)_3(PW_4O_{24})_2$. Although these samples could not be dissolved in any solvents for a proper UV-vis analysis, the activity of the catalyst could still be visually correlated with the color of the catalyst.

Of particular interest was the optimization of the ratio between $\mathbf{DP}^{2+}$ and $H_3PW_{12}O_{40}$ used (Table 2, entries 4, 6 and 7). When using a 3:2 ratio (Table 2, entry 4) to produce $(\mathbf{DP}^{2+})_3(\mathbf{PPW}^{3-})_2$, the solid obtained was a pale yellow, which we attributed to the contamination of $(\mathbf{DP}^{2+})_3(\mathbf{PPW}^{3-})_2$ with inactive $(\mathbf{DP}^{2+})(WO_6^{2-})$. When using an excess of $\mathbf{DP}^{2+}$ in a 5:1 ratio (Table 2, entry 6), the solid obtained was orange. Under these conditions, there is enough excess of $\mathbf{DP}^{2+}$ to precipitate all of the phosphptungstate species, leaving 2.5 equivalents of $\mathbf{DP}^{2+}$, which is able to entrain a large amount of WO_6^{2-}. So now a large amount of $(\mathbf{DP}^{2+})(WO_6^{2-})$ is produced, consistent with the orange color observed. When using an excess of $H_3PW_{12}O_{40}$ in a 1:2 ratio (Table 2, entry 7), a white product was obtained, which was much more active than previous experiments. The white color is consistent with absence of $(\mathbf{DP}^{2+})(WO_6^{2-})$.

The speed of reagent addition was also a critical point in our experiment. The synthesis of $(\mathbf{DP}^{2+})_3(\mathbf{PPW}^{3-})_2$ was repeated by adding the solution of $\mathbf{DP}^{2+}$ at different rates. It was found that a fast addition would always yield a yellow, less active catalyst, no matter how high the excess of $H_3PW_{12}O_{40}$ and H_2O_2 used. In order to obtain a white active catalyst, the solution of $\mathbf{DP}^{2+}$ had to be added dropwise. The slow addition enhances the difference of reaction rates between $PW_4O_{24}^{3-}$ and WO_6^{2-}, in favour of the active product. Since the solvent used is polar (a mixture of acetonitrile, water and hydrogen peroxide), the higher charge trianion of $PW_4O_{24}^{3-}$ will bind to the cationic **DP**$^{2+}$ faster than the dianion WO_6^{2-}.

7.1.3. NMR study of solvent effects

In order to produce the catalyst, the phase transfer agent (**DP**$^{2+}$)(Br^-)$_2$ had to be dissolved and added to the solution of phosphotungstic acid in hydrogen peroxide. This requires an additional solvent to dissolve (**DP**$^{2+}$)(Br^-)$_2$. Since (**DP**$^{2+}$)(Br^-)$_2$ was purified by recrystallization in boiling water, this was the obvious solvent to use, as hydrogen peroxide is already diluted in water. However, water was found to be a poor solvent because the product would precipitate too quickly and it would always yield a yellow product, which shows the presence of the inactive (**DP**$^{2+}$)(WO_6^{2-}). (**DP**$^{2+}$)(Br^-)$_2$ could only be dissolved using small alcohols (methanol, ethanol), $CHCl_3$, DMF, DMSO and warm acetonitrile (above 50 °C). DMSO was immediately discarded as it reacts violently with the phosphotungstate in hydrogen peroxide. DMF gave similar results to methanol but was discarded for its toxicity and price.

The effect of solvents on the equilibrium of peroxidized phosphotungstate species was studied by ^{31}P NMR before the addition of (**DP**$^{2+}$)(Br^-)$_2$. The results are shown in Figure 17 in appendix.

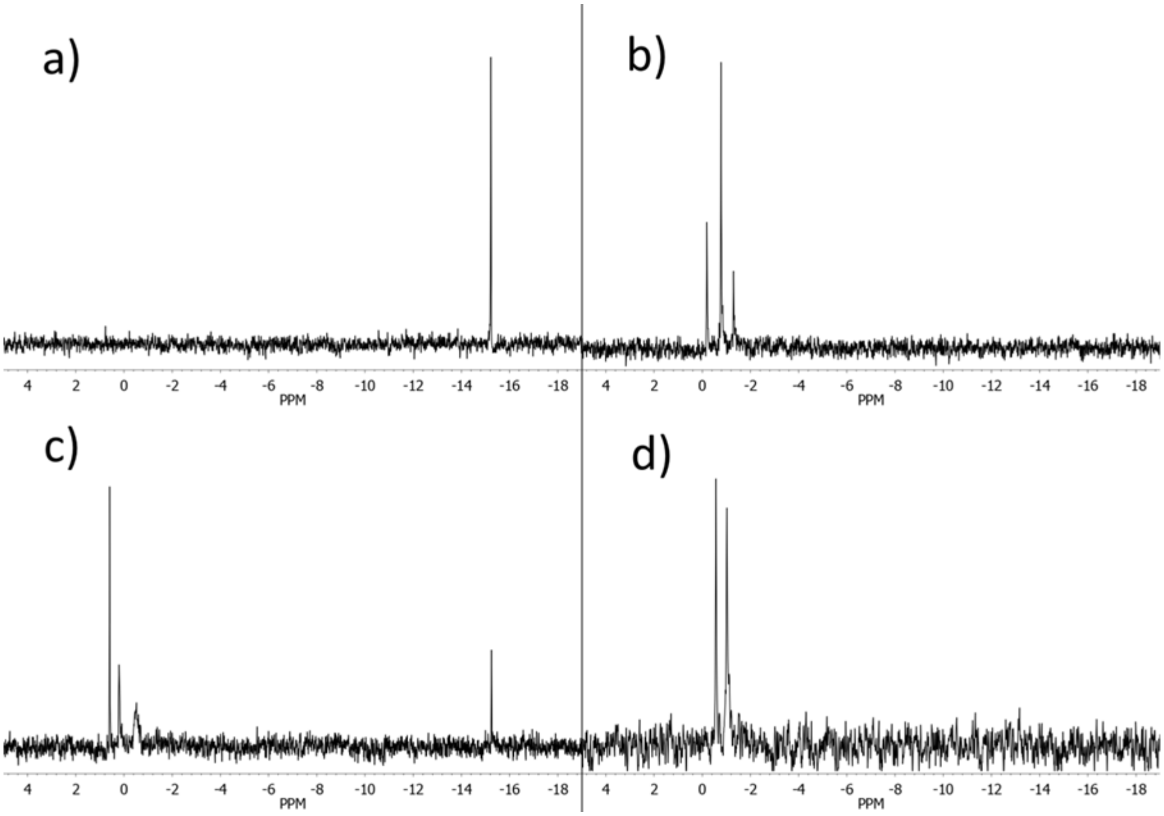

Figure 17: ^{31}P NMR spectra. a) $H_3PW_{12}O_{40}$ in D_2O, b) $H_3PW_{12}O_{40}$ with 200 eq. of H_2O_2 in D_2O, c) $H_3PW_{12}O_{40}$ with 200 eq. of H_2O_2 in CD_3OD, d) $H_3PW_{12}O_{40}$ with 200 eq. of H_2O_2 in D_2O/MeCN.

The first notable result was that when phosphotungstic acid is oxidized with hydrogen peroxide, the ^{31}P NMR spectrum shows three peaks at -0.3 ppm, -0.9 ppm and -1.4 ppm. This result shows that the formation of the Venturello anion PW_4O_{24} does not occur exclusively in absence of a stabilizing counter cation. When methanol was used as co-solvent, the peaks shifted to 0.3 ppm, -0.2 ppm and a broadened peak at -0.8 pm, but more importantly, a peak at -15.3 ppm appeared, which belongs to the precursor, $H_3PW_{12}O_{40}$. This is possibly due to methanol being oxidized to formaldehyde as a side reaction, which depletes the active peroxophosphotungstate and allows the precursor to regenerate. Acetonitrile gave rise to two clean peaks at -0.6 ppm and -1.0 ppm with no precursor, which explains why the catalyst synthesized in acetonitrile gives better results.

A similar solvent effect can also be observed via MAS ^{31}P NMR (Figure 18 in appendix).

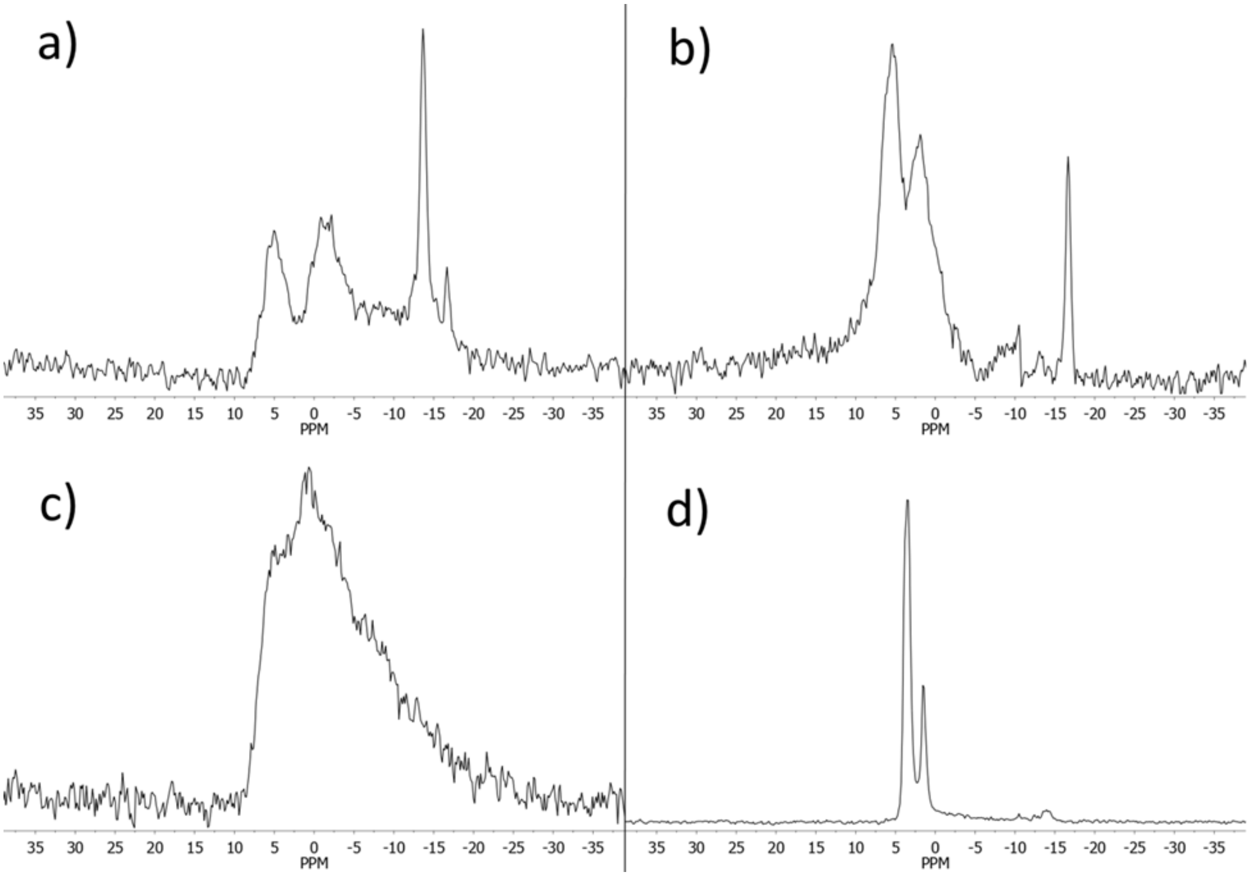

Figure 18: MAS ^{31}P NMR spectra of catalyst $(C_{41}H_{72}N_2)_3(PW_4O_{24})_2$ synthesized with a) H_2O b) MeOH c) $CHCl_3$ d) MeCN.

When the catalyst was synthesized using water, multiple peaks were observed between 8 and -16 ppm, with the largest signal at -13.7 ppm, which belongs to an intermediate with a low degree of peroxidation. When using methanol, two broad signals were observed between 10 ppm and -5 ppm, which should be highly peroxidized species, as well as a peak at -16.5 which shows that some of the inactive non-oxidized phosphotungstate co-precipitated. When using chloroform, a very broad peak was observed between 8 and -20 ppm, which is likely a complex mixture of partially peroxidized phosphotungstates. The catalyst synthesized with acetonitrile shows the peaks of highly peroxidized species at 3.5 ppm, and 1.5 ppm, both peaks being much better resolved than with the other solvents. There is also a very small peak at -13.9 ppm, which should be an intermediate with a low degree of peroxidation. It is important to notice that the catalysts produced in water and chloroform were visibly yellow which demonstrates the presence of the inactive (**DP**$^{2+}$)(WO_6^{2-})$_2$, which does not contain phosphorus and is therefore not visible by ^{31}P NMR.

7.1.4. SEM characterization

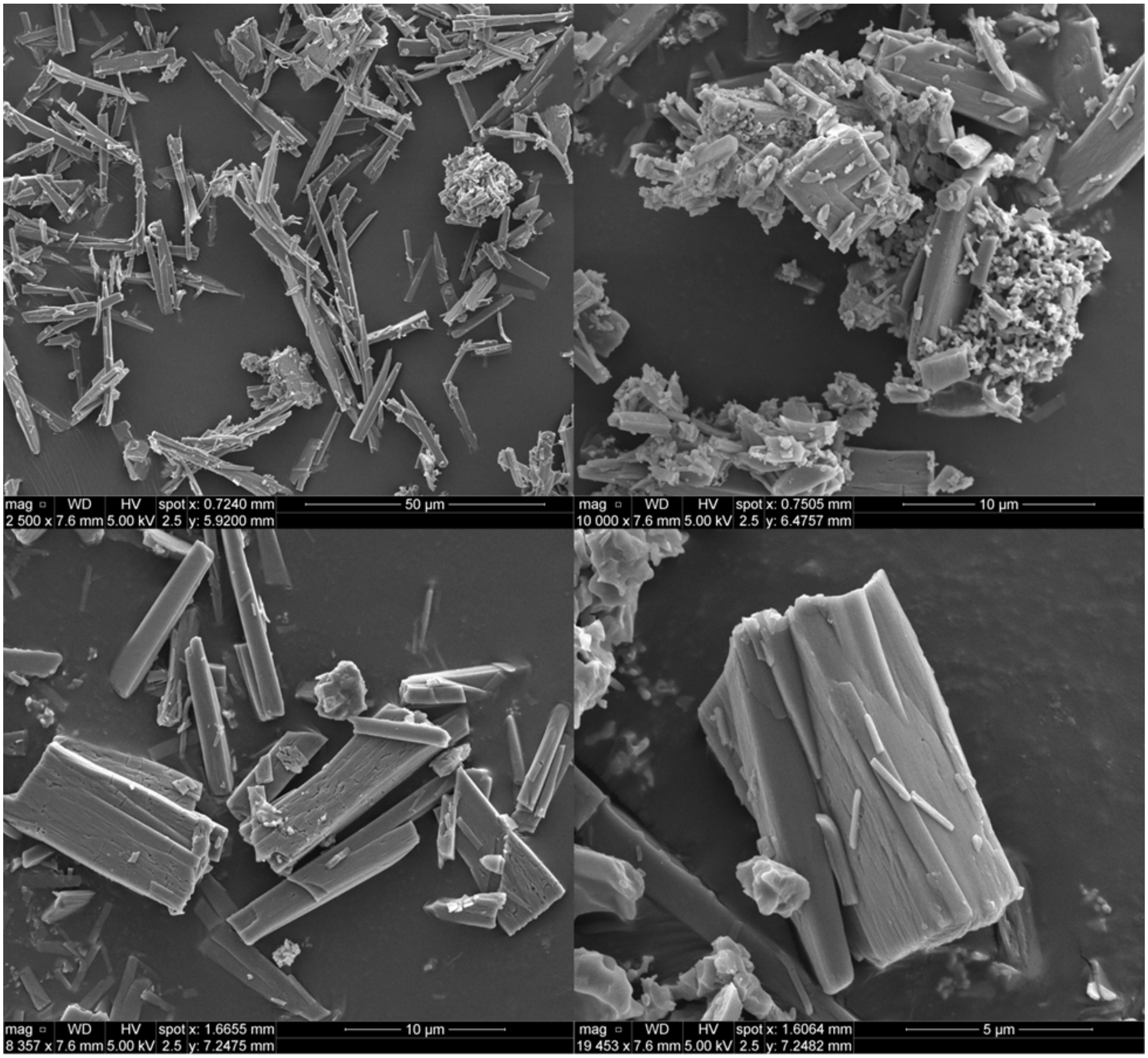

Figure 19: SEM pictures of ([**DP**$^{2+}$]$_3$[**PPW**$^{3-}$]$_2$) as synthesized using conditions from Table 2 entry 9.

From the SEM pictures, it can be observed that the product has two distinct regions. The majority of the sample observed arranged itself in the shape of rectangular prisms, which range between 1 μm and 50 μm in length, with height and width between 0.5 and 5 μm. These slabs agglomerate at random while retaining their shape. The second region observed is an amorphous agglomeration with no determined size or shape, which appears to be the result of particle growth in random directions, and is consistent with the ^{31}P MAS NMR analysis that shows the product is not a single pure compound, but a mixture.

7.1.5. Catalyst recovery and recycling

Figure 20: Picture of a typical catalytic test for the epoxidation of methyl oleate. The catalyst ([**DP**$^{2+}$]$_3$[**PPW**$^{3-}$]$_2$) floats between the organic phase (top) and the aqueous phase (bottom).

The catalyst ([**DP**$^{2+}$]$_3$[**PPW**$^{3-}$]$_2$) was designed to be immiscible in both the organic and the inorganic phases, as can be clearly seen in Figure 20. In order to recycle the catalyst, we tested a few strategies. Simple filtration allowed to recover clean product, but made catalyst recovery largely inefficient. Given the small amounts of catalyst used for most experiments (7.6 mg of catalyst for a 0.22mol% test), we turned to centrifugation which allowed to have the solid catalyst adhere strongly to the bottom of the flask, while both liquid phases could be removed with a pipette.

Recycling tests using 1mol% catalysts allowed for efficient recycling and high activity and selectivity upon 5 cycles. When 0.022mol% was used the catalyst activity dropped after 3 cycles. The low loading, however, allowed after 5 cycles to achieve a high cumulated TON of 1868 (Table 7 in appendix). Specifically, significant loss of activity was observed after TON exceeded 1300. This drop is not consistent with loss of catalyst as a leaching of 5.3% in tungsten was measured in the larger scale experiment (Table 3, entry 8). Thermal degradation was ruled out as a cause of degradation by pre-heating the catalyst for 24 hours, after which the catalyst showed normal activity. Therefore the loss of catalytic activity appears to correlate with catalyst degradation after extensive number of cycles.

Table 7: High TON recyclings.

Cycle	**Conversion**	**Selectivity**	**Accumulated TON**	**Accumulated TOF**
1	98.3%	96%	446	149
2	96.9%	96%	886	148
3	92.1%	98%	1304	145
4	70.8%	100%	1626	135
5	53.4%	100%	1868	125

Reaction Conditions: 500 mg of methyl oleate (1 eq.), 7.6 mg of $[\mathbf{DP}^{2+}]_3[\mathbf{PPW}^{3-}]_2$ (0.0022 eq.), 222 μL H_2O_2 30% (1.32 eq.). Reaction is heated to 60 °C and stirred for 3 hours at this temperature.

Recycling conditions: The reaction mixture was diluted with 10 mL of ethyl acetate, centrifuged, and both liquid phases removed with a pipette. The solid catalyst remaining in the flask was dried with air for 1 minute.

7.1.6. References

(24) Kamata, K.; Yonehara, K.; Sumida, Y.; Yamaguchi, K.; Hikichi, S.; Mizuno, N., Efficient epoxidation of olefins with >= 99% selectivity and use of hydrogen peroxide. *Science* **2003,** *300,* 964-966.

(25) Kamata, K.; Yonehara, K.; Sumida, Y.; Hirata, K.; Nojima, S.; Mizuno, N., Efficient heterogeneous epoxidation of alkenes by a supported tungsten oxide catalyst. *Angew. Chem. Int. Ed.* **2011,** *50*, 12062-12066.

(29) Leng, Y.; Wu, J.; Jiang, P.; Wang, J., Amphiphilic phosphotungstate-paired ionic copolymer as a highly efficient catalyst for triphase epoxidation of alkenes with H_2O_2. *Catal. Sci. Technol.* **2014,** *4*, 1293.

(30) Leng, Y.; Zhao, J.; Jiang, P.; Wang, J., Amphiphilic polyoxometalate-paired polymer coated Fe_3O_4: magnetically recyclable catalyst for epoxidation of bio-derived olefins with H_2O_2. *ACS Appl. Mater. Interfaces* **2014,** *6*, 5947-5954.

(31) Yamada, Y. M. A.; Guo, H. Q.; Uozumi, Y., Tightly convoluted polymeric phosphotungstate catalyst: An oxidative cyclization of alkenols and alkenoic acids. *Org. Lett.* **2007,** *9*, 1501-1504.

(32) Khlebnikova, T. B.; Pai, Z. P.; Fedoseeva, L. A.; Mattsat, Y. V., Catalytic oxidation of fatty acids. II. Epoxidation and oxidative cleavage of unsaturated fatty acid esters containing additional functional groups. *React. Kinet. Catal. Lett.* **2009,** *98*, 9-17.

(161) Landry, M. J.; Gellé, A.; Meng, B. Y.; Barrett, C. J.; Moores, A., Surface-Plasmon-Mediated Hydrogenation of Carbonyls Catalyzed by Silver Nanocubes under Visible Light. *ACS Catal.* **2017,** *7*, 6128-6133.

(180) Clapham, S. E.; Hadzovic, A.; Morris, R. H., Mechanisms of the H_2-hydrogenation and transfer hydrogenation of polar bonds catalyzed by ruthenium hydride complexes. *Coord. Chem. Rev.* **2004,** *248*, 2201–2237.

(181) Baig, R. B. N.; Varma, R. S., Magnetic Silica-Supported Ruthenium Nanoparticles: An Efficient Catalyst for Transfer Hydrogenation of Carbonyl Compounds. *ACS Sustainable Chem. Eng.* **2013,** *1*, 805−809.

7.2. Appendix II: Supporting information for chapter 3

7.2.1 Nanoparticle characterization

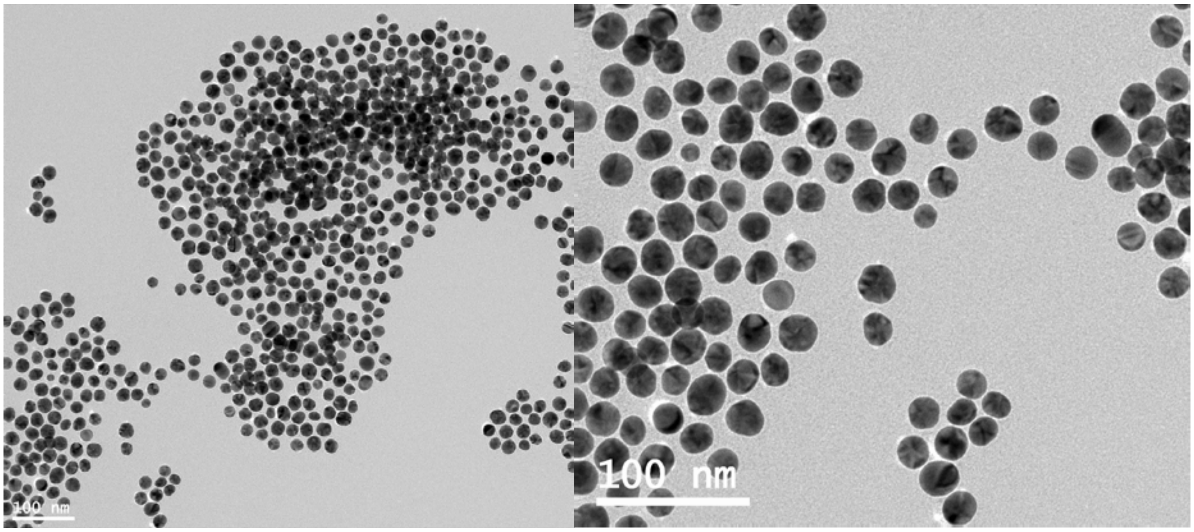

Figure 21: Bright-field TEM images of pristine Au NPs.

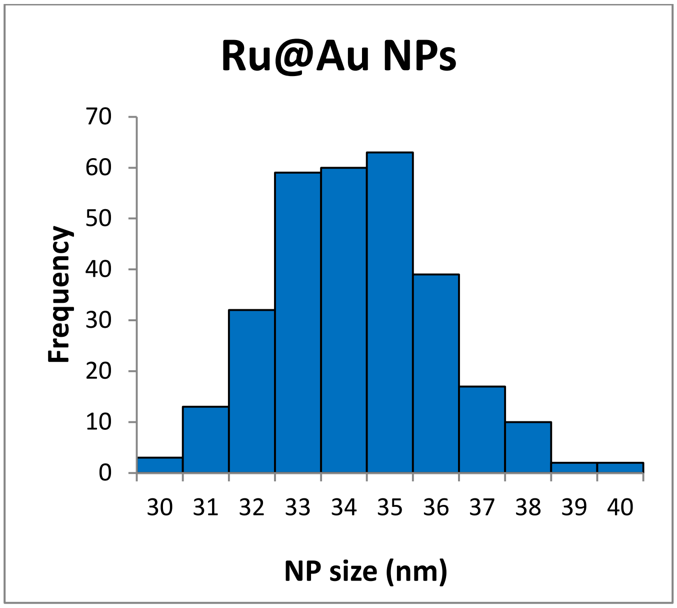

Figure 22: Histogram of 300 Ru@Au NPs. Average size: 34.3 nm. Standard deviation: 1.8 nm.

Due to the low contrast of Ru on Au NPs by Bright-field TEM, an additional sample was prepared with a 1:2 Ru:Au loading to better visualize that Ru was indeed growing on the surface of the Au NPs. However, this sample was not used for catalysis, since the increased proportion of Ru significantly dampens the LSPR band.

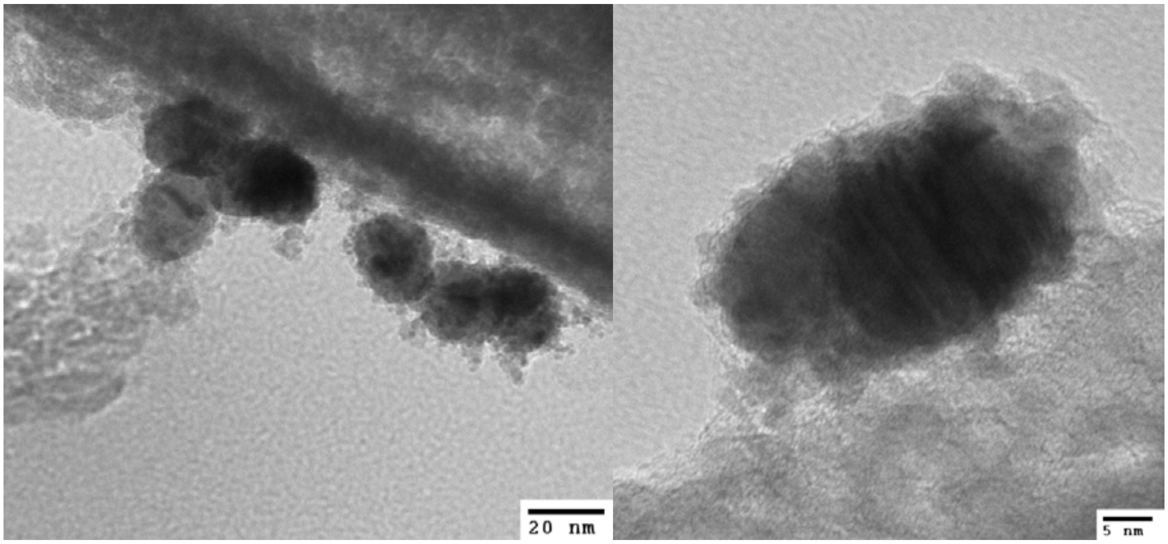

Figure 23: Bright-field TEM images of Au@Ru/Al_2O_3 with 1:2 Ru:Au loading.

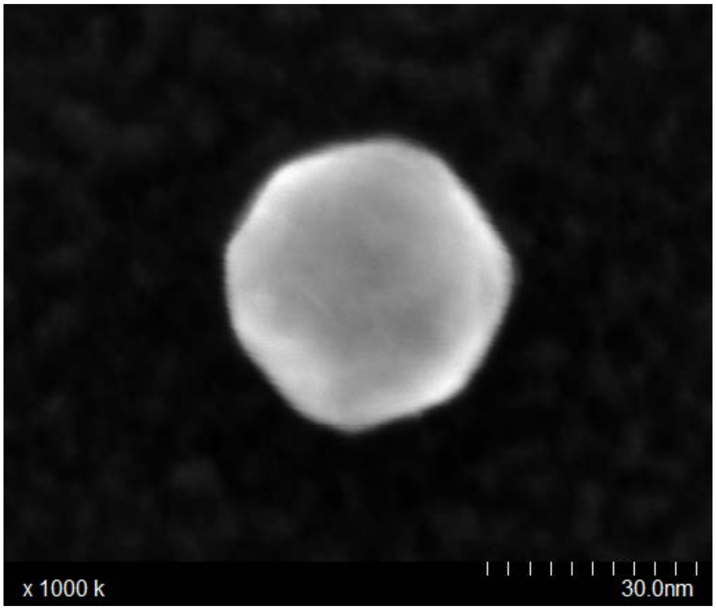

Figure 24: Secondary electron image of pristine Au NPs, demonstrating that the surface is very smooth.

7.2.2. LED emission spectra

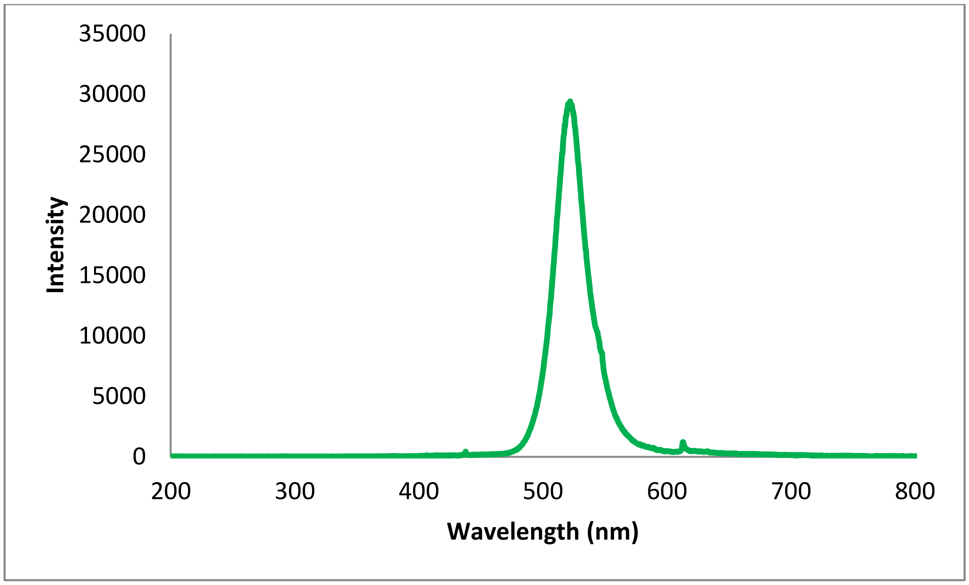

Figure 25: Emission spectrum of Green LEDs. Peak maximum at 519 nm.

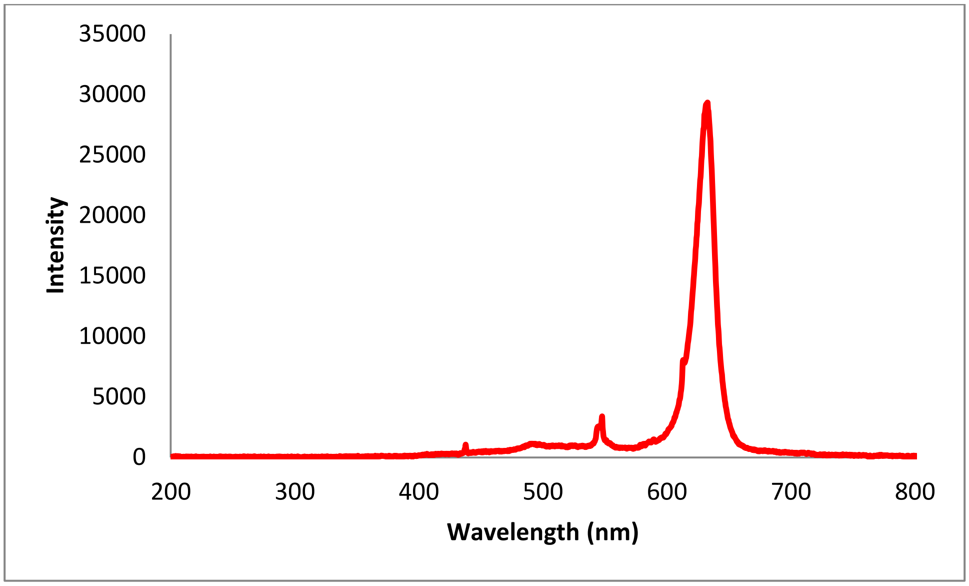

Figure 26: Emission spectrum of Red LEDs. Peak maximum at 630 nm.

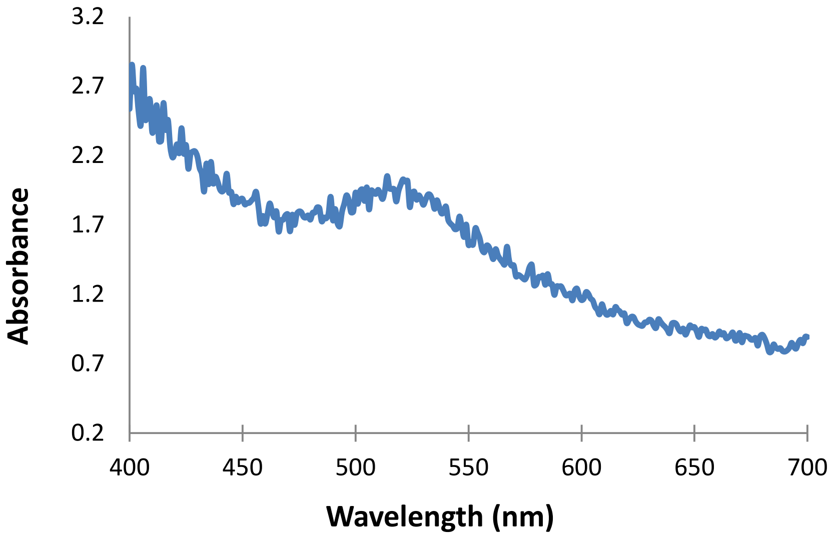

Figure 27: UV-Vis spectrum of Au/Al_2O_3.

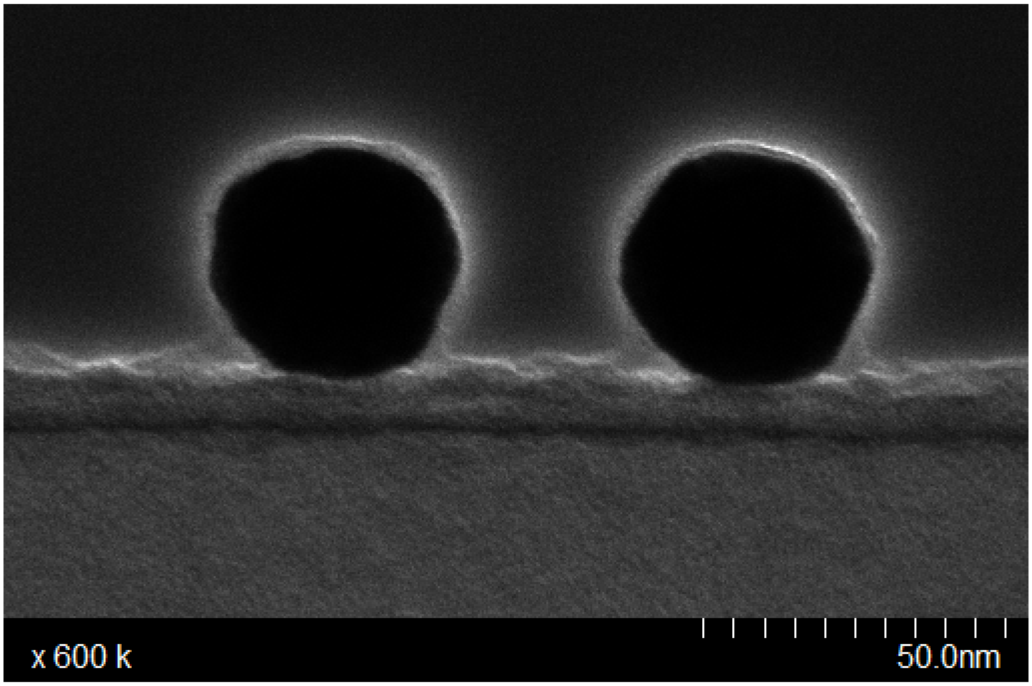

Figure 28: EF-STEM-EELS image of Au NPs showing the LSPR band.

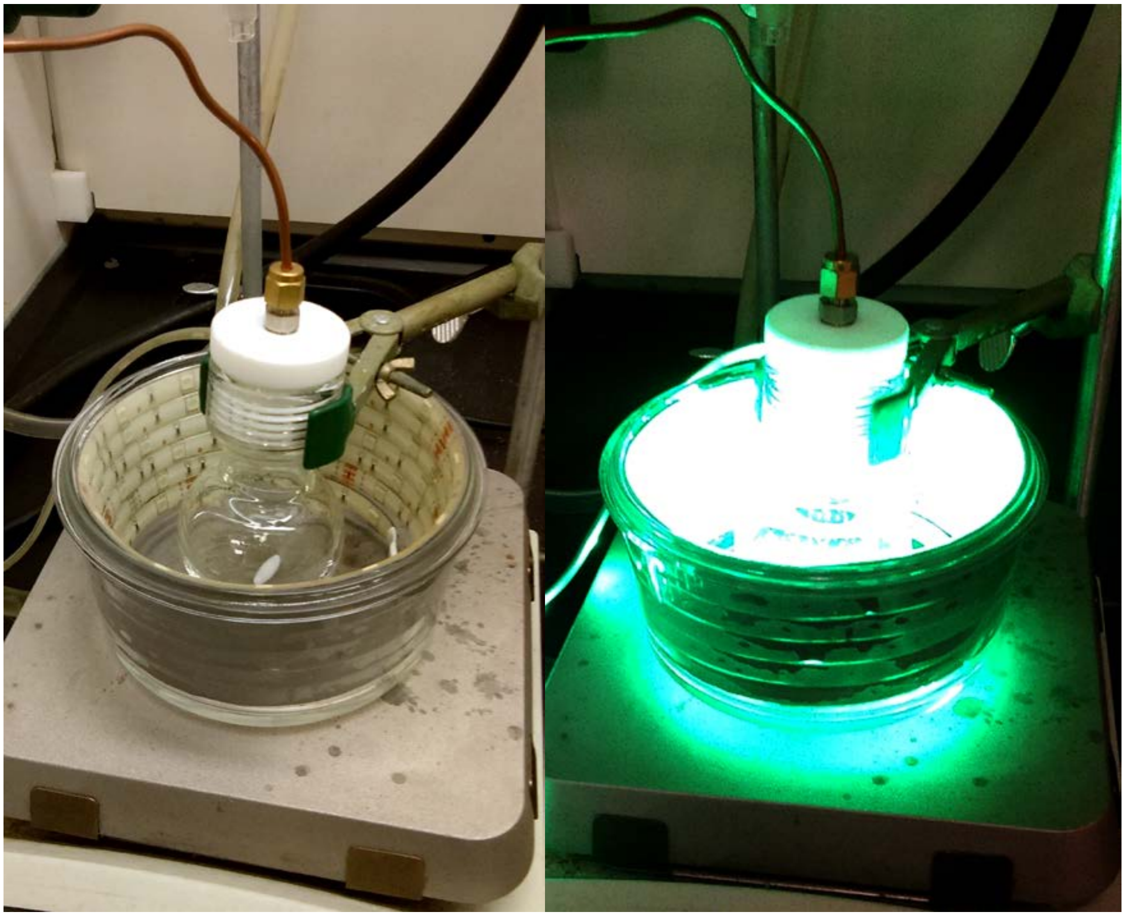

Figure 29: Reaction setup.

7.3. Appendix III: Supporting information for chapter 4

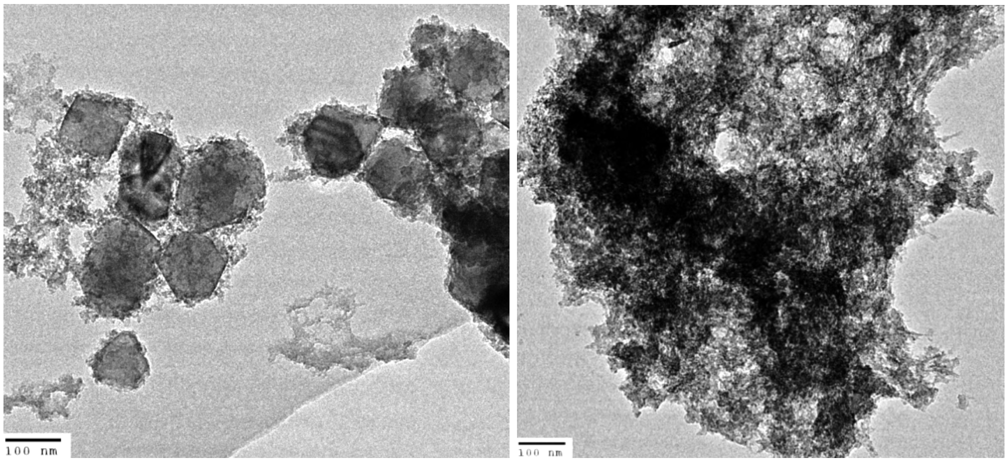

Figure 30: TEM images of oxidized Al NPs.